Durham E-Theses

A search for non-integral charge particles in cosmic rays

J. King

How to cite:

King, J. (1970) *A search for non-integral charge particles in cosmic rays.* Doctoral thesis, Durham University.

Use policy

A SEARCH FOR NON-INTEGRAL CHARGE

PARTICLES IN COSMIC RAYS

by

J. KING, B.Sc.

A Thesis submitted to the

University of Durham

for the

Degree of Doctor of Philosophy

November, 1970

CONTENTS

ABSTRACT

Large area proportional counters were developed and used to study
the charge distribution of interacting particles incident at Durham
in the near vertical direction. The experiment was operated in the
search for non-integral charge particles in cosmic rays at sea level.
The apparatus was sensitive to relativistic particles of charge in the
range 2e/3 to 7e/3. No strong signal was obtained in the running time
and the rate of non-integral charge particles was set as a limit. This
limit was :-

$$I < (4.2 \pm 1.9)10^{-9} cm^{-2} s^{-1} sr^{-1}$$

A second experiment was developed to detect e/3 charge particles
close to the core of extensive air showers at sea level. The response
of the detector for relativistic single muons was measured and the
equivalent characteristics for relativistic e/3 quarks calculated.
The change in response for the more energetic muons close to the air
shower core was also measured and agreed with the calculated prediction.

A system of electronics was constructed and was used in the two
experiments and subsidiary investigations.

PREFACE

This thesis describes the work performed by the author in the Physics Department of the University of Durham while he was a research student under the supervision of Dr. F. Ashton.

Large area proportional counters were developed, constructed and tested by the author. Eight of these counters were incorporated into an experiment to measure the charge distribution of nuclear-active particles at sea level. The day-to-day running of this experiment and the analysis and interpretation of the data has been the author's sole responsibility.

A second experiment was performed to test the feasibility of using flash tubes to detect $e/3$ charged quarks close to the core of air showers. Again the development, building, running, analysis and interpretation has been the responsibility of the author, with assistance from Mr. R. M. El-Helo.

The author also developed and constructed a series of electronic circuits suitable for use in cosmic ray experiments.

Other work in which the present author was a co-author and which has been published, but is not referred to in this thesis, comprises: a study of the neutron energy spectrum in sea level cosmic radiation (Ashton et al., 1969); and a search for magnetic monopoles in cosmic rays (Ashton et al., 1969a). Both these papers were reported at the Russian Cosmic Ray Conference (Tashkent, 1968).

CHAPTER   1

INTRODUCTION

1.1 Elementary Particles

Physicists have always studied matter by trying to reduce it into

its smallest component parts, However, today one is left with a

bewildering confusion of 'elementary' particles both subnuclear and

heavier than the proton (baryonic).   Prior to 1930, it was believed that

most physical phenomena could be represented by three elementary particles,

the proton, the electron and the photon - interacting through two basic

types of force - electromagnetic and gravitational.   It soon became

clear that the nucleus lay outside this scheme.   A nuclear force had to

be postulated that would balance the strong coulomb repulsion of the

protons inside the nucleus.   By analogy with the photon in electromagnetic

interactions, Yukawa (1935) postulated that the force between nucleons

could best be described as an exchange of intermediate 'virtual' particles.

Based on the range of the force, $\sim 10^{-13}$ cm, Yukawa predicted the π-meson

as the intermediary.   This particle was subsequently discovered in cosmic

rays and it became clear that the protons and neutrons (which had

previously been discovered in 1932) were not structureless points but

clusters of subnuclear material of radius about 10^{-13} cm.   The advent of

accelerating machines and bubble chambers has meant that this structure

of the nucleons has been studied and a wide spectrum of particles has

been discovered.   The classification and understanding of these particles

is one of the major problems in nuclear physics today.

Considerable advances in classification have been made by studying

the conservation laws which govern particle interactions.   In strong
interactions of the baryon group, for example, three conservation laws
are obeyed:-

1. The conservation of electronic charge Q, which is thought to be
    absolute.

2. The conservation of baryonic charge B, which is, again, thought to
    be absolute and accounts for the abundance and stability of the
    proton.

3. The conservation of hypercharge, Y, to account for the associated
    production of the K meson with the Λ or Σ hyperons in strong
    interactions.

It has been found that the elementary particles can be divided into
groups, for example the spin $\frac{1}{2}$ baryons.

The question then arises of what mechanism could produce these
observed regularities.   The theory of Unitary Symmetry will explain
grouping and the physical interpretation of this theory could be the
existence of three (because of the three charges Q, B and Y) subnuclear
particles (p,n,λ).   'Quarks', as these particles are called, were proposed
by Gell-Man (1964) and independently by Zweig (1964).   The p and n quarks
form an isodoublet $(I = \frac{1}{2})$ of strangeness S = 0;   the λ quark is an
isoscalar $(I = 0)$ to which the strangeness S = -1 is assigned.   Since,
as discussed below, three quarks are **necessary to construct** a baryon,
and a quark-antiquark pair to construct a meson, each quark will have
baryon number (charge) $B = \frac{1}{3}$.   Hence the hypercharge, defined by:

$$Y = S + B$$

is $\frac{1}{3}$ for the p and the n, and $-\frac{2}{3}$ for the λ. The Gell-Man-Nishijima relation

$$Q = I_3 + \tfrac{1}{2} Y$$

then gives values of the charge of p, n, λ as $\frac{2}{3}$ e, $-\frac{1}{3}$ e, $-\frac{1}{3}$ e. The quantum numbers of these quarks and the antiquarks are described in table 1.

TABLE 1   The Quantum Numbers of the Quarks

Symbol	Q	Spin	B	S	Y=S+B	I_3	Mass
P	$+\frac{2}{3}$e	$\frac{1}{2}$	$\frac{1}{3}$	0	$\frac{1}{3}$	$\frac{1}{2}$	M
n	$-e/3$	$\frac{1}{2}$	$\frac{1}{3}$	0	$\frac{1}{3}$	$-\frac{1}{2}$	M
λ	$-e/3$	$\frac{1}{2}$	$\frac{1}{3}$	-1	$-\frac{2}{3}$	0	M + 146 MeV/c^2
$\bar{p}$	$-2e/3$	$\frac{1}{2}$	$-\frac{1}{3}$	0	$-\frac{1}{3}$	$-\frac{1}{2}$	M
$\bar{n}$	$+e/3$	$\frac{1}{2}$	$-\frac{1}{3}$	0	$-\frac{1}{3}$	$\frac{1}{2}$	M
$\bar{\lambda}$	$+e/3$	$\frac{1}{2}$	$-\frac{1}{3}$	$+1$	$\frac{2}{3}$	0	M + 146 MeV/c^2

where M ~ several GeV/c^2

Q is the electric charge

B is the baryon number

S is the strangeness

Y is the hypercharge

I_3 is the third component of isospin.

Unitary symmetry required the quark content in any system to be conserved, but for any given dynamical situation involving p, n, and λ, a new dynamical situation can be obtained by rearranging the initial combinations. Quarks can then be regarded as the basic building blocks of hadrionic particles, and thus define their properties and conservation laws. The mesons can then be represented by bound states of a quark-antiquark pair, giving a spin of 0 or 1 according to the alignment of the quark spins. As can be seen from Figure 1.1 the two nonets of mesons can thus be made up from this arrangement.

Similarly, the spin $\frac{1}{2}(3/2)$ baryons, can be made up of a bound state of three quarks. Taking spin $3/2$ one arrives at the baryon decuplet and for spin $\frac{1}{2}$ the baryon octet, as shown in Figure 1.2. From this model it was possible to predict the existence of the Ω^- particle, its electric charge, hypercharge and mass.

The ratio of the magnetic moments of the neutron and the proton is also correctly predicted by the quark model, - 0.667 compared with the experimental value of - 0.685.

The theory of unitary symmetry and the quark model has thus brought order to the previous chaos of elementary particles. However, the full details of the model are still not fully understood; Kokkedee (1969). The binding energy between quarks must be very large to reduce the total mass to the level required, and no convincing model has been put forward for the quark force. One also wonders why, if quark-antiquark and three quark bound states occur in the mass range < 4 GeV/c^2, a four quark state does not exist, as it would be lighter. The question remains whether the quark actually exists as a subnuclear element which could
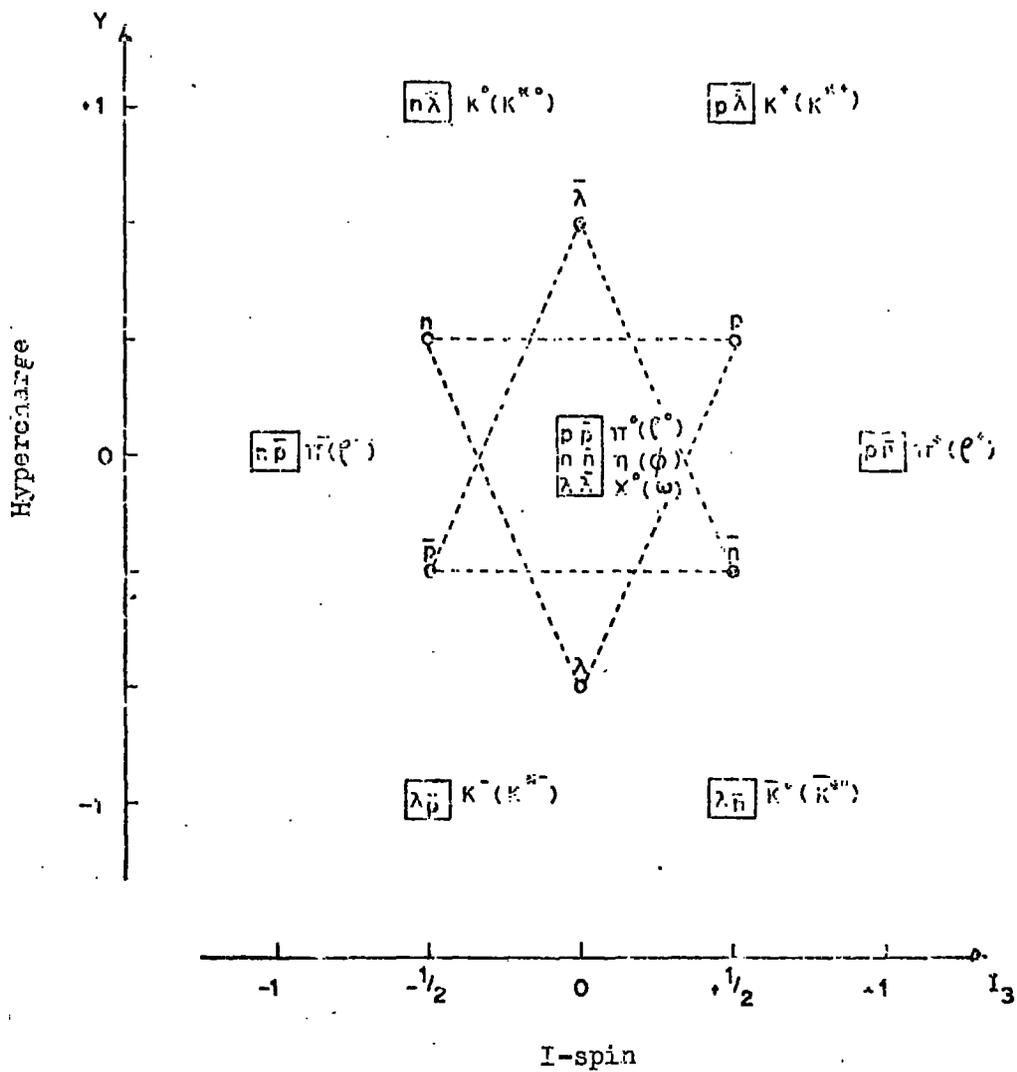
Spin C (1) mesons

Figure 1.1 The quark-antiquark pairs which produce
the two nonets of mesons.
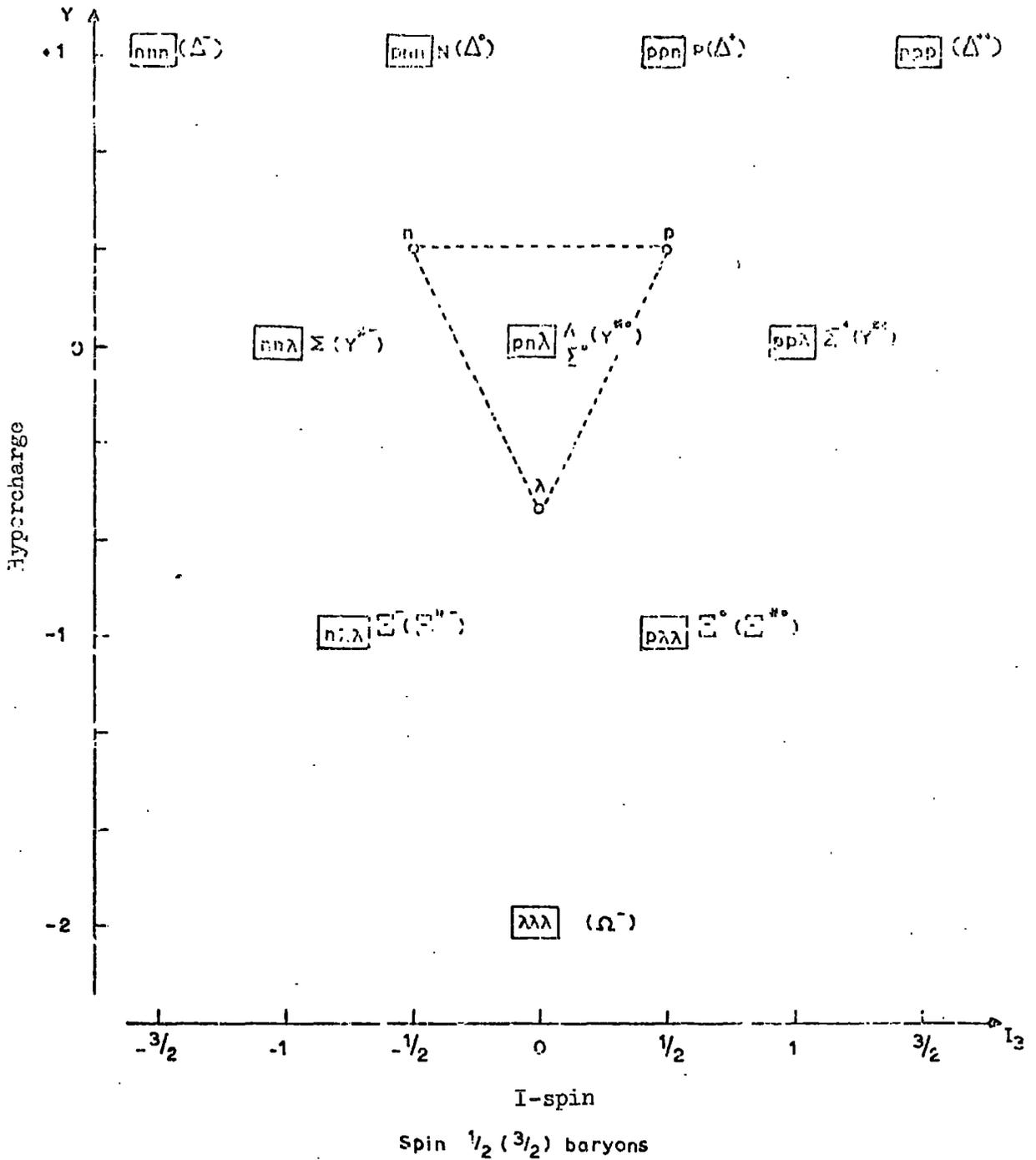
Figure 1.2 The three-quark combination which makes up the
baryon, spin ½ decuplet and the spin 3/2 octet.

be detected or whether it is just the physical interpretation of a convenient mathematical device.

1.2 Search for Quarks

Since the theory of quarks was first postulated many experiments have been performed to search for fractionally charged, massive particles. All the experimental results published up to 1968 have been summarized in a report by Massam (1968). Accelerator experiments at CERN and Brookhaven have failed to substantiate the theoretical prediction for the production of quarks. However, this could be due to the heavy mass of the quark. The energy provided in the centre of mass system by a 30 GeV proton beam is approximately 4 GeV. This would then set a lower limit of ~ 2 GeV/c^2 on the quark mass.

Cosmic rays offer protons of much higher energies. However, the primary energy spectrum is so steep (the rate decreases as $E^{-1.3}$, where E is the kinetic energy in GeV) that most of the quarks produced in proton-air nuclei collisions will be close to the threshold energy. The protons will diffuse through the atmosphere and reach sea level with ~ 0.05 times their primary energy after ~ 5 interactions. The majority of the secondary particles in the interactions are pions which will decay to muons, such that 70% of the intensity of cosmic rays at sea level are made up of these muons of median energy ~ 2 GeV. Thus any quarks produced in the interaction must be viewed through a background of many muons, although, if the transverse momentum given to the quark is great enough the quark will clear the main shower of particles.

Cosmic ray experiments have been performed at sea level, at mountain altitudes and deep underground. They have all, with one exception, been limited by their ability to detect only single unaccompanied quarks. No definite quarks have been discovered and the rate of quarks is therefore set as an upper limit. The best value for these limits, to date, for unaccompanied events is set by Ashton et al (1968a). At the 90% confidence limit these rates are:-

$$e/3 \; < \; 1\text{:}2.10^{-10} \; cm^{-2} \; s^{-1} \; sr^{-1}$$

$$2e/3 \; < \; 8\cdot0.10^{-11} \; cm^{-2} \; s^{-1} \; sr^{-1}$$

Experiments have also been performed to search for quarks absorbed in the nuclei of the material on the earth's surface, including the atmosphere. The results are difficult to interpret and a table of concentrations obtained are shown by Massam (1968) and Nir (1967). The large range of concentrations obtained experimentally are, according to Massam, comparable with the limit of the rates from counter experiments. A flux of $10^{-10} cm^{-2} sr^{-1} s^{-1}$ incident for 10^9 years and stopped in the first kilometre of the earth's crust would give 100 quarks per cc i.e. 10^{-22} quarks/nucleon. This concentration could lead to an underestimation of the quark flux as the effect of the earth's electric field has not been taken into account. A 'quarked' atom whose charge will be, generally - 2e/3 could be expected to be swept up by the field into the ionosphere, McDowell and Hasted (1967), and there is the finite possibility that they will be swept into interplanetary space by the solar wind as proposed by Axford (1968).

Optical spectra, from the sun, have also been studied looking for shifts in the spectral lines that would be due to quarked atoms. Several shifts have been found (Massam (1968)) but there is great difficulty in their interpretation.

There are two main objections to a realistic quark model, namely that despite great efforts by experimentalists the quark has not been found, and that no mechanism has been found which explains the low-lying integral charge states ($q\bar{q}$ and qqq) and which prevents other non-integral charge states of quark and antiquarks. Buhler-Broglin (1967) and de Swart (1967) have speculated that experimentalists should not only look for $|Q| = \frac{1}{3}$ and $\frac{2}{3}$ charged states but also search for particles with charges $|Q| = 4/3, 5/3, 7/3$ etc. It is possible that although $e/3$ and $2e/3$ quarks exist, they may be unstable to decay into compounds of 2 or 3 quarks or 2 quarks and antiquark, i.e. -

$$q \to \bar{q}\bar{q} + (qqq)$$
$$q \to qqqq + (\bar{q}\bar{q}\bar{q})$$
$$\text{or} \quad q \to qq\bar{q} + (q\bar{q})$$

where (qqq) is a baryon

and $(q\bar{q})$ is a meson.

The mass of the $4q$, $2q$ or $2q\cdot\bar{q}$ states might be smaller than that of the single quark, though much larger than the baryon. If the lightest member of these super-multiplets is the member of largest Y, as suggested by the known baryon states, the stable, fractionally charged state could well have the charges stated above.

Buhler-Broglin (1967) has investigated the flux of $4e/3$ charged

particles using six layers of scintillation counters under $780 \cdot gm \ cm^{-2}$ of iron absorber. Two spark chambers provided visual information. Only leptonic particles could be detected and the efficiency of the apparatus for 4e/3 was stated as 53%.

The sensitivity of this experiment to the rate of 4e/3 charged particles was found to be restricted by the background of muons, and, at 90% confidence, the limit was found to be:

$$\leqslant (1.6 \pm 0.8) \cdot 10^{-7} \ cm^{-2} \ s^{-1} \ sr^{-1}$$

Adair (1968) has considerably lowered this limit using a hodoscope of 48 liquid scintillation counters set up in 8 layers. The apparatus was sensitive to all charges $\geqslant$ 4e/3 and, in 1,000 hours, achieved the limit of

$$\lesssim 1.3 \ 10^{-10} \ cm^{-2} s^{-1} \ sr^{-1}$$

The search for quarks has now been taken into the region of air showers. This leads to difficulties, the main being that the quark must be detected with an accompaniment of many other particles. It is possible to absorb out the electron accompaniment, but one is still left with the muon and nuclear active components. McCusker (1969) and Cairns (1969), working on the same experiment, on examining 5,500 showers of mean primary energy $\sim 4 \times 10^{15}$ eV have reported four tracks which could be considered as 2e/3. The experiment consisted of an air shower array of 64 plastic scintillators, which were triggered by a coincidence from three small Geiger counter trays at the apices of a $\sim$ 2m triangle. The ionising particles were viewed with 4 Wilson cloud chambers, each 30 cm in diameter, of which three were 20 cm deep and the fourth, 10 cm deep. Only the 20 cm deep cloud chambers were shielded

but each chamber had an illuminated depth of 5 cm. The scintillator array, which was within 3 m of the cloud chambers, provided core position data.

There are several mechanisms which could produce a low ionising track in a cloud chamber, and, although these events have been rigorously tested, there is still some doubt as to their validity as $2e/3$ charged particles. A high pressure cloud chamber is at present being constructed by this group to search for charge $e/3$ in air showers.

1.3 The charge distribution of interacting particles

An experiment was carried out which measured the charge distribution of interacting particles, and specifically looked for non-integral charges $\geqslant 2e/3$. The experimental layout is described in detail in Chapter 4. It consisted of a layer of proportional counters positioned above 20 cm of iron absorber. The energy of the secondary components from the interaction in the iron was measured by a large liquid scintillator. Crossed flash tubes provided visual track information in three dimensions. The expected pulse height distributions in the proportional counters is considered in Chapter 5. The construction, design, and testing of the proportional counters used is discussed in Chapters 2 and 3.

1.4 A search for $e/3$ charged particles close to the core of air showers

An experiment was built up and tested that would distinguish an $e/3$ charged particle among a host of charged e particles. This experiment

is described fully in Chapters 6 and 7. It had the advantage over a
cloud chamber of having a considerably larger sensitive volume. The
expected rate of quarks that would have to be detected in this apparatus
to be comparable to McCusker results would be 1 event in every 370
hours. Flash tubes, although unable to separate $2e/3$ from e were found
to be very capable of distinguishing $e/3$ although the efficiency of
detection might be less than the cloud chamber because of the confusion
at high track densities.

The electronic system which was developed for these two experiments
is displayed in Appendix A. Appendix B described the small telescopes
used and Appendix C compares the response of the three types of
scintillator encountered during the work on the two experiments.

CHAPTER 2

THE DEVELOPMENT AND PERFORMANCE OF LARGE PROPORTIONAL COUNTERS

2.1 Introduction

The proportional counter is one of the classical devices of
nuclear physics, and was used by Rutherford in 1908, although it was
not until quite recently that its principles of operation were at all
fully exposed.

The proportional counter is a device, which operates by collecting
the ionisation, caused by an incident charged particle, and displaying
it as an electrical pulse. Unlike the Geiger counter, it produces a
pulse which is proportional to the initial ionisation over a wide range,
and unlike a scintillator, it has the added advantage (Ashton et al,
1968) of uniformity of response, no matter how large the counter. A
large proportional counter is also considerably less expensive than a
scintillator, for large sensitive areas. Moreover, use can be made of
the relativistic logarithmic rise in ionisation to distinguish between
particles of varying Lorrentz factor, (Ramana Murthy, 1967).

However, the size of electrical pulse produced by the proportional
counter requires a high amplification, and if many proportional counters
need to be used, this could be prohibitive. Until now, most conventional
counters have been cylindrical, which means that one has to be very
careful of geometrical effects. This can be overcome by suitable over-
lapping of visual track position information.

If one wants to increase the size of a proportional counter keeping
the response the same, the electric field inside the counter must be

kept high. This would mean that either the supply voltage must be raised or the inner electrode must be decreased in size. This would therefore limit the size of proportional counter that one could make.

2.2 The theory of proportional counters

Let us consider a proportional counter, which is made up of two coaxial cylinders with a gas filling, such as argon at atmospheric pressure, between them. The outer cylinder, radius b, and the inner cylinder, radius a, are maintained at potentials zero and +V respectively. If a nuclear particle traverses the gas it will produce ionisation, and the electrons and positive ions formed will drift to the electrodes under the attraction of the electric field. An electrical pulse can then be seen at the central electrode, or wire, due to the arrival of the ionisation at the electrodes. As the mobility of the electrons is much greater than that of the positive ions, this pulse will consist of a fast rise caused by the arrival of the electrons in microseconds, followed by a much slower rise in the final height, caused by the slower (milliseconds) arrival of the positive ions. If this pulse is differentiated, by a suitable choice of RC, one can obtain a pulse with microseconds decay time, and yet which is still proportional to the original ionisation and above noise (Wilkinson, 1950).

Consider the voltage applied to the electrodes to be increased so that the electrons are given sufficient energy to produce more electrons by collision. Gas multiplication will occur. The field, E, necessary to accelerate an electron from rest to the energy required to produce

extra ionisation in argon at atmospheric pressure is approximately 10 kV cm^{-1}. For a cylindrical counter the field at radius, r, is given by:-

$$E = \frac{V}{r \log_e \frac{b}{a}}$$

For the counter described below, $b/a = 1840$ and $V = 3kV$, the field required for ionisation by collision in argon at atmospheric pressure is reached at a radius, $r = 0.04$ cm. An electron from the ion pairs produced anywhere in the counter will drift toward the wire and, once it reaches the radus, r, will produce an 'avalanche' of electrons, which is collected by the wire. The pulse height produced is therefore independent of the position of the original ionisation in the counter, as the 'multiplication' occurs only very close to the wire.

The gas multiplication M, is defined as the number of electrons reaching the electrode for each initial electron, and this is very dependent on the photons present producing more electrons by the photo-electric effect. The number of photo-electrons will be proportional to the number of electrons, n, present in the first 'avalanche', with γ the constant of proportionality. The first avalanche will then produce γn photoelectrons which in turn will 'avalanche' to γn^2 etc. The total number of electrons reaching the wire for each electron formed in the gas will then be:-

$$n \;+\; \gamma n^2 \;+\; \gamma n^3 \;+\; \ldots\ldots$$

with n increasing with the voltage.

If one wants the counter to be proportional to the initial ionisation, then V must be kept low so that $\gamma n < 1$. The addition of methane to the counter gas, which will absorb the photons, will also help to keep γ low. The total number of electrons reaching the wire will then be:-

$$M = \frac{n}{1-\gamma n}$$

The proportional region of this type of counter is then governed by the voltage, and its limits are from $M > 1$ to the voltage where γn approaches unity. Where the latter applies, the gain will increase with voltage much more strongly (the region of limited proportionality).

The proportional counter is therefore a device, which will distinguish between particles differing in total ionisation. By gas amplification, it will produce a 'signal' well above noise, when only a few electrons are released in the initial ionisation. It is robust and flexible, and microphonic disturbances and electromagnetic pick-up are much less important, since the genuine 'signal' is amplified.

Most of these advantages would be offset if the gas gain M, was not constant from one particle to the next. If straggling in the number of electrons in the 'avalanche' occurred, the device would not be able to measure particle energy with sufficient accuracy.

One would expect large straggling for single avalanches, as confirmed by Wilkinson (1950), who shows the value for the variance V, in the gas amplification, M, to be:-

$$v = \bar{M^2} - \bar{M}$$

If the width of the distribution is measured by $\sqrt{v}$, then for large gains the straggle in the multiplication will be nearly equal to the mean value of the multiplication.

The situation is greatly improved, if one takes a number of initiating electrons, m. One then has m independent avalanches, each with $v \sim \bar{M}^2$. If the mean value of the initial ionisation is $\bar{m}$ and its variance w, then Frisch has shown that the variance v_p in the total number of electrons collected in a multiple avalanche is:

$$v_p = w\bar{M}^2 + v\bar{m}$$

$$= w\bar{M} + (\bar{M}^2 - \bar{M})\bar{m}$$

The relative variance is then

$$\frac{v_p}{(\bar{m}\bar{M})^2} = \frac{w}{\bar{m}^2} + \frac{1}{\bar{m}} - \frac{1}{\bar{M}\,\bar{m}}$$

and for $\bar{M} \gg 1$

$$\frac{v_p}{(\bar{m}\bar{M})^2} = \frac{w}{\bar{m}^2} + \frac{1}{\bar{m}}$$

If an ionising particle of well defined energy spends all its energy in the counter, Fana (1947) has found that the variance w is $< \bar{m}$ as a fluctuation of ionisation, giving more ion pairs in one length of the track, leaves less energy for the rest of the track. The counter effect will then be noticeable but, as $1/m$ must be small for accurate energy measurement the effect will not be serious.

If, on the other hand, an ionising particle, such as a fast muon,

spends very little of its energy in the counter, the variance in the total ionisation will be greater than normal, because of the exaggerating effect of δ rays. Thus $w > \bar{m}$ and the additional variance imposed by the counter is correspondingly less important. The proportional counter is thus a useful device in specific ionisation studies in cosmic rays.

When one considers that the electrons are not in equilibrium with the field close to the wire, the calculations carried out by Hanna, Kirkwood and Pontecorvo (1949) show that the effect of straggling is still less pronounced. Curran, Cockcroft and Angus (1949) have also investigated straggling within a single avalanche, and have shown this to be less than expected. Space charge effects at high multiplications would also tend to sharpen the distribution by opposing large M values.

2.3 Construction of the large proportional counters

A diagram of the proportional counters constructed is shown in Figure 2.1a. It consists of a drawn cylinder of 85% aluminium and 15% silicon, of diameter 14 cm and length 3.67 m, with a 3×10^{-3} inch (0.0076cm) tungsten wire positioned coaxially as the central electrode. The ends were sealed with discs of half inch thick perspex, the wire being supported by bolts tapped into this perspex. The joins, as shown in the diagram, were sealed with catalloy-paste metal filler, to give a vacuum-tight seal. In addition, a high vacuum tap was mounted on one of these perspex ends, through which the counter was filled with gas, 90% argon and 10% methane, to atmospheric pressure. The differentiating circuit and the emitter follower used are shown in Figure 2.1b.
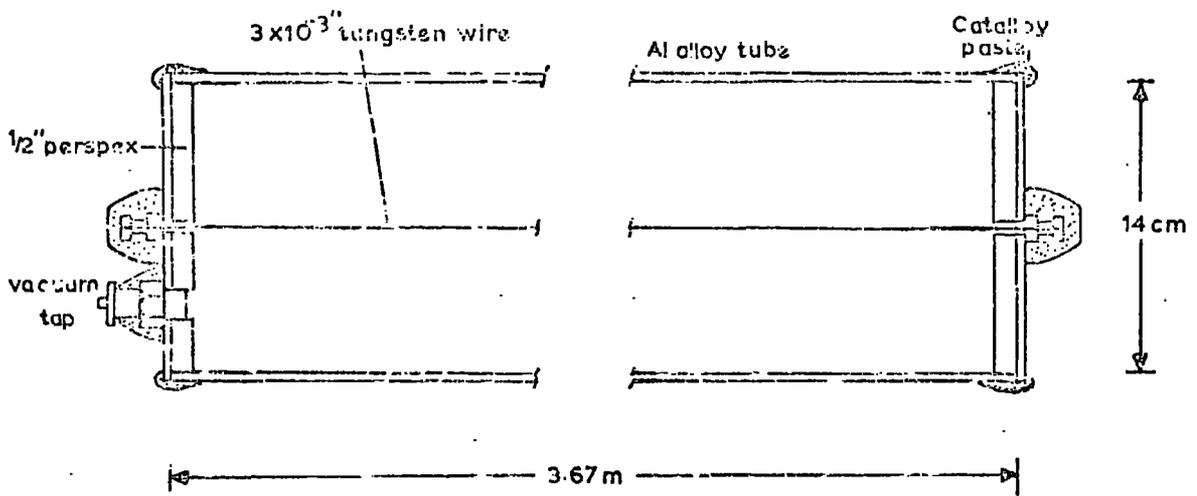
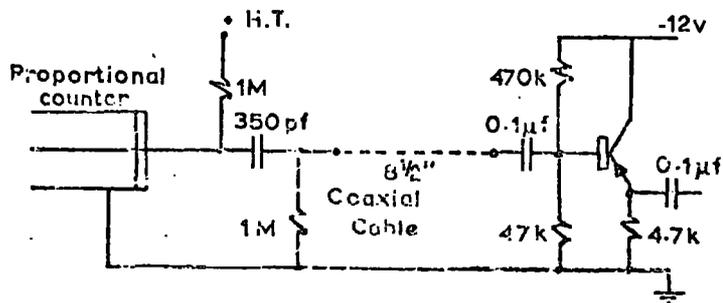Figure 2.1a The construction of the proportional counters.

Figure 2.1b The proportional counter head unit.

It is important that all traces of any electro-negative gas or
impurities should be removed from the counter before operation. Care
was taken that the inside walls of·the counter were thoroughly cleaned
with suitable solvents before construction. The counter was then
evacuated, using the system shown in Figure 2.1, to remove as much of
the air as possible. Each cylinder was pumped down, using the backing
pump and the liquid nitrogen trap, to pressures in the region of 0.04
torr, and left under vacuum for several hours for a leak test. Leaks
of less than 0.04 torr over the first 12 hours were found to be accept-
able. The cylinder was then flushed with the filling gas to 1 cm of
mercury, and re-evacuated as low as possible. The backing pump and the
nitrogen trap were then switched out of the system and the cylinder
filled with the argon mixture to 5 mm Hg above atmospheric pressure. As
the cylinders could not be sealed to an extremely high degree, the
slight over-pressure in the counter would prolong its life, but
frequent checks had to be made on the condition of the gas.

2.4 The performance of the counters

Cosmic ray muons which traversed the counter were selected by means
of a Geiger telescope (Section 6). At selected voltages the distribu-
tion in output voltage for a particle traversing the telescope was
measured. Figure 2.3 is an example of the single particle distribution
obtained in this way from proportional counter, P5, at an operating
voltage of 3.0kV. The pulse height-supply voltage plot could then be
drawn for the counter (Figure 2.4). As can be seen from this figure,
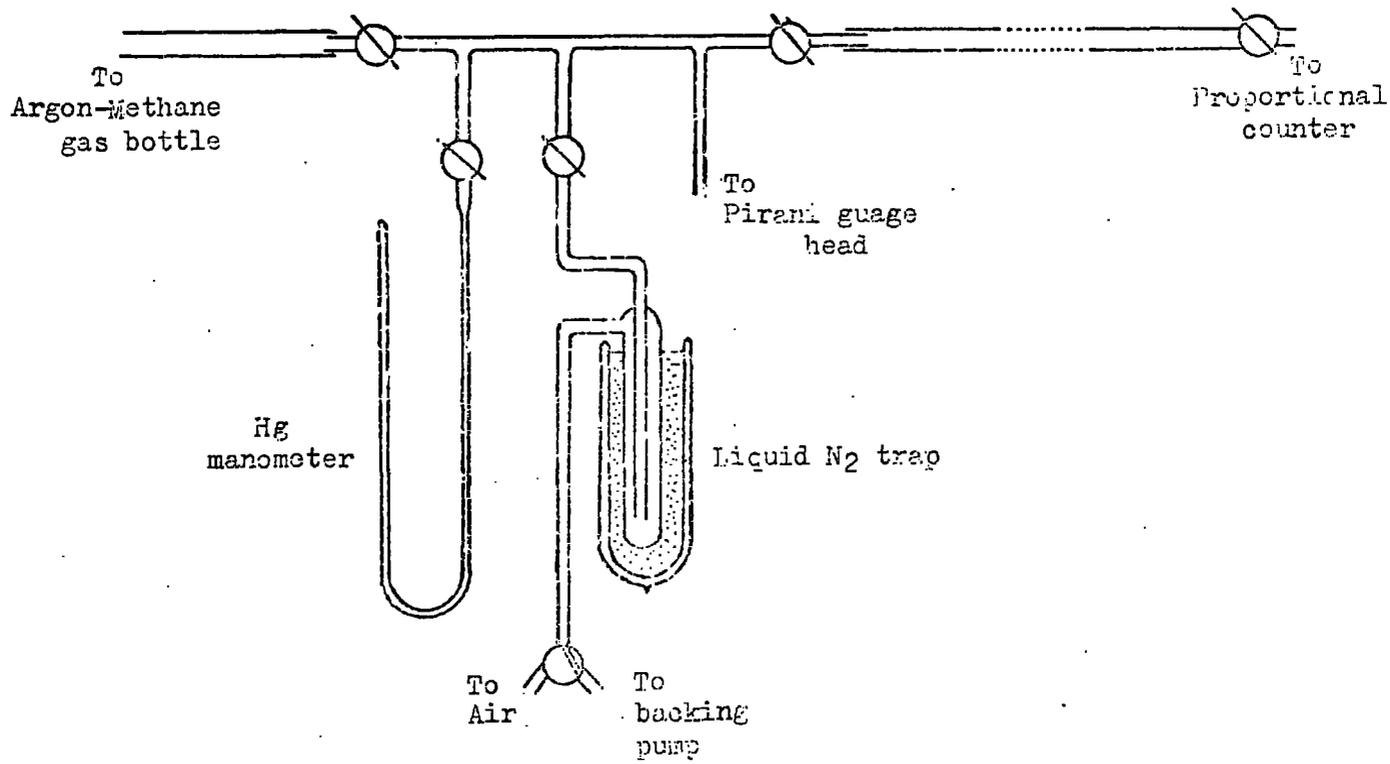the pulse height has a constant exponential slope, i.e. it is in the

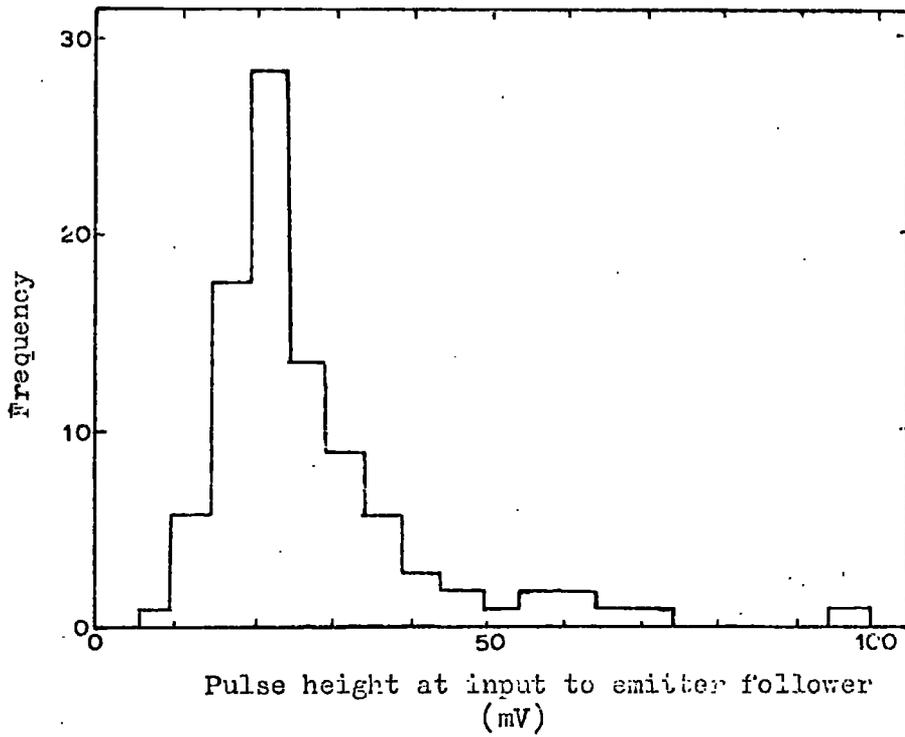Figure C.2   The evacuation and filling system.

Figure 2.3 The single particle distribution obtained from proportional counter, P5, operating at 3.0kV using the Geiger telescope arrangement.
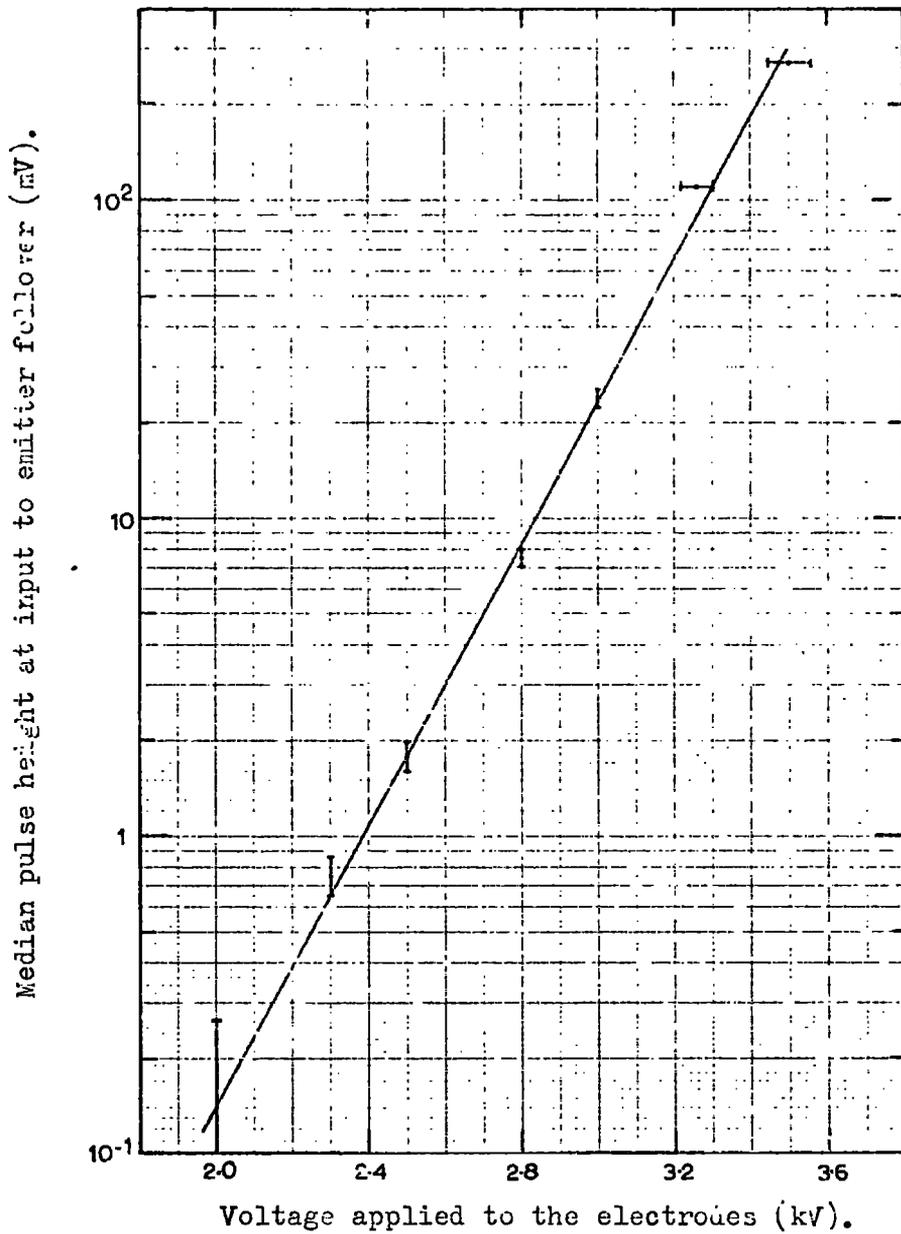
Figure 2.4 The variation of the median pulse, produced
using the Geiger telescope, with operating
voltage for the proportional counter.

proportional region, for over three decades of pulse height. At the lower limit the pulse height tends to disappear into noise, apparently caused by the telescope. At the higher limit of pulse height, for two of the proportional counters manufactured, there is a slight suggestion of an increase of slope at approximately 3.6kV. However, in this region one is restricted by the nearness to saturation of the electronics.

2.5   The ionisation energy loss by charged particles

2.5.1   The most probable ionisation loss

A charged particle moving through matter loses energy by several different mechanisms, namely by collisions with the atomic electrons of the medium, by direct pair production, by bremsstrahlung, by Cerenkov radiation and by nuclear reactions.

In a thin absorber, such as the proportional counter, the higher energy loss such as direct pair production etc. cannot be measured because the electrons may have greater range than the thickness of the counter. It is not then the average ionisation loss that is measured by a thin absorber, but the most probable ionisation loss, which is caused by the more frequent low energy transfer collisions of the charged particle with the atomic electrons.

Symon (1948) has worked out a complete solution to the most probable ionisation loss, and his results are summarised by Rossi (1952). The most probable energy loss, Ep, is given by:

$$E_p = \frac{2Cm_e c^2 x}{\beta^2} \left(\ell n \left\{ \frac{4Cm_e^2 c^4 x}{(1-\beta^2) I^2(Z)} \right\} - \beta^2 + j \right)$$

where

$$C = 0.15 \frac{Z}{A} \ gm^{-1} cm^2$$

$I^2(Z)$ - average ionisation potential 13.5Z(eV)

x - the thickness of the aborber, gm cm^{-2}

and j - a special function given graphically by

Rossi in terms where

$$G = \frac{2Cm_e c^2 x}{\beta^2 \ E'_m} \ , \quad E'_m \quad \text{the maximum transferable energy.}$$

At the energies and thickness dealt with here j can be taken as a constant 0.33, for the whole range of γ.

For the proportional counter, for a track of 14 cm through argon-methane mixture at one atmosphere, the most probable ionisation loss will then be given by:

$$E_p = \frac{1.71}{\beta^2} \left(ln \left\{ \frac{2.98.10^4}{(1-\beta^2)} \right\} - \beta^2 + 0.33 \right) KeV$$

A plot of this function of the most probable energy loss against the Lorrentz factor, γ, is given in Figure 2.5.

This function has been evaluated under the assumption that the atoms of the medium are isolated. However, one cannot assume this when the impact parameter is larger than the atomic distances. For such distant collisions screening of the electric field on the passing particle will reduce the interaction. Since distant collisions become more important as the velocity increases, the correction to be applied to the expression for the energy loss is an increasing function of velocity.

According to Fermi (1939) the quantity Δ, to be subtracted from the

most probable energy loss is:

$$\Delta = \frac{2Cm_e c^2}{\beta^2} \, \ell n \, \epsilon \qquad \text{for } \beta < \frac{1}{\sqrt{\epsilon}}$$

and
$$\Delta = \frac{2Cm_e c^2}{\beta^2} \left(\ell n \frac{\epsilon - 1}{1 - \beta^2} + \frac{1 - \epsilon\beta^2}{\epsilon - 1} \right) \text{ for } \beta > \frac{1}{\sqrt{\epsilon}}$$

where $\epsilon = 1 + \dfrac{ne^2}{\pi m_e \nu_o^2}$ with $I(Z) = h \nu_o$

and n the number of electrons per unit volume of average dispersion frequency ν_o.

In the present case $\epsilon - 1 = 1.07.10^{-5}$

$\therefore$ for $\beta < \dfrac{1}{\sqrt{\epsilon}}$, $\Delta \to 0$ as $\ell n \simeq 0$

and for $\beta > \dfrac{1}{\sqrt{\epsilon}}$, $\Delta = 2 Cm_e c^2 [\ell n(\epsilon - 1) \cdot \gamma^2 - 1)$

This expression has been subtracted from Symon's curve and the result is shown in Figure 2.5.

More recent calculations on energy loss have been carried out by Sternheimer (1952, 53 and 56) and he has obtained a function:

$$E_p = \frac{At}{\beta^2} \left\{ B + 1.06 + 2 \ell n \left(\frac{p}{Mc} \right) + \ell n \left(\frac{At}{\beta^2} \right) - \beta^2 - \delta \right\}$$

where p is the momentum of the particle mass M

A,B,t are constants of the medium

and δ the density correction, has the form:

$$\delta = 2 \ell n \left(\frac{p}{Mc} \right) + C \qquad \text{for } \frac{p}{Mc} > 100$$

Most probable energy loss, T_p, (keV)

40

30

20

1   10   100   1,000
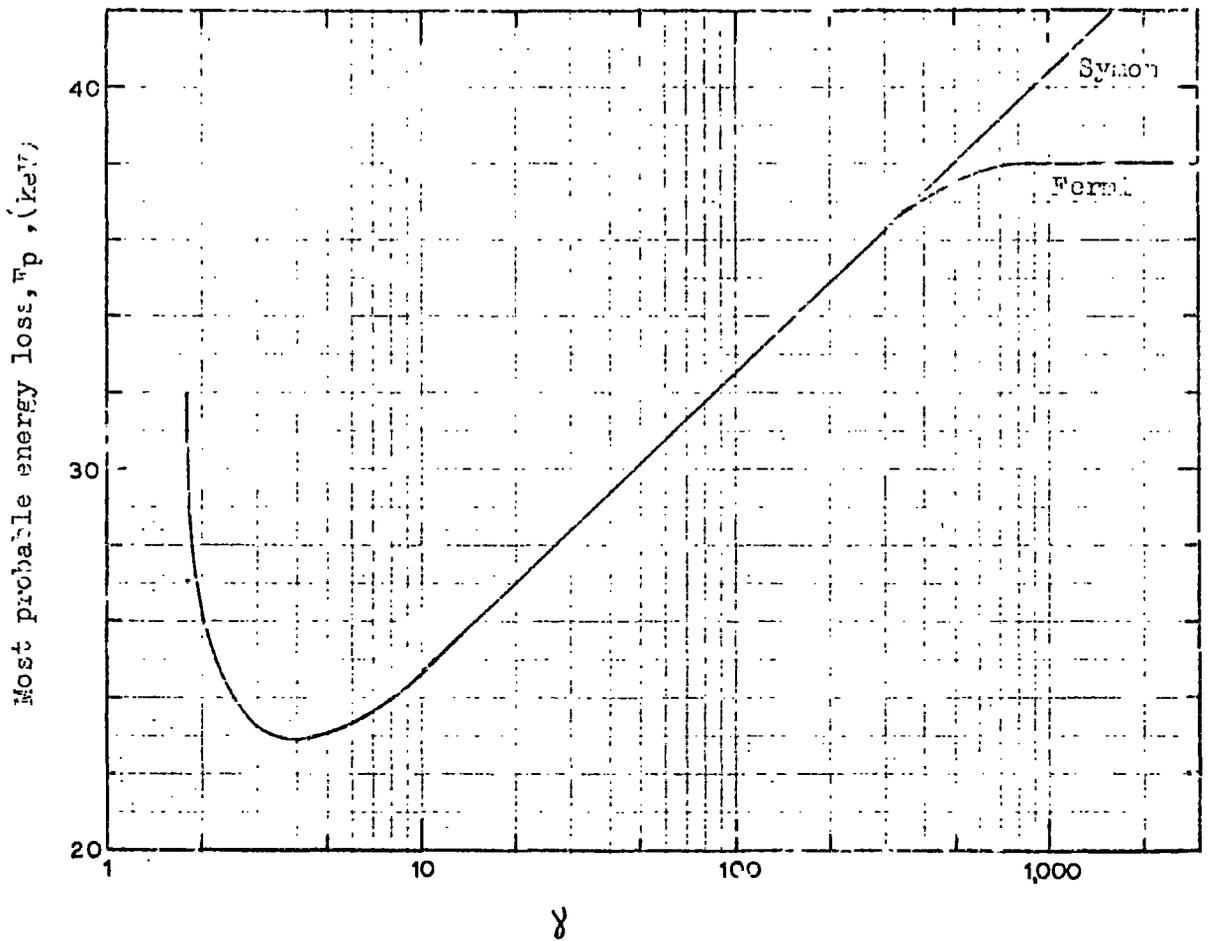
γ

Symon

Fermi

Figure 2.5   The most probable ionization loss as a function of
the Lorrentz factor, γ, for 14cm of proportion gas.
The Symon curve takes the density effect into
account.

for $0.1 < \frac{p}{Mc} < 100$ an extra term

$$0.514 \left\{ 2 - \log_{10} \left(\frac{p}{Mc} \right) \right\}^{2.595}$$

is included.

For the proportional counters one finds that Symon's and Sternheimer's expressions agree.

2.5.2 The distribution in ionisation

Particles of a given kind and incident energy do not lose the same amount of energy in traversing a given thickness of material, because the collisions which are responsible for the energy loss are independent. Symon (1948) has worked out a complete solution of the probability of energy loss for thick and thin absorbers. Rossi (1952) plots Symon's results for thin absorbers as:

$$\frac{\Delta_0 \omega}{F} \quad \text{against} \quad \frac{Ep-E}{\Delta_0}$$

where Ep and E are the most probable and the actual energy losses.

$$\Delta_0 = \frac{2Cm_e c^2 xb}{\beta^2}$$

and F is given in graphic form as a function of β and the maximum transferable energy, E'_m.

These distributions are plotted by Rossi for various values of the parameter λ, which is related to the assymetry of the distribution, and is also given graphically by Rossi.

For the energies dealt with here these parameters are all at their asymptotic value of b = 1.45, λ = 1.48, F = 0.6 and therefore Δ_0 = 2.49keV.

The distribution thus obtained is shown in Figure 2.6. Qualitatively, the peak of the distribution is due to the loss of excitation, and the long tail due to knock-on electrons. The tail should then fall off as E^{-1}, from Rutherford's formula, and this is the case when λ = 1.48.

However, recent work on very thin absorbers (Ramana Murthy 1968) has shown the distribution to be very much wider than expected. The theoretical distributions of Landau (1944), Symon (1948) and Vavilov (1957) will not apply to pions, muons etc. traversing this proportional counter, as the effects of the atomic binding of electrons have not been taken into account. Blunck and Leisegang (1950) and Blunck and Westphal (1951) have modified the Landau theory to include these effects, and they define a parameter, b^2, as:

$$b^2 = \frac{20\,\Delta z^{4/3}}{\left\{0.3\left(\frac{Z}{A}\right) x \left(\frac{m_e c^2}{\beta^2}\right)\right\}^2}$$

where Δ is the average energy loss in traversing the counter of x gcm^{-2} and the other terms have their usual meaning.

These authors plot the energy loss distribution as a function, $F_{\alpha R,b}(\lambda)$ against λ for various values of b, where λ is a linear function in energy loss, and:

$$\alpha R = 1.4 \cdot 10^{-3}\frac{Z}{A} x \left(\frac{4}{3}\ n(183\ z^{-\frac{1}{3}}) + \frac{1}{9}\right)$$

which in this case can be taken as zero.

For values of $b^2 \ll 3$ the distribution obtained is identical to the Landau, but when $b^2 \ll 3$ the width of the distribution is much wider. The functions $F_{\alpha R,b}(\lambda)$, for $R = 0.000$, and λ for $b^2 = 0$, 3 and 9 were normalised and plotted on the same axes as the Symon distribution (Figure 2.7). Comparing the distributions obtained with the Landau distribution (Figure 2.6) one can see that for $b^2 = 0$ the two distributions are identical, but at $b^2 = 9$, the Blunck distribution is twice as broad.

Substituting values for the experimental arrangement here, one finds that b^2 is given by

$$b^2 = 0.3175 \; \beta^4. \; \bar{\Delta} \; (keV)$$

2.6 The calibration arrangement

As described previously, the proportional counters were calibrated using a Geiger telescope. This telescope consisted of three trays of Geiger tubes, two positioned above the counter and one below, as shown in Figure 2.8. A coincidence from all three of these trays would necessitate a particle having traversed the proportional counter gas.

However, the uncertainty in track length in the counter gas would impose an extra width on the distribution obtained. Some estimate should therefore be made of the distribution in track length.

Consider a parallel plate counter with its plates also parallel to the Geiger telescope. The track length between the plates will be given by the angle to the vertical of the incident track.
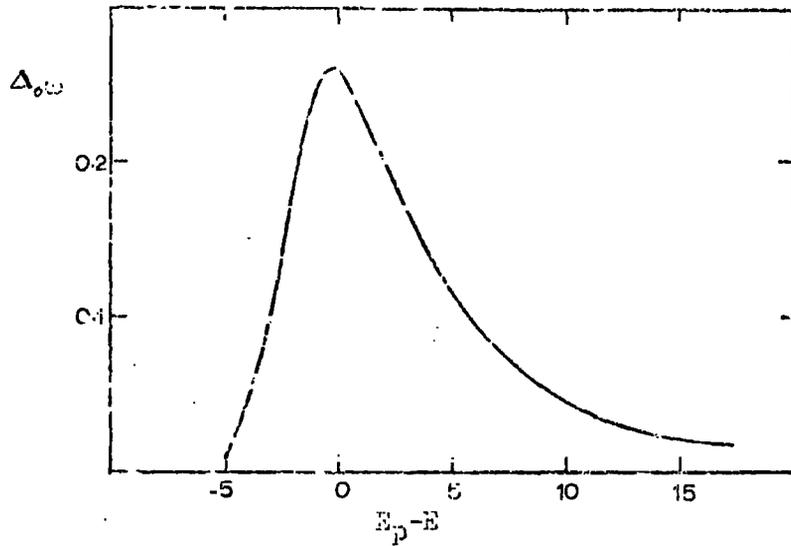
Figure 2.6   The Landau distribution in energy loss
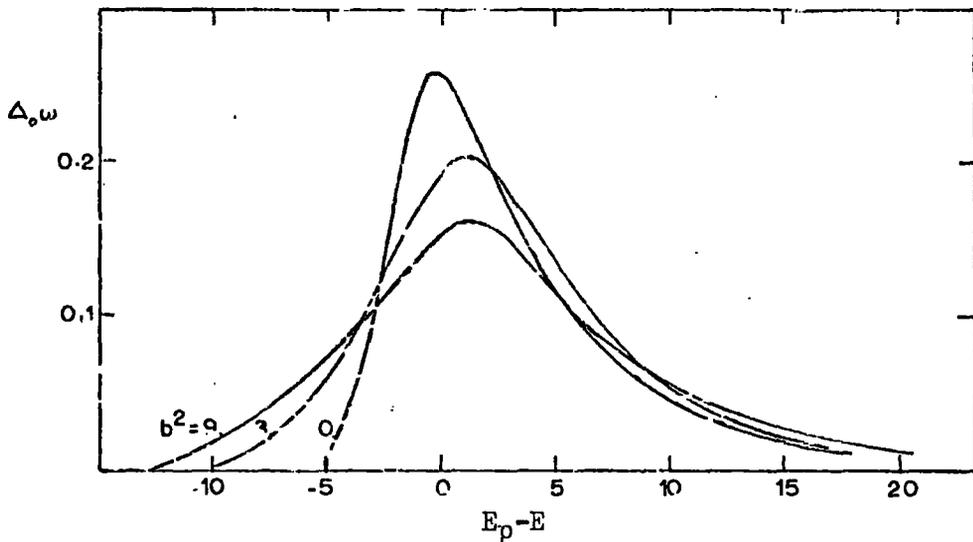calculated using the theory of Symon for
the proportional counter used.

Figure 2.7   The Blunck and Westphal distributions in
energy loss for various b^2, normalised to
compare with the Landau distribution.
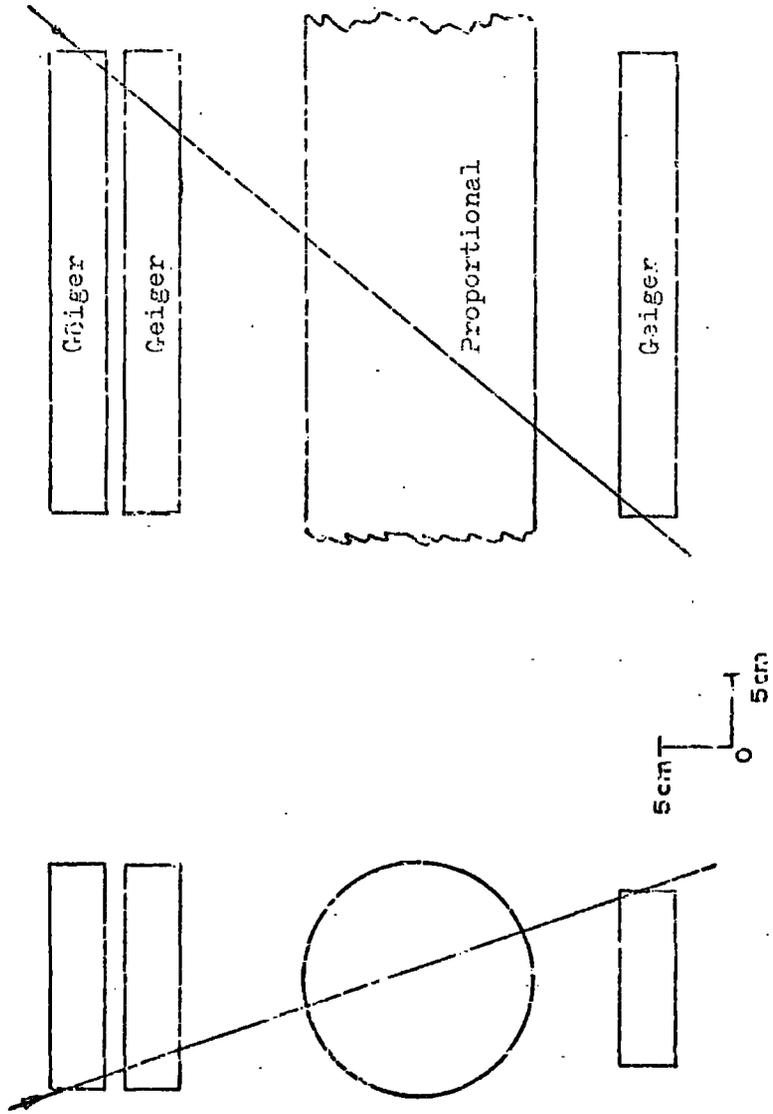The $b^2 = 0$ curve is identical to the Landau.

Figure 2.8 The Geiger counter calibration arrangement.

i.e. track length, $T_r = \dfrac{2b}{\cos\theta}$ where 2b is the distance between the plates (i.e. the diameter).

To obtain the track length distribution one therefore needs the distribution in intensity against zenith angle,θ . Now, for isotropic radiation the intensity at angle θ is proportional to the solid angle described by the apparatus at that angle. The distribution in track length can then be obtained from a plot of the solid angle per radian, described by the telescope against the zenith angle, θ. This can be obtained graphically and is explained with the aid of a diagram (Figure 2.9).

The area of the bottom of the Geiger telescope was divided into 16 equal areas, four of which are shown in the diagram. Considering one of the small areas, the solid angle per radian subtended between θ and $\theta +$ and $d\theta$ is given by

$$2\pi \sin\theta . \; \frac{\phi}{360}$$

This function was evaluated graphically at specific values of θ for all four of the areas, dA, and the values for the single angle at each θ were added to obtain the necessary result.

One can make some estimate of the effect of a cylindrical counter by considering only vertical radiation. When this is folded into track length distribution above, an approximate distribution for the track length in the cylindrical counter, using the Geiger telescope, is obtained (Figure 2.10).
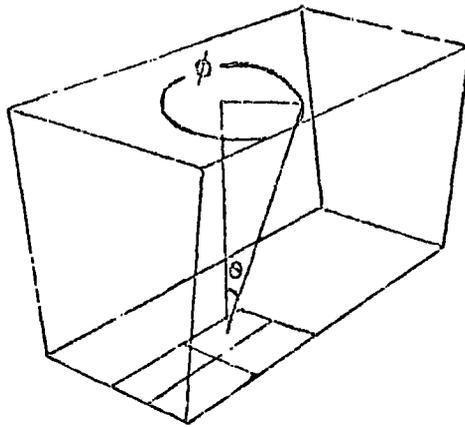
Figure 2.9   The method of calculation of track length for a
parallel plate counter. The two limits of the
volume are given by the upper and lower Geiger
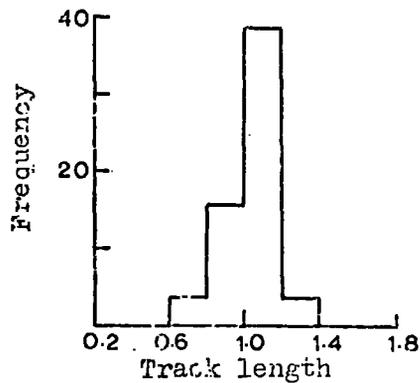trays.

Figure 2.10   The expected distribution in track length for
a cylindrical counter. Track length has been
normalised to 14cm=1.0.

The distributions in initial ionisation, for the calibration and the track length, have now been evaluated, so that, if the effects of straggling are considered negligible, one can calculate the total expected distribution in pulse height for this arrangement. Figure 2.11 compares this calculated distribution with that obtained experimentally from proportional counter P5, at an operating voltage of 3.0 kV.

2.7 Measurement of the capacitance of the counter

The proportional counter will have its own intrinsic capacitance, C_o. The introduction of the emitter follower and its input connections will affect the value of this capacitance, and as the counter is always operated with this as a unit, it is better to take C_o as the total capacitance of the system.

The value of this capacitance will affect the voltage pulse height obtained at the input of the emitter follower by the simple relation:

$V = \dfrac{Q}{C_o}$ where Q is the total charge collected by the wire and $Q = Mq$

where M is the gas gain

and   q the initial ionisation.

If one includes in the circuit an additional capactor, C, in parallel with the intrinsic capacitance (Figure 2.12a) then the voltage measured becomes

$$V = \frac{Q}{C + C_o}$$

Thus a plot of C against 1/V will give a straight line with intercept on the vertical axis equal to the intrinsic capacitance of the proportional
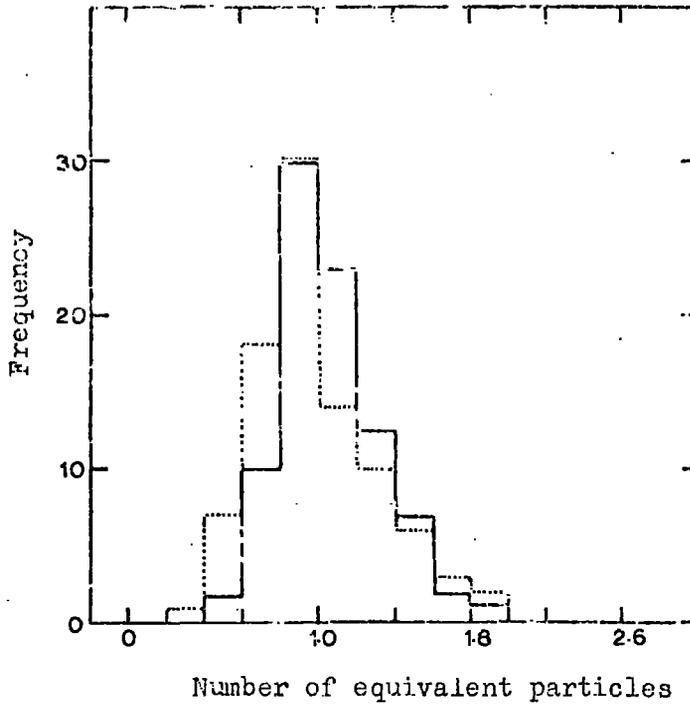
Figure 2.11   The expected single particle distribution calculated
from the Landau and track length distributions
compared with the dotted single particle peak from
proportional counter,5,at 3.0kV.

counter-emitter follower arrangement.

The medians of the pulse height distributions obtained for the Geiger telescope arrangement for selected values of the capacitance, C, were plotted as above (Figure 2.12b). Care was taken that the voltage applied to the counter was kept constant for all values of C. The value obtained for the capacitance of the counter arrangement was 61 ± 25 pF.

The expected ionisation loss in the proportional counter for particles selected by the telescope has been calculated below (Chapter 5, Section 2). This ionisation was found to be 28.9 keV. This energy is then converted into a number of ion pairs which will initiate the avalanches. Schmeider (1939) and Melton, Hurst and Burtner (1954) have obtained values for the energy required in argon to produce one ion pair. These values are 26.9 and 26.2 eV respectively, and one would therefore expect approximately 1200 ion pairs to be released. Using the value for the capacitance, the gas gain obtained at the voltage of the capacitance measurements is then given by:

$$M = \frac{C_o V}{q}$$ where V is the median pulse height obtained when no parallel capacitance is used.

then M   (318 ± 130)v where v is measured in millivolts.

A plot of the gas gain- voltage curve is shown in Figure 2.13 and, as can be seen, the proportional counters will operate at gains of approximately 10^5 without any instability setting in.
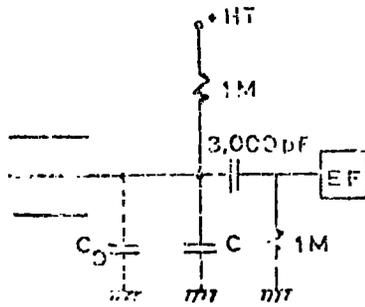
Figure 2.12a   The measurement of the capacitance, C_O, of the
proportional counter, emitter follower arrangement.
At constant voltage supply, the median single
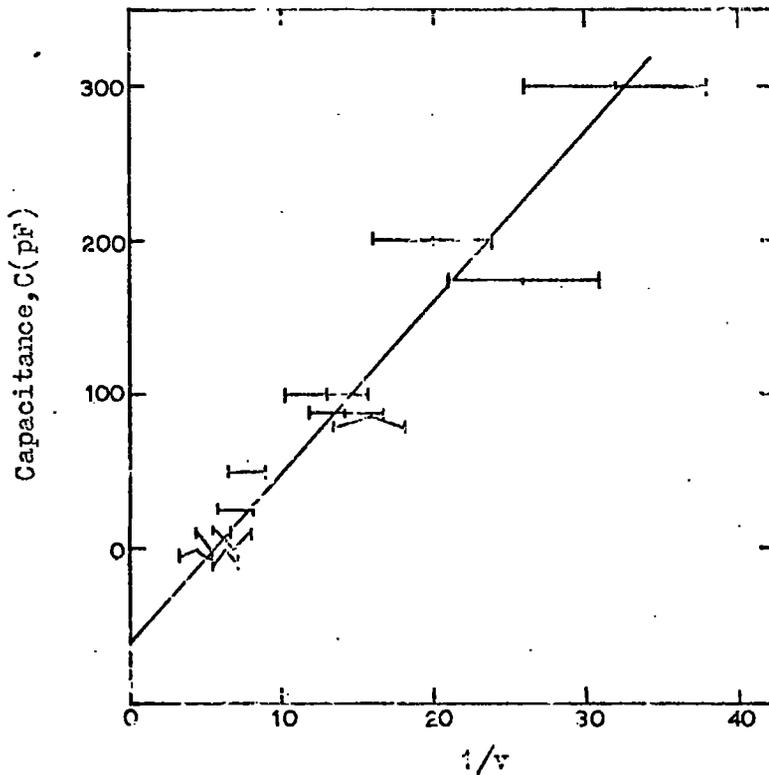pulse height, v, is given by:-

$$C + C_O = \frac{Q}{v}$$

Figure 2.12b   Reciprocal of the median pulse height, in
millivolts, obtained for values of the
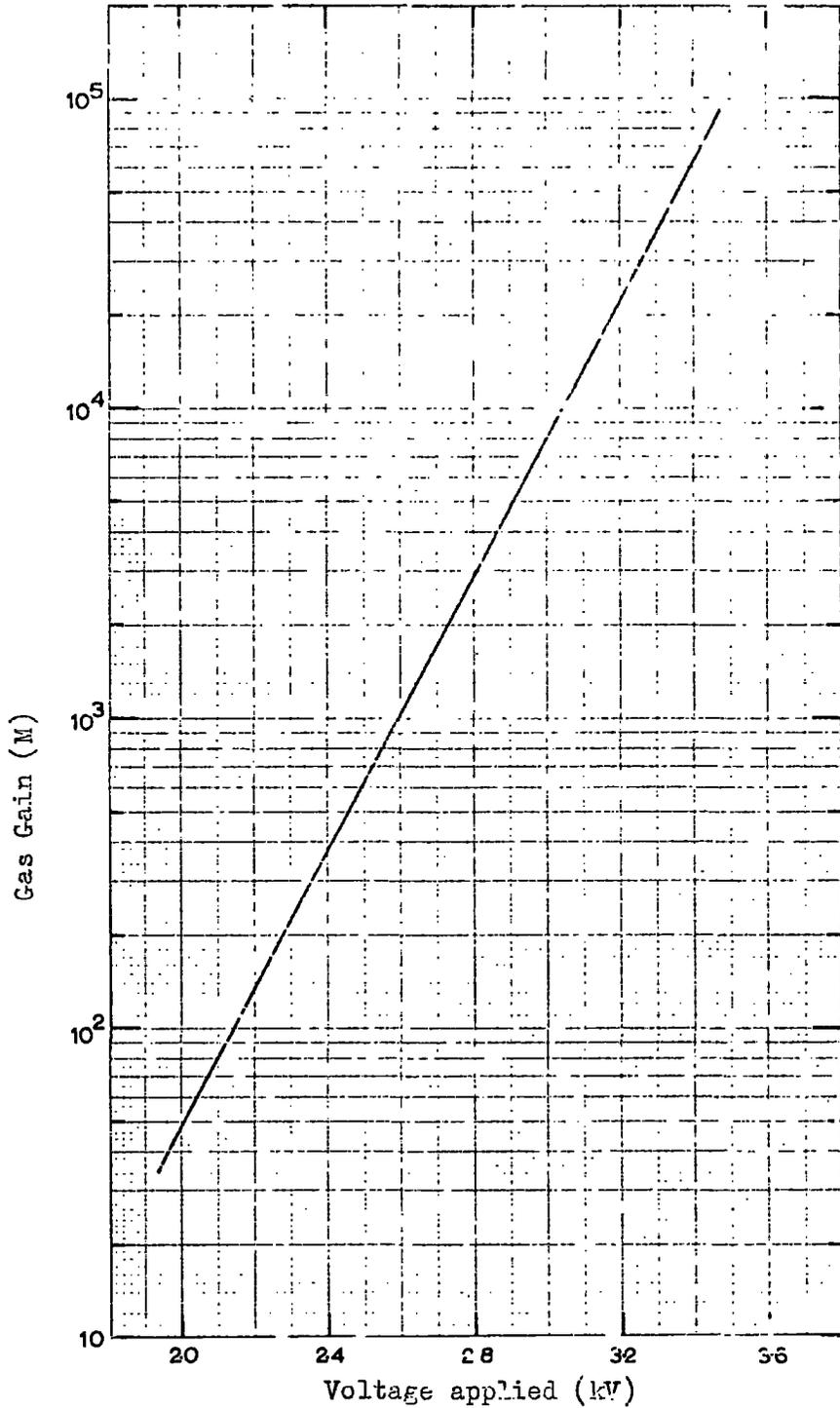capacitance, C, inserted in the circuit.

Figure 2.13 The gas gain-voltage characteristic for proportional
counter, P5.

CHAPTER 3

AN EXTENSIVE AIR SHOWER EXPERIMENT TO INVESTIGATE THE LINEARITY
OF THE PROPORTIONAL COUNTERS AT LARGE PULSE HEIGHTS

3.1 Introduction

In order to use the proportional counters confidently, it is
necessary to know their range of proportionality. The density spectrum
of extensive air showers has been measured accurately, (Galbraith 1958 ,
and Cocconi 1961) and this information was used to test the proportional
counters.

3.2 Description of the experimental arrangement

The experiment consisted of eight of the large cylindrical propor-
tional counters laid out horizontally and in close contact. The area
of the detector was then 3.5 m^2, and the mean density of particles in
this area was measured. Two experimental runs were carried out with
different selection systems, and it was only in the second run that air
showers were detected.

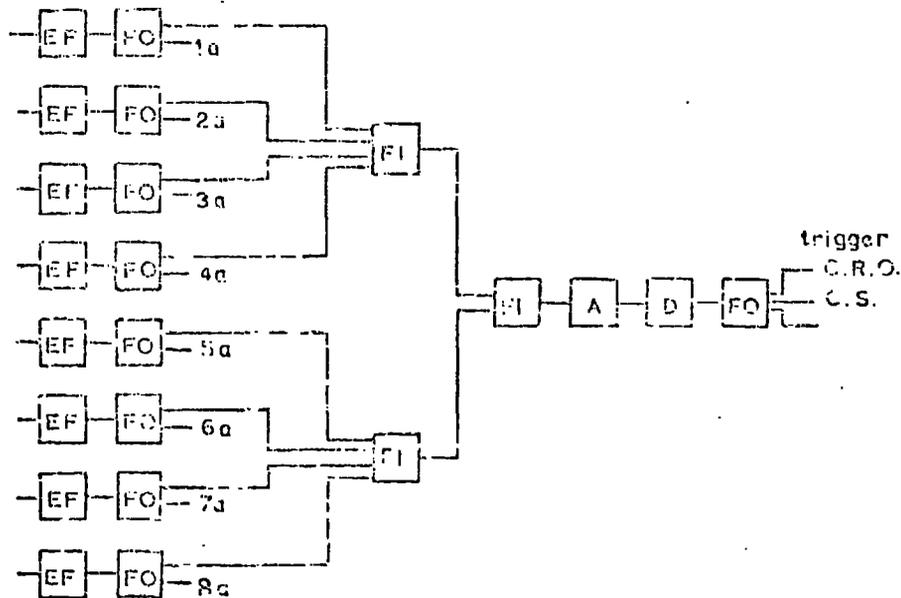3.3 The single pulse experiment

3.3.1 The selection system

A block diagram of the selection system is shown in Figure 3.1. The
pulses from each proportional counter were taken through an emitter
follower to a fan-out, where they were split, one channel going to the
display system and the other to the selection system. The pulses in the
selection channels for each proportional counter were then brought

together via two fan-ins to an amplifier and a discriminator. In this way one could select, in any of the eight proportional counters, on one pulse, of value greater than that set by the discriminator. The output from the discriminator was split in a fan-out into two channels, one to trigger the oscilloscope to record the pulses, and the other to trigger the cycling system. The cycling system would then rotate and, by micro-switches, would wind on the camera, which viewed the CRO, whilst paralysing the electronics and accepting no more triggers until the end of the cycle.

3.3.2   The display system

The display system is shown in Figure 3.2. It consisted of a set of eight 6µs delay lines linked together, and terminated with the characteristic impedance (1650Ω) only at the two ends. The pulses from the proportional counters were introduced into the delay line via variable amplifiers at 6µs intervals. Diodes were placed at each input to cut down multiple reflections from these inputs. The output pulses, each separated by 6µs were taken out through an amplifier to the CRO, where they formed a 48µs long trace. The variable amplifiers at each input were adjusted to give equal output pulse heights at the CRO, for equal inputs.

Photographs of the type of pulses observed with this system, for a single pulse and for eight pulses, are shown in Plates 3.1 and 3.2. respectively. It can be seen in Plate 2 that the eight pulses, when large, are not well separated, and care had to be taken when measuring the pulse heights to take this into account.

Key: E.F.   emitter follower   A   amplifier
      F.O.   fan out   D   discriminator
      F.I.   fan in   C.S. cycling system

Figure 3.1   The selection system used for the single pulse
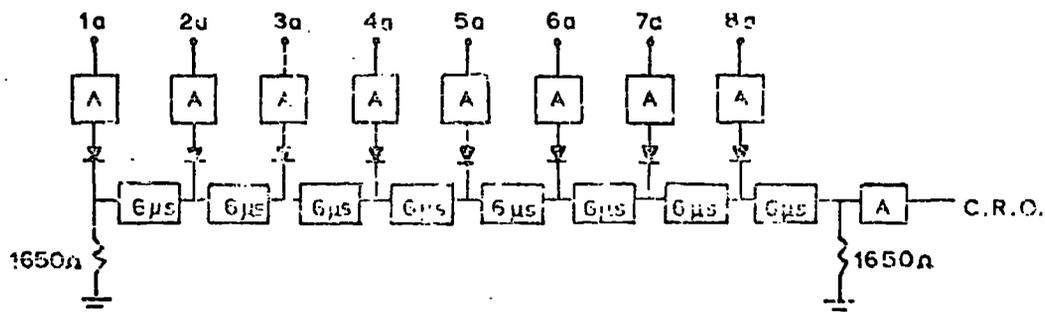   experiment.

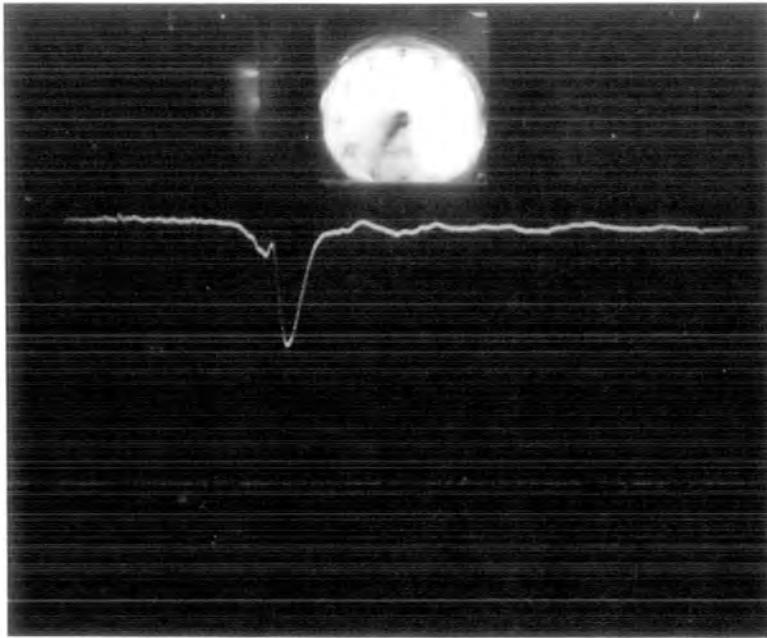Figure 3.2   The display system used for the proportional
             counters.

Plate 3.1   An example of a single pulse obtained
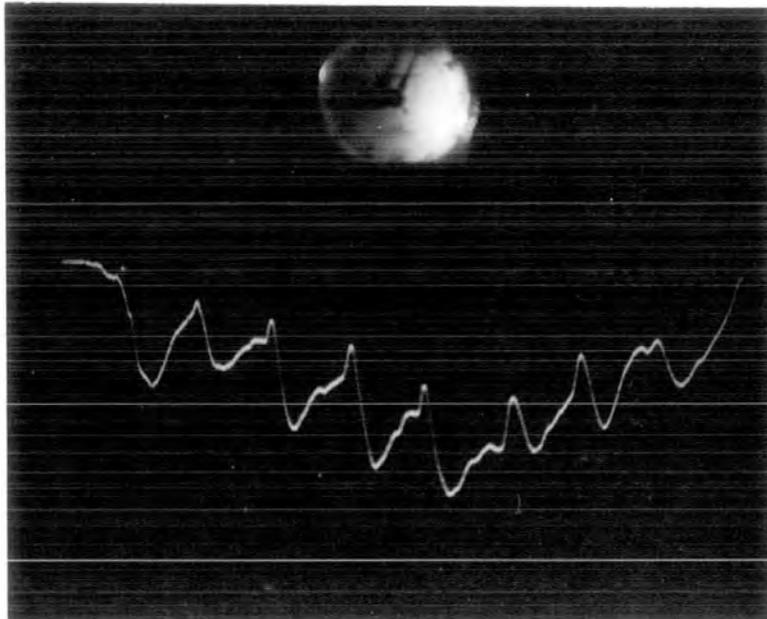using the display system described.

Plate 3.2   An example of eight coincident pulses
obtained using the display system.

3.3.3 Results

The integral density spectrum obtained with this selection is shown in Figure 3.3. Very few air showers were detected, for densities less than 400 particles per counter. Large single pulses predominated the triggers.

Some attempt has been made to explain the width of this single particle distribution, and the positions where the various effects become important, are shown in Figure 3.3. The total rate expected has been calculated from the area to be, approximately, $6 \ 10^3 min^{-1}$. It can thus be seen that there is a certain amount of noise in the system. All the other effects have been calculated from this rate, and therefore all the positions shown in Figure 3.3 are dependent on it.

The first effect that could broaden this distribution is the production of electron-photon cascades in the walls of the counter. The critical energy, ϵ_c, is 84 MeV in air and 49 MeV in aluminium, and, therefore one could expect some shower formation. As the electron to muon ratio in cosmic rays at sea level is 1 to 4 (Fazzini et al., 1968), one would expect to see the effect of multiplicity on the integral density spectrum at the following rate:-

$$1.5. \ 10^3 min^{-1} \text{ per counter}$$

Knock-on electrons from the wall would also broaden this spectrum. The probability of producing a knock-on electron of energy ($> E'$), where $E' \ll E'_m$ is the maximum transferable energy, is given by the integral of Rutherford's formula:-
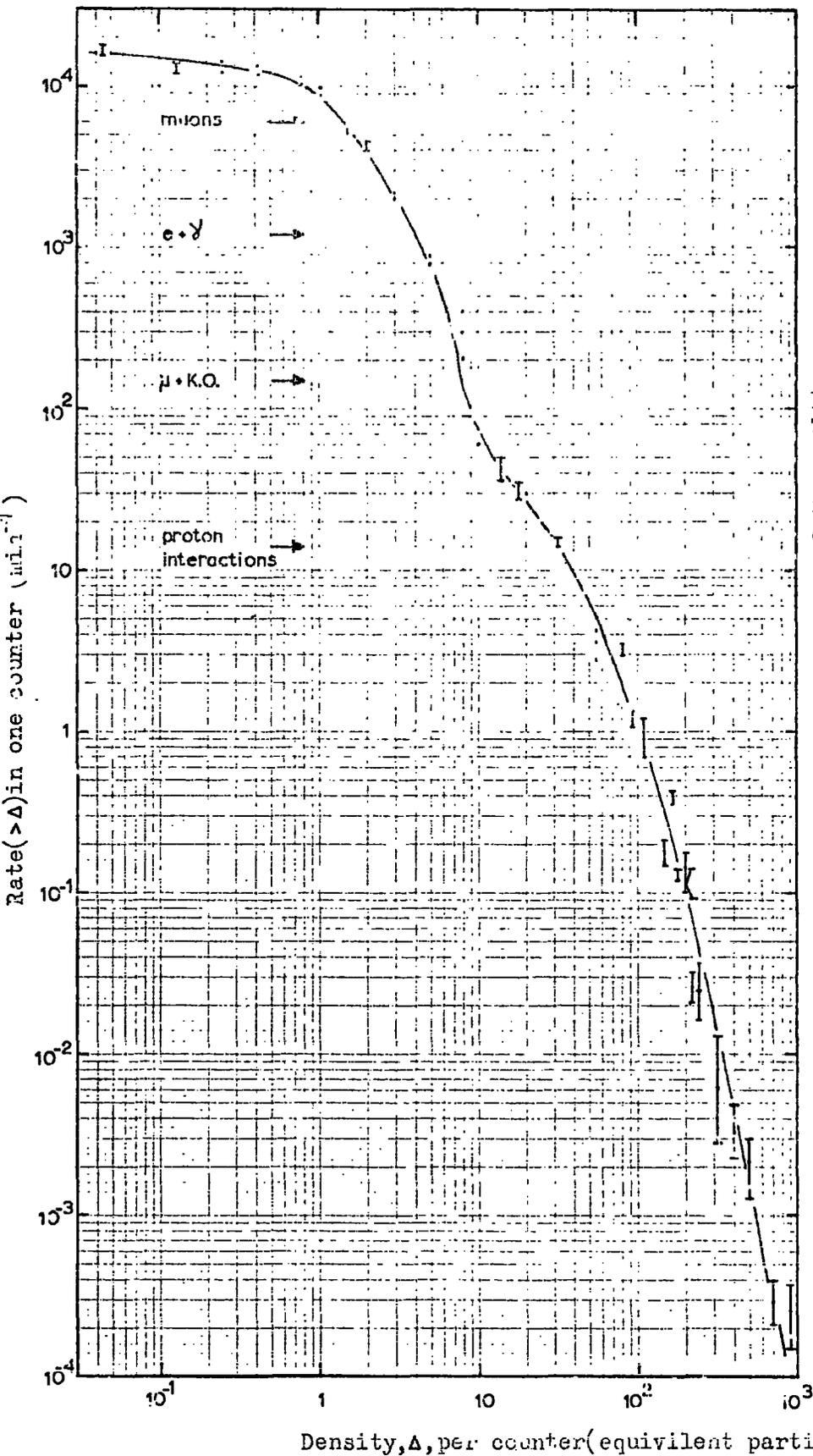
Figure 3.3
The integral density
spectrum obtained by
selecting pulses (>Δ)
in one proportional
counter.

Rate(>Δ)in one counter (μin.1⁻¹) (y-axis label)

Density,Δ,per counter(equivilent particles) (x-axis label)

muons

e+γ

μ+K.O.

proton
interactions

$$\phi(> E') = \frac{2Cm_e c^2}{\beta^2} \; z^2 \int_{E'_o}^{\infty} \frac{1}{(E')^2} \; dE'$$

where $C = 0.15 \frac{Z}{A}$

β is the velocity of the incident particle

E'_o is the minimum energy of the knock-on electron.

Here, taking the simplest case of a knock-on occurring at the centre of the aluminium wall, E'_o is the energy required to traverse half the thickness of the wall, to reach the counter gas. This energy will then be given by the Feather rule, as stated by Burcham (1963),

$$E = \frac{R_e + 0.16}{0.54}$$
where R_e is the range of an electron in Al

E is the energy in MeV

and is 2.06 MeV.

Evaluating the expression, the probability of producing a knock-on electron which will penetrate to the counter gas, is 2.6% and hence the expected rate of knock-on events will be $1.5 \; 10^2 \text{min}^{-1}$ per counter.

Proton interactions will also broaden this distribution, but as the μ to p ratio is 1 to 100 the rate will be greatly reduced. The probability of interaction can be found by using the geometric interaction length in aluminium, $L_g = 87$ gm cm^{-2}. Taking the thickness of the counter wall, x, the number of particles, N, that will interact for N_o incident particles is given by:-

$$N = N_o \left(\exp \left\{ \frac{-x}{L_g} \right\} - 1 \right)$$

Substituting the values for x and L_g, one obtains a value of 2.4% interactions. The rate of proton interactions will then be 1.4 min^{-1} per counter.

Another possible effect, which has been observed in cloud chambers, is the emission of radioactive α particles from the walls of the counter. For example, a 1 MeV α particle will deposit all its energy into ionisation of the gas, and will produce 5 10^4 ion pairs. On the other hand, a muon of energy, 2 GeV, will deposit only 27 keV in the gas to produce 10^3 ion pairs. This α particle will therefore produce a pulse of size 50 equivalent particles.

As the integral density spectrum of air showers has an exponent of $\gamma \simeq$ 1.4, the air shower spectrum is not reached, using this selection, until at least > 1,000 particles per counter have been selected.

3.4 The coincidence experiment

3.4.1 The selection system

To select air showers with these proportional counters, it was found necessary to take two physically separated counters in coincidence. Figure 3.4 shows the selection system used. Coincident pulses from proportional counters P1 and P2, of a level set by the two discriminators, were used to trigger the oscilloscope and the cycling system. The pulses were displayed using the same system as above and the density of particles measured was the mean density obtained in the eight proportional counters.

3.4.2 Results

Figure 3.5 shows the integral density spectrum obtained from this
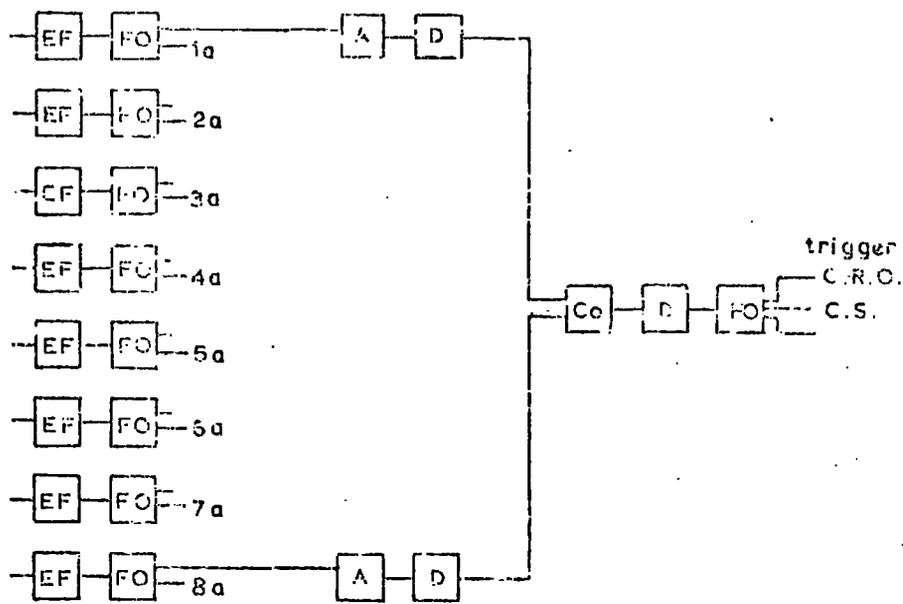
Co   coincidence unit

Figure 3.4   The selection system for the coincidence
experiment.

arrangement, compared with the spectrum quoted by Galbraith (1958). This spectrum was obtained from work done by Singer (1951) for densities in the region 15 to 1,000 particles m^{-2}. The measured exponent was 1.4 ± 0.2 compared with 1.4 as stated by Galbraith. It can be seen that the rate observed at each density is less than the rate expected, but this is within experimental errors and, probably, a factor of normalisation.

3.5 Summary

The proportional counters were used to look at the single particle distribution from one counter, and to look at the air shower density spectrum. The two results obtained are compared in Figure 3.6.

The single particle distribution was found to be very broad, mainly because of the interaction of the aluminium walls with the incident cosmic rays. It can be seen (Figure 3.6) that only at densities greater than 1,000 particles can one select air showers using a single proportional counter of this type.

The air shower density spectrum obtained from the coincidence run agreed, within its large errors, with the measured spectrum of other workers. There was no evidence of any non-linearity in response, for the high ionisations occurring, and one can conclude that the proportional counters are a useful, reliable method of measuring the ionisation caused by cosmic rays.
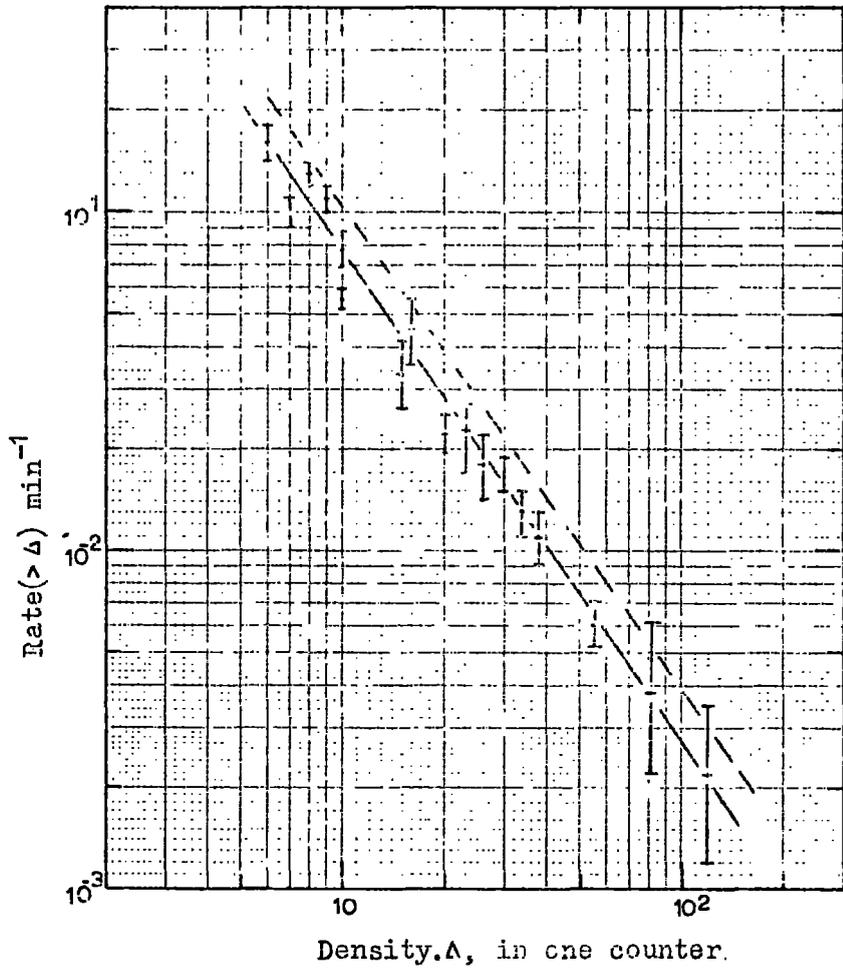
Figure 3.5 The integral density spectrum of coincident pulses in the outermost proportional counters, P_1 and P_8, compared with the dotted spectrum quoted by Galbraith.
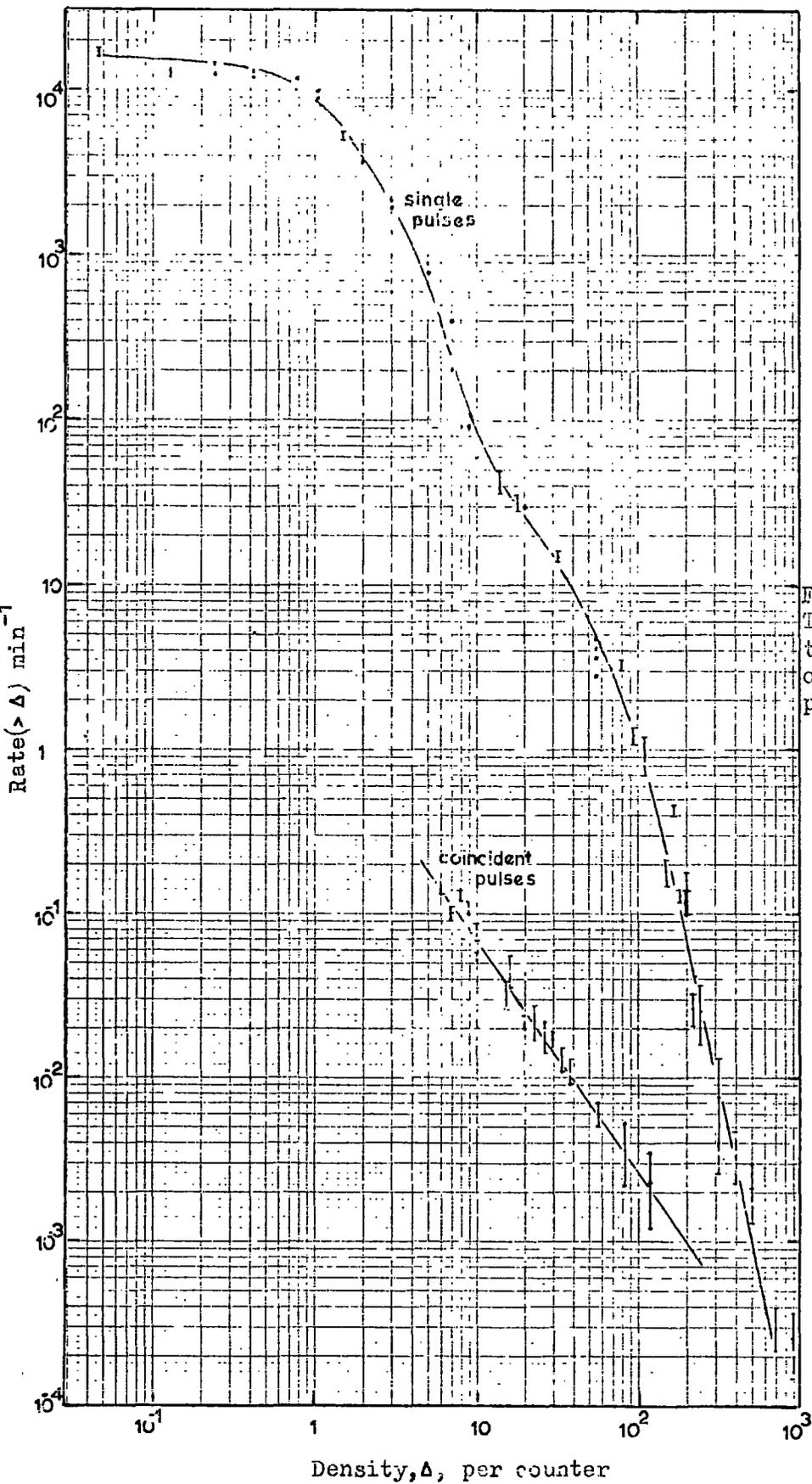
Figure 3.6
The comparison of the two density spectra obtained from the proportional counters.

CHAPTER 4

A SEARCH FOR INTERACTING PARTICLES OF CHARGE 2e/3, 4e/3,
5e/3 IN COSMIC RAYS

4.1 Introduction

The object of this experiment was to measure, using proportional

counters, the ionisation of particles which undergo an interaction, in an

iron absorber, of energy exchange greater than 30 GeV.

A scale diagram of the apparatus used is shown in Figure 4.1. It

consists of a layer of large proportional counters, 22.9 cm of iron

absorber, and a liquid scintillator. Flash tube trays A,B,C,D,E,F and G

were included to provide visual information of the interaction.

A hadrionic particle incident on this apparatus will produce an

interaction in the absorber with a probability which depends on its

interaction length; for nucleons (λ = 129 gm cm^{-2}) the probability of

interaction is 0.74. In this interaction pions will be produced, the

neutral pions will decay into two gamma rays to produce an electron-photon

shower, and the charged pions will go on to interact further, producing

more charged and neutral pions. This burst of pions, electrons and

photons will be detected in the scintillation counter. The passage of

the particle will also be detected by the proportional counters, and the

ionisation produced, as it is dependent on the γ and the charge of the

particle, can be used to give a measure of its charge.

4.2 The proportional counters

The proportional counters used were the same as those described

Side view   Front view
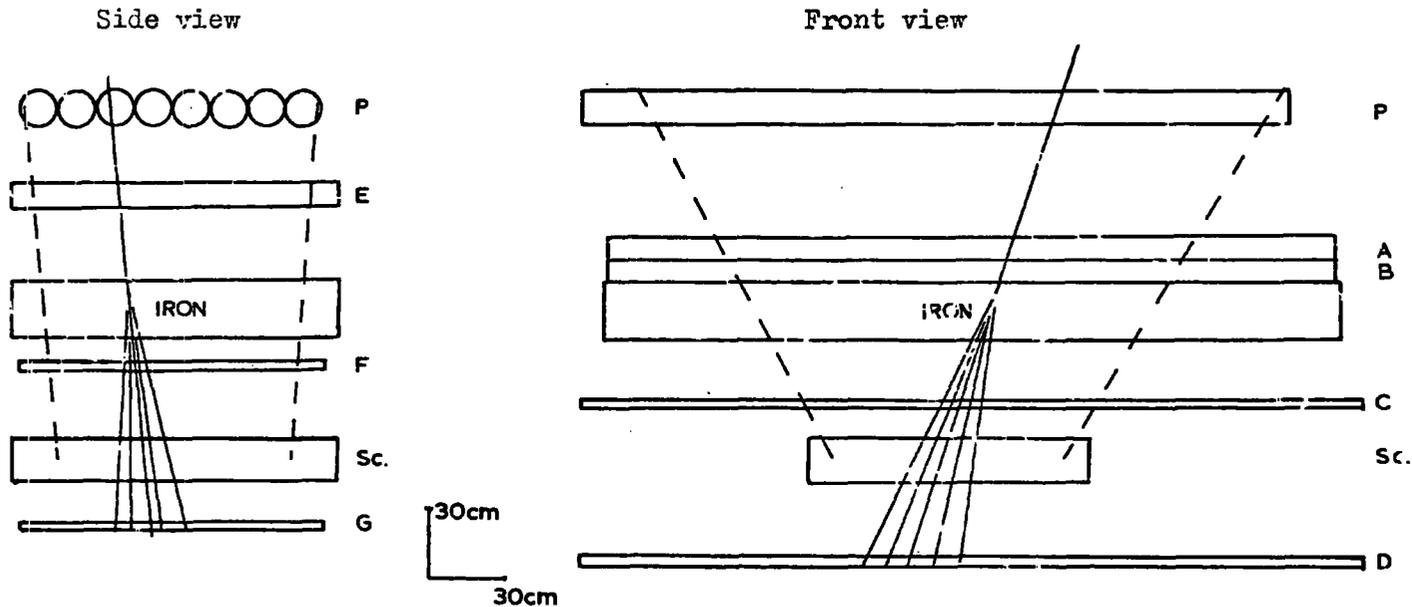
Figure 4.1   The burst experiment apparatus.
              1 layer of 8 cylindrical proportional counters,P.
              4 flash tube trays in the front view,A-D.
              3 flash tube trays in the side view,E-G.
              1 large scintillation counter,Sc.
              The dotted line shows the sensitive volume.

previously, consisting of an aluminium alloy cylinder ~ 15 cm in diameter, and 3 m long with a 3.10^{-3} inch tungsten wire down the centre and filled with a 90% argon, 10% methane mixture of gas to atmospheric pressure.

The counters were calibrated individually with cosmic ray electrons and muons of known mean ionisation using a geiger telescope. For convenience the median pulse height of the distribution obtained in this arrangement was taken as one equivalent particle. The pulse height-voltage curve for each counter was thus obtained and the counters were matched by adjusting the voltage to give the same median voltage pulse for the calibration telescope.

The counters were recalibrated regularly during the experimental run by two alternative methods. A very approximate but very quick check was to compare the rate of pulses greater than a specific voltage, with the rate in each counter, and the previous rates obtained. This test was carried out at regular intervals to guard against gas contamination in the counter. At less frequent intervals the output from the counter was fed directly into a pulse height analyser so that a distribution of incident particles of all possible energies, angles, and positions in the proportional counter was obtained. This distribution would not generally form a peak, but a plateau in the falling rate, due to electronic noise, etc., and this had to be accounted for to give the value of pulse height required.

4.3 The scintillation counter

The scintillator used consisted of a perspex box, of dimensions

130 x 90 x 17.8 cm filled with medicinal paraffin plus 0.5 gms per litre
p-terphenyl and 0.005 gm per litre of POPOP. This was enclosed in a
light-tight wooden box and was viewed by two five inch photo-multipliers.
These were mounted at each end of the box with a system of mirrors in the
space between the phosphor and the photomultipliers acting as a light
guide. The E.H.T. supply to the photomultipliers was of positive polarity
and the output was taken from the anode to give a negative pulse with a
delay time of 1 microsecond.

The response, that is the variation in pulse height with distance
from the source of ionisation to the photomultiplier, for scintillators
of this type has been investigated by Ashton et al (1965). The response
curves obtained showed an 18% difference between an ionising particle
passing vertically through the centre of the phosphor and one passing
near one end.

To avoid any broadening of the single particle distribution from
the counter, care had to be taken that the gains of the two photomulti-
pliers were matched. Initially this had been done by testing each
photomultiplier in turn in a light-flasher box. This consists of a light-
tight box, inside which light pulses are produced by the arc-discharge of
a mercury wetted relay (Kerns et al., 1959). The variation in pulse
height and supply voltage could be measured and hence the E.H.T. values
for the same gain in each photomultiplier could be found. The matching
of the photomultipliers could be checked 'in situ' by looking at the
pulse height in each counter produced by a single relativistic muon
passing through the centre of the counter. The muons were selected

using a small scintillator telescope positioned centrally above and below the large scintillator. The pulse height for each photomultiplier was displayed on an oscilloscope and photographed. By comparing the two distributions of pulse height obtained one could verify that the photomultipliers were matched.

In a previous experiment using this type of scintillation counter, Coats (1967) checked the linearity of response of the photomultipliers to different light intensities. Using the light-flasher box with the photomultiplier set at its operating voltage he introduced an optical wedge to vary the intensity in the range of 250:1. The results showed that the pulse heights obtained were proportional to the number of incident photons for a range well encompassing the range required for this experiment.

The scintillator was regularly recalibrated during the experiment using the scintillator telescope as above. The pulse height distributions obtained (Figure 4.2) gave a mean pulse height in the region of 1 mV with a full width at half height of approximately 80%. This mean pulse height was defined as one equivalent particle, that is, the mean pulse height produced by single relativistic muons passing vertically through the centre of the scintillator. The size of a burst detected in the scintillator was then expressed as equivalent particles, the ratio of the burst pulse height and the calibration pulse height.

4.4   Flash tube trays

The position of the seven trays of flash tubes used in this experiment
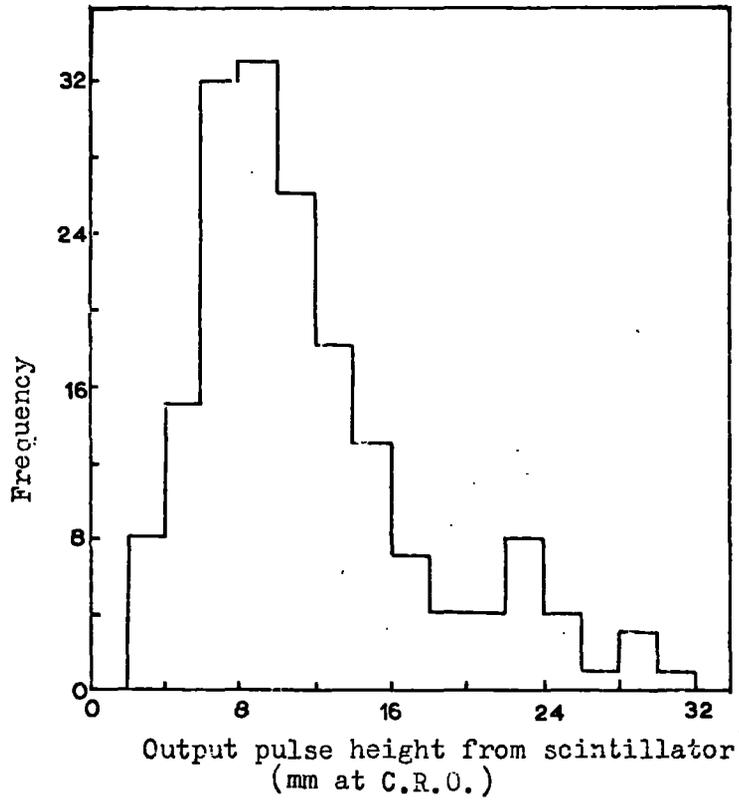
Figure 4.2 A typical single particle distribution obtained
            from the scintillation counter using a small
            scintillator telescope.

is shown in Figure 4.1. As can be seen trays A,B,C,D and trays E, F, and G were placed orthogonally to provide visual information, of a particle track, in three dimensions. Each tray basically consisted of an earthed electrode separated by two layers of flash tubes from an insulated electrode, to which a high voltage pulse is applied. Trays A and B were made up of two earthed electrodes, one on either side of the high voltage electrode giving four layers of flash tubes each. Trays C,D,F and G were of the simple configuration of two electrodes for two layers of flash tubes, and tray E had six layers of flash tubes with four electrodes alternately earthed and insulated.

The 3.6 kV/cm high voltage pulse required to trigger the flash tubes was generated using a thyristor to trigger four air spark gaps which discharged a bank of condensers. This pulse was applied to the insulated electrodes 60 μsecs. after an event was selected by the logic circuitry, and the flashes obtained were recorded photographically on Ilford Mark V film by two cameras.

The 60 μsec delay before applying the high voltage pulse was necessitated by the proportional pulse display system and this meant that the efficiency of the flash tubes suffered slightly. The layer efficiency of each tray could be measured by selecting, with a small telescope, single particles traversing the stack. The tracks were recorded and the layer efficiency was converted to internal efficiency by correcting for glass thickness and for gaps between the tubes. The average efficiencies for each tray are as follows:-

A = 81%, B = 81%, E = 82%, C = 77%, D = 75%, F = 70%, G = 71%

An event is taken as a track in A and B in line with groups of flashes in C and D, and a track in E in line with groups of flashes in F and G. For analysis purposes a track in A and B or E is defined as being ≥ 3 flashes in a straight line. Because of the low efficiencies of the flash tubes this definition would mean that, perhaps, a small percentage of true singles producing a burst might be rejected. On rare occasions this rule was waived in the analysis for tray E where, for example, there were two flashes in line with the burst and the correct proportional counter showed a pulse.

4.5 The electronic and display system

4.5.1 The electronics

A block diagram of the logic system for the experiment is shown in Figure 4.3. A preliminary run was carried out using only the scintillator pulse in the selection system. However, it was found that at the discrimination level required (burst sizes > 30 equivalent particles) this produced a large percentage of spurious triggers, and events which missed the proportional counters, especially in the side view. It was decided that the experiment should be run with a coincidence between the proportional counters and the scintillator to reduce this rate of unwanted events. In order to include possible particles of $\frac{2}{3}$ charge, the discrimination level for the proportional counters had to be kept below the level of approximately half the single particle peak. For this reason the level for the proportional counters was set at 0.2 equivalent particles from any proportional counter. This did cut down the rate of
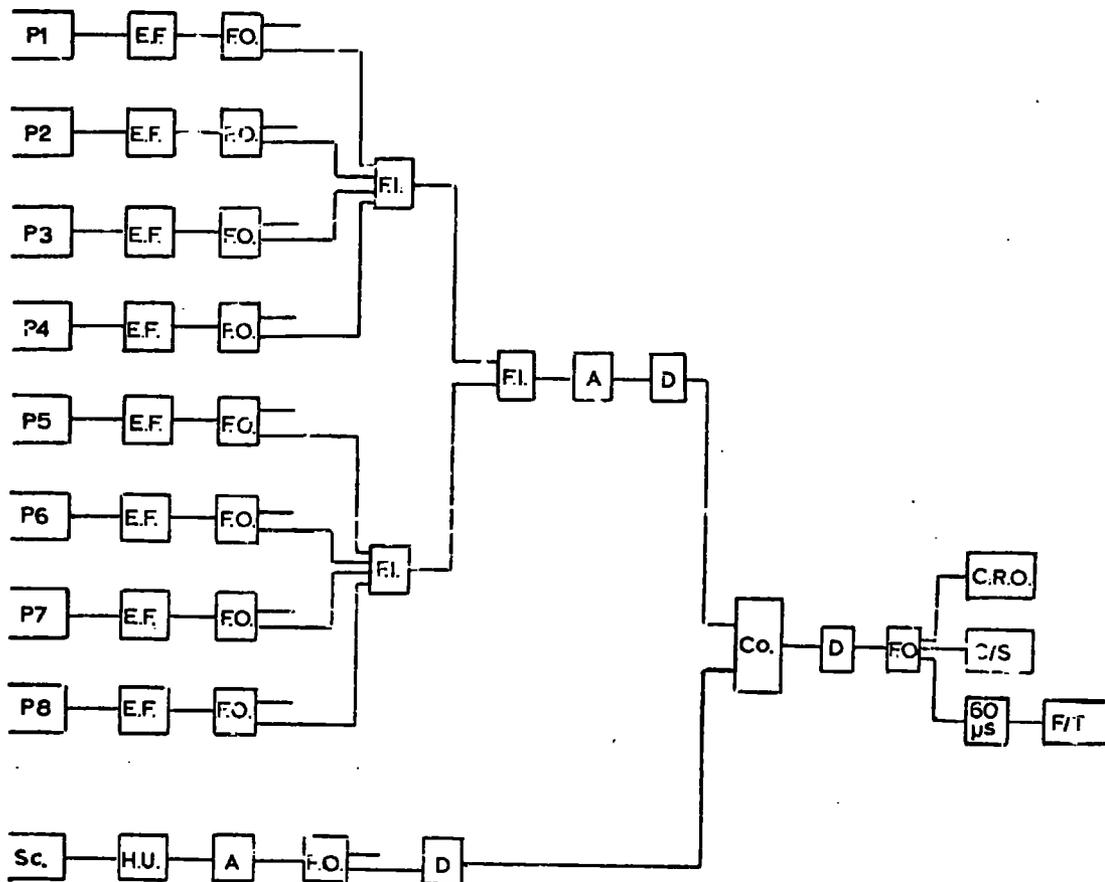
Key: P   proportional counter.   F.O.   fan out.
     Sc scintillation counter.   F.I.   fan in.
     E.F. emitter follower   D   discriminator.
     H.U. head unit.   Co.   coincidence.
                     C/S cycling system trigger.
                     F/T flash tube pulsing unit.
                     CRO oscilloscope trigger.

Figure 4.3   A block diagram of the electronics used in the burst
             experiment.

spurious events, as the expected rate of spurious coincidences at these settings would be

$$2n, \, n_2 \, \tau \; = \; 1 \text{ in 16 minutes}$$

but air showers and multiple events would still trigger the apparatus. An anticoincidence arrangement between each proportional counter would have stopped the air shower triggers but it would also mean that multiple events, which might be of interest, would not be recorded.

The pulses from each proportional counter were fed through 21 cm of coaxial cable to an emitter follower. From here they were led through equal lengths of cable to the electronic rack and through a fan-out unit which reproduced an identical pulse on two output channels. One of these channels was used for display and the other for selection. The pulses in the selection channel were then mixed, taking two groups of four proportional counters each, in two four-channel fan-ins and the outputs of these two were mixed again in another fan-in whose output would be the mixed output of all eight proportional counters. To achieve the necessary low discrimination level the resultant pulses were then amplified using two identical amplifiers to give a gain of approximately 100. This amplified pulse was then fed into a discriminator.

Similarly, the pulses from the two photomultipliers were fed directly into one head unit and the output pulses amplified (approximately x 10) and split in a fan-out. The pulse in the selection channel was then discriminated.

The pulses from the 'proportional' discriminator and the pulses from

the 'scintillator' discriminator were then fed into a coincidence unit.
When a coincidence occurred the resultant pulse was discriminated and
aplit in a fan-out, the oscilloscope was delayed by 60 μsecs, using a
delay pulse generator, to avoid pick-up on the oscilloscope from the high
voltage pulse. This pulse then triggered a unit consisting of a valve
monostable, which in turn triggered a thyristor and a pulse transformer.
The resultant pulse triggered an air spark gap discharging a bank of
condensers to provide a 12 kV, 10 microsec pulse which was fed to the
electrodes of the flash tube trays. The third output pulse from the fan-
out started the cycling system, which first paralysed the input to all
triggering systems and then, by microswitches, illuminated the fiducials
and the clocks in the two views of the flash tube trays. It also illumin-
ated a watch situated in the oscilloscope system, and then wound on the
three cameras used. Finally, the paralysis was removed at the end of a
seven second cycle and the system was ready to record another selected
event.

4.5.2 The display system

The pulses from the proportional counters and the scintillator were
displayed on a four-tube oscilloscope, and, for each event, the four
traces were photographed as explained above using Ilford Mark V film.
The scintillator display pulse was taken from the output of the fan-out
to feed through a 6 μsec delay line into the input of the oscilloscope
(tube 1). The other three tubes of the oscilloscope were then left for
the display of the proportional pulse. Using these tubes, each at various

stages of amplification, the output pulses from the counters could be viewed in the range from 0.2 to 8 equivalent particles. The display system for the proportional counters has been described previously. It consists of eight separate units of 6 μsecs delay line, linked to each other in a line and terminated with its characteristic impedance only at the two ends. The proportional display pulses, 1a-8a, were fed through a variable amplifier and a diode into the delay line in such a way that pulses from adjacent counters were separated by 6 microsecs. The variable amplifiers were adjusted to give equal outputs in each channel for the same input, and the output pulses were again amplified and split in a fan-out to feed the three oscilloscope inputs.

4.6   Running time

This arrangement was run for a total sensitive time of 86 hours in the months of September and October, 1969, and 2,973 frames were recorded and 110 'good' measurable events obtained. In deriving the value of the sensitive running time, the dead time, while the cycling system was in operation, was taken into account. This accounted for 5.3% of the total running time.

Many of the events selected were either air showers or spurious coincidences between the proportional counters and the scintillator and could be selected out immediately in the scanning.

4.7 Experimental data

4.7.1 Analysis of results

When an event was detected with a pulse > 30 equivalent particles in the scintillator in coincidence with a pulse > 0.2 equivalent particles in any one proportional counter, the oscilloscope and the flash tubes were automatically photographed. The three films used in this process were scanned and the events classified.

It was necessary in scanning the flash tube film to define the sensitive volume of the apparatus clearly (Fig. 4.1). The line of the track and of the centres of the bursts produced were required to be in this volume, and an event which went 'out of geometry' in the flash tubes was immediately discarded. It must be noted that these limits were such that the whole of the burst of particles for a primary of any reasonable energy, was required to pass through the scintillator phosphor. All events which gave a track within 1 cm of the side of a proportional counter were also rejected as the ionization produced would be small and errors in track length evaluation large.

The flash tube parameters measured from the film are shown (Fig. 4.4). From these measurements the angles to the vertical of the track and of the line of burst, θ_1, θ_1' in the front view and θ_2, θ_2' in the side view could be evaluated. The true zenith angle of the event could then be calculated using the relation:-

$$\tan^2\theta = \tan^2\theta_1 + \tan^2\theta_2 .$$

The pulse heights obtained were also recorded as a voltage pulse in mV and, in the case of the proportional counters the particular counter
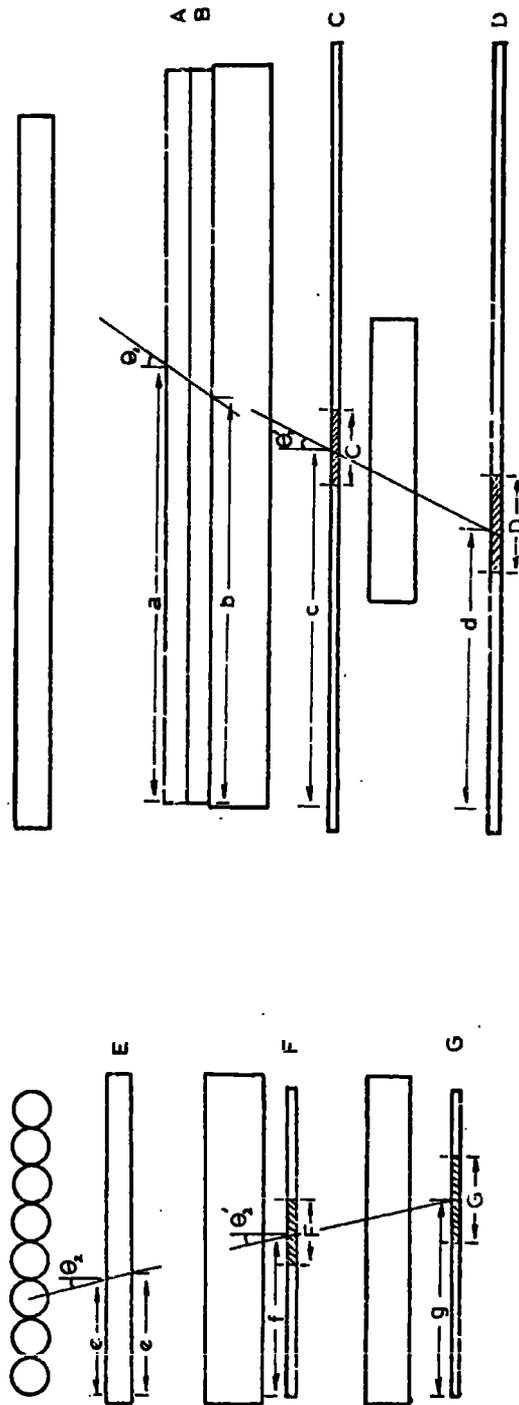
Figure 4.4 The flash tube parameters.

noted. These pulses were then converted into 'equivalent particles' using the electronic calibration graphs of the respective run. In the case of the scintillator the value (N) obtained needs no further analysis as, from above, the response is approximately constant over the whole area of the counter. The results obtained for the scintillator are shown as a pulse height- frequency plot (Figure 4.5). The proportional counters, on the other hand, are cylindrical, and great care had to be taken in working out the response of the counter for each specific event.

4.7.2 Proportional counter pulse height evaluation

The response of a proportional counter to an ionising particle is proportional to the length of track of the particle in the counter. All the pulse heights obtained were normalised to a track length of 14 cm (the diameter of the counters) using the method described below.

A large scale diagram of the side elevation was drawn. For each event the line of flight, according to measurements e, e', f, g, was fitted with a rule. The projected track length, t, in this elevation could then be measured and from this value the real track length, T, could be evaluated using the relation:-

$$T = t \sqrt{(1 + \tan^2\theta_1 \cos^2\theta_2)} \text{ where } \theta_1 \text{ and } \theta_2 \text{ are of the notation}$$

above.

The pulse height could then be normalised to a track length of 14 cm.

It is important, to ensure the reliability of the normalised proportional pulse, that some measure of the accuracy in track length measurement
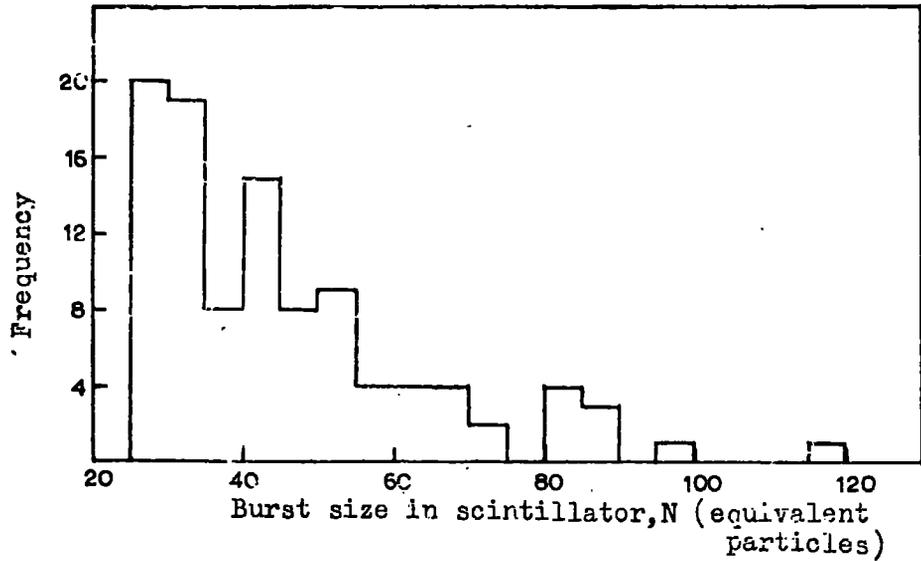
Figure 4.5 The distribution in burst size for the events in which there measurable proportional counter pulses.

is made. All the selected events were taken and, in the fitting of the line of track to the flash tube co-ordinates, the worst fit was used to obtain a different value of t. The error in track length estimation was then taken as the difference in the two values of T evaluated, and the distribution of these errors formed a Gaussian, as expected, of standard deviation 2.8 cm. Figure 4.6 plots the relative error in track length against the normalised proportional pulse height (P) as a scatter plot for all good events. Events that were seen to have a large value in the error term were discarded, and these numbered about 2%.

A scatter plot of pulse height (P) against track length (T) (Figure 4.7) was also drawn to check for any anomalous connection between the two especially for large or small pulse height. As can be seen, there appears to be no connection and the mean track length was ~ 14 cm.

The final accepted proportional counter pulse heights are shown as a frequency plot (Figure 4.8).

4.8 The acceptance function

The acceptance limits for this experiment have already been shown as Figure 4.1. The acceptance aperture was calculated graphically and is best described with the aid of a diagram (Figure 4.9) which shows the volume through which single, burst-producing, particles must pass to be accepted as good events. It must be noted that the 'null' areas between the proportional counters are not shown in this diagram but a 3 cm gap between each counter was taken as the 'null' area in the calculation.
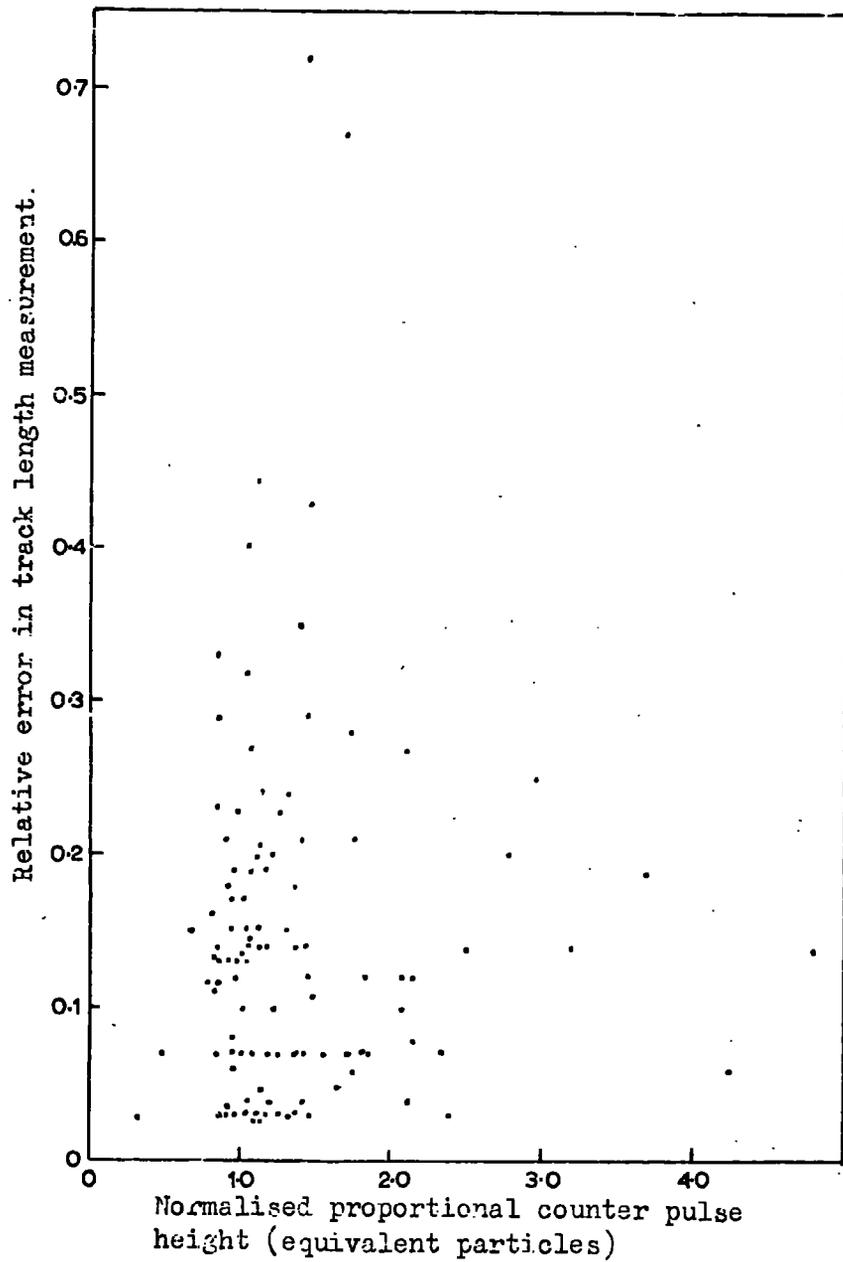
Figure 4.6 Scatter plot of the relative error in track length
measurement against the normalised proportional
counter pulse height.
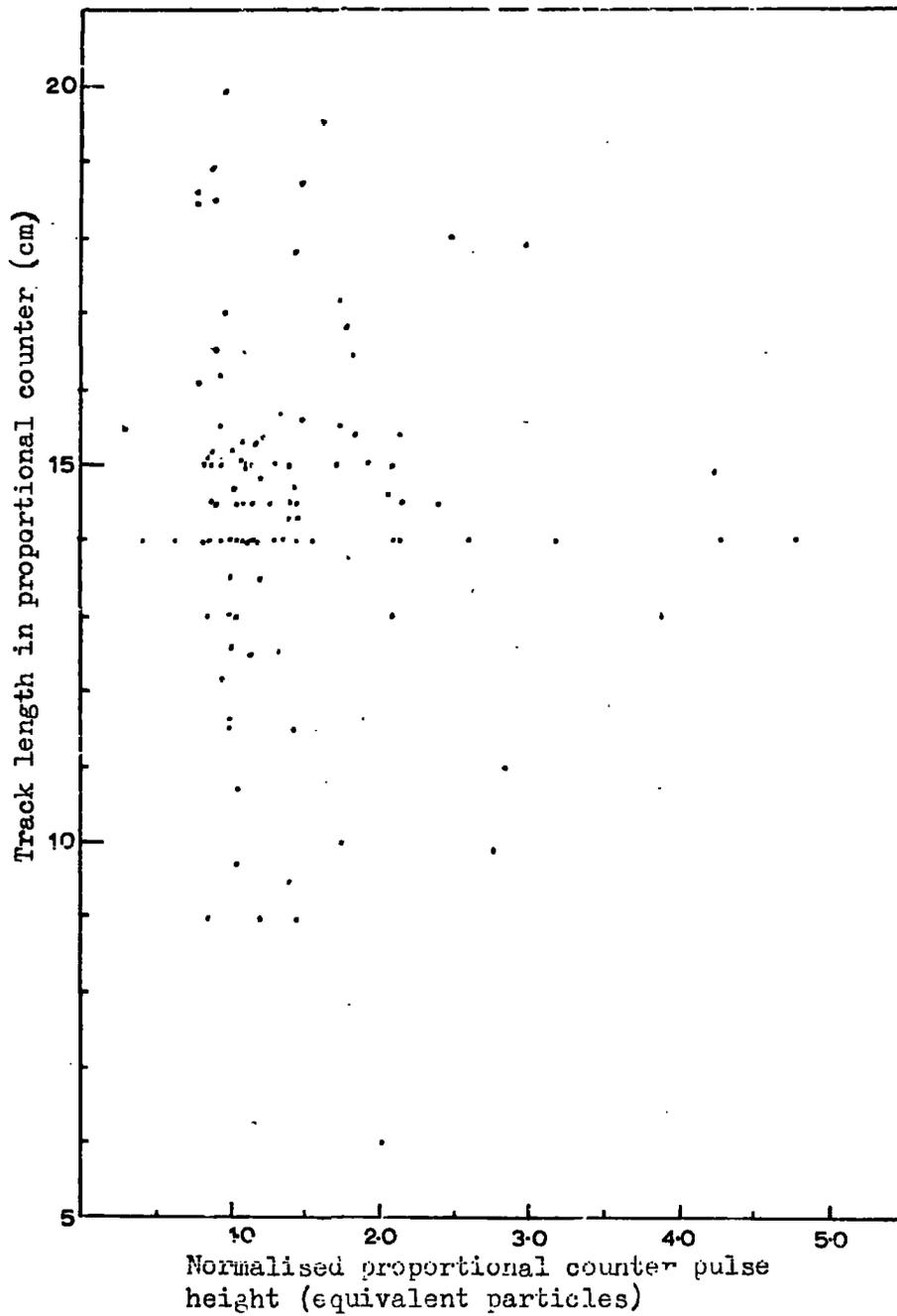
Figure 4.7   Scatter plot of measured track length against
its normalised proportional counter pulse height.
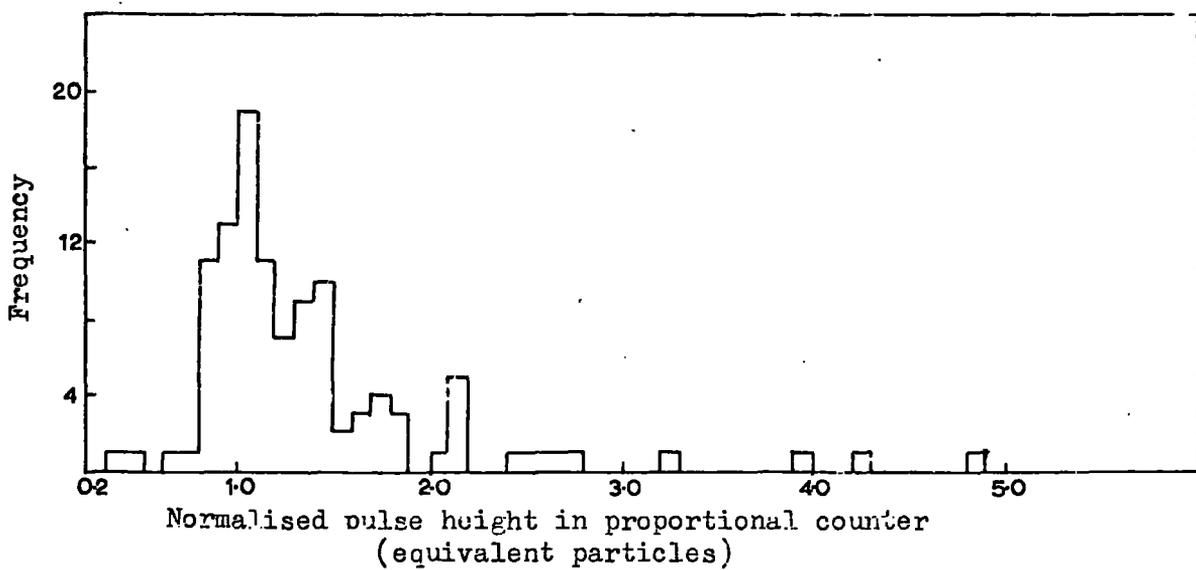
Figure 4.8   The distribution in pulse height in the proportional
             counter for all the measurable events in the experimental
             run. All proportional counter pulse heights were
             normalised to a standard track length of 14cm.

The area ABCD was divided into four equal areas and each of these was further divided into four equal areas, one case being shown in the diagram. Considering one of these small areas, dA, the element solid angle subtended between θ and $\theta + d\theta$ is given by -

$$2\pi \sin\theta \cdot \cos\theta \cdot \frac{\phi}{360} \quad \text{where } \phi \text{ is in degrees}$$

and the acceptance aperture is therefore:-

$$2\pi \sin\theta \cdot \cos\theta \cdot \frac{\phi}{360} \; dA$$

This function was evaluated for each of the areas, dA, at specific values of θ. The values obtained at each value of θ for all areas of dA were added to give the curve shown in Figure 4.10. This curve gives the number of m^2 steradian per radian presented, by the apparatus, to incoming isotropic radiation as a function of zenith angle. The area under this curve, therefore, represents the total acceptance aperture for isotropic radiation and was found to be $0.49m^2$ steradian.

For non-isotropic radiation one must fold into this acceptance-zenith angle curve a function with a dependence on zenith angle. The expression chosen was of the form:-

$$I = \exp\left(\frac{-1030}{\lambda_a \cos\theta}\right)$$

It must be noted that, although λ_a is an attenuation length, in this case it has little physical significance, as the primaries dealt with are
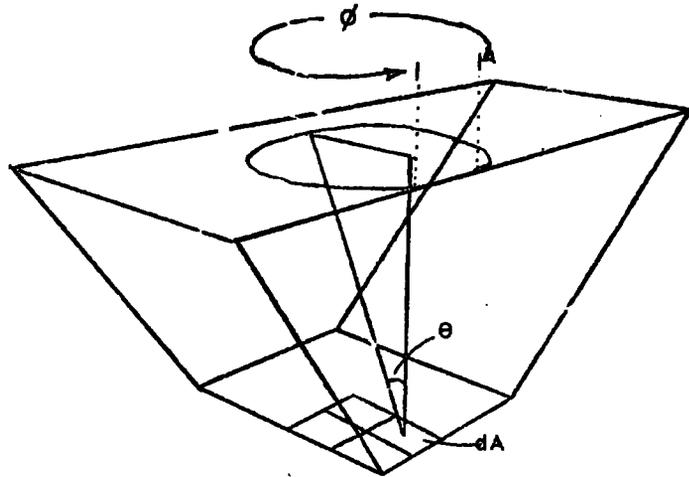
Figure 4.9   The acceptance volume of the apparatus.
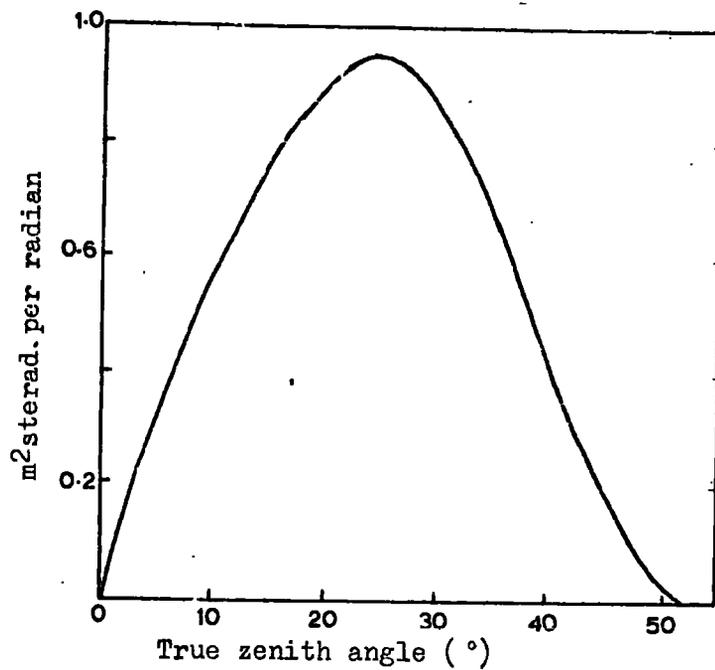
True zenith angle (°)

Figure 4.10   Number of m²sterad. presented by the apparatus
to incoming isotropic radiation as a function
of the zenith angle.
(Null areas between the counters taken into
account.)

a mixture of pions, protons and mu-mesons. It was necessary to do a minimum ψ^2 fit to the experimental angular distribution obtained (Figure 4.11), to find the best value for λ_a. Figure 4.12 shows the curve of number of m steradian per radian presented to the incoming non-isotropic radiation of intensity dependence

$$\exp \left(\frac{-1030}{\lambda_a \cos\theta} \right)$$

where λ_a is the best ψ^2 fit to the data and is 233 ± 20. The total acceptance aperture for non-isotropic radiation of this form was found to be 0.32 m^2 steradian.
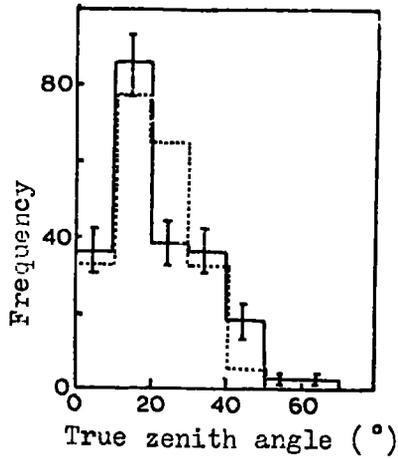
Figure 4.11 Angular distribution of all accepted events and the,
dotted, best χ^2 fit to this data for nonisotropic
radiation.
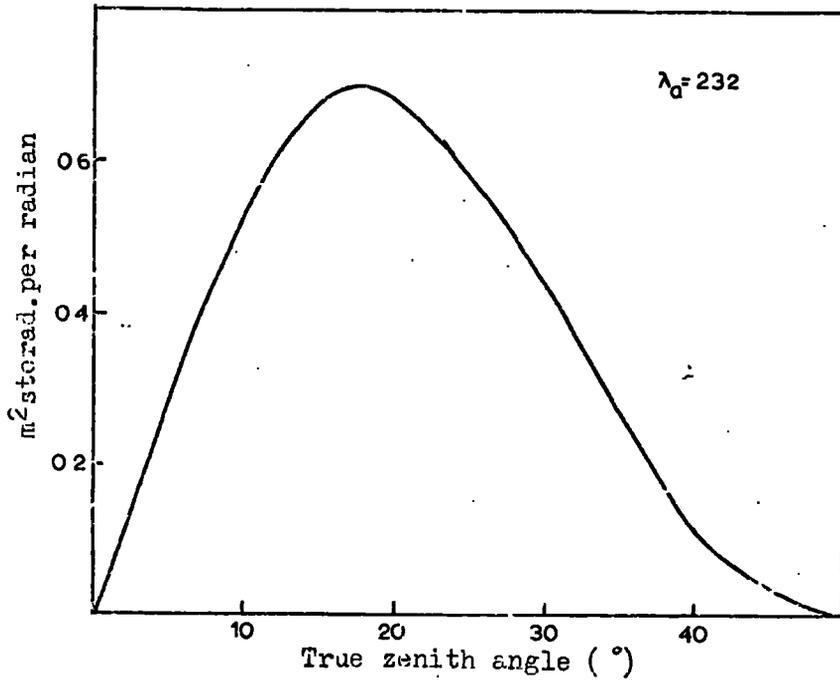
Figure 4.12 Number of m sterad. presented by the apparatus to
incoming nonisotropic radiation of the form
$I \propto \exp\left[\dfrac{-1030}{\lambda_a \cos\theta}\right]$ Here λ_a is given by the best χ^2 fit
to the angular distribution and is 232.

CHAPTER 5

INTERPRETATION OF THE RESULTS IN THE 2e/3,4e/3 ETC. SEARCH

5.1 Introduction

In this search all charged particles producing an interaction of
energy exchange greater than 30 GeV in an iron absorber were accepted
and the pulse height produced in the proportional counters recorded.
These interacting particles will be a mixture of pions, protons and
muons of all energies and, to obtain a form for the expected distribution
in ionisation, one must obtain the relative rates and energies of these
particles. However, to relate the distribution derived from this
information with the experimental distribution, one must first obtain
the relation between ionisation loss in the gas of the counter and the
equivalent particles in which the pulse height is measured.

5.2 Calibration of energy loss in terms of equivalent particles

As described above the proportional counters were calibrated using
a Geiger telescope. A particle, which triggered this telescope would
have to traverse an amount of matter, made up mainly of the glass in the
tubes and the aluminium proportional counter walls, which amounted to
6 gm cm^{-2}. These particles would be mostly μ-mesons and electrons whose
minimum energies could be calculated. For electrons the Feather rule
may be used giving $E(min) = 11.75$ MeV and for muons, the range-energy
relation, $E(min) = 36.0$ MeV.

The mean energies of muons and electrons above these minima and their relative rates could be obtained, providing the energy spectra in cosmic rays at sea level is known. Fazzini et al (1968) quote the differential energy spectrum for both electrons and muons and this was used to give, for muons, mean energy 2 GeV, 71.4% of flux, and for electrons 36 MeV, 28.6%.

The most probable energy produced by charged particles traversing the proportional counter gas may be calculated from the expression given by Rossi as:-

$$E_p = \frac{2Cm_e c^2 x}{\beta^2}^2 \left(\ln\left\{ \frac{4C(m_e c^2)^2 x}{(1-\beta^2)I^2(Z)} \right\} - \beta^2 + j \right)$$

where $C = 0.15 \frac{Z}{A}$ gm cm^{-2}

$\quad\quad$ I (Z) - Average ionisation potential $\simeq$ 13.5Z(eV)

$\quad\quad$ m_e $\quad$ - mass of the electron

$\quad\quad$ j $\quad\quad$ - a special function tabulated by Rossi.

For 14 cm of proportional gas this expression becomes

$$E_p = \frac{17.2z^2}{\beta^2} \left(\ln\left\{ \frac{2.98.10^4}{(1-\beta^2)} \right\} - \beta^2 + j \right) \text{ MeV}$$

The value for E_p calculated for muons and electrons of the median energies was therefore 38 keV and 31 keV respectively.

Taking the contributions of the electrons and muons together one can say that, for the calibration telescope, the average median ionisation was 28.9 keV. Since the median of the Landau distribution obtained in

this arrangement was defined as one equivalent particle one therefore has a relation between ionisation and pulse height.

5.3 Energy of burst-initiating events

R.B. Coats (1967) and N. I. Smith (1969) have made detailed studies of bursts produced by cosmic rays in this type of apparatus. From their results one can obtain the relative rates and mean energies of the proton, pion and muon components of the primary flux. Both Smith and Coats have carried out detailed calculations of the relationship between burst size and energy for the absorber used in their respective experiments. Hence, normalising these results to the absorber used in this experiment one can obtain, for a given burst size the energies and the relative contributions of the three components.

The distribution in burst size obtained for all good events is shown in Figure 5.1, and its median value was calculated to be 41 equivalent particles. To obtain a form for the expected distribution in the proportional counters it was taken that all the events were of this median burst size and the median energy and contribution of the proton, pion, and muon primaries were calculated. The values obtained were

34.6%, 82 GeV protons

32.7%, 34 GeV pions

32.7%, 69 GeV muons
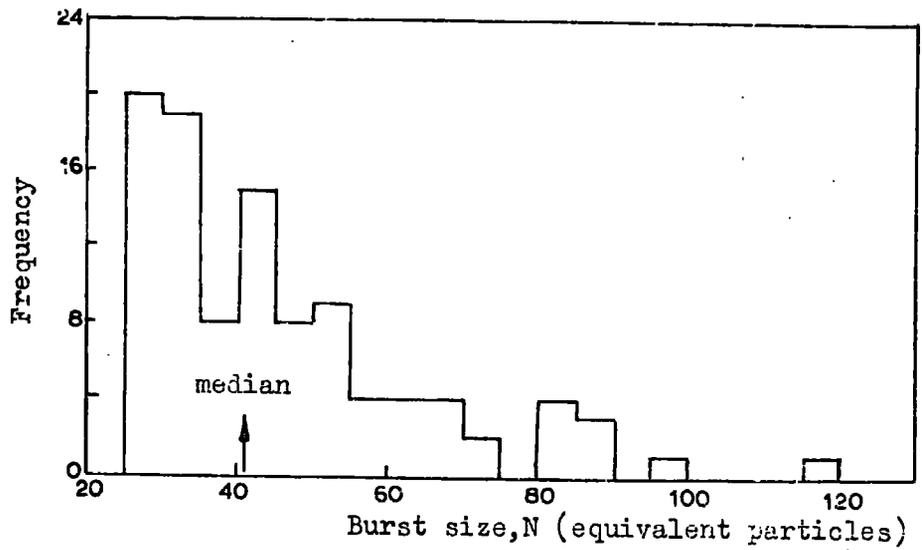
Figure 5.1   Frequency distribution in burst size in the scintillator
for all accepted events.

5.4 The energy loss in the proportional counter and its distribution

Nuclear particles of equal mass and energy in traversing the counter gas will produce a distribution in energy loss, whose most probable value can be evaluated from the equation above. Each of the three primary components will therefore produce different energy losses and distributions in the proportional counter. The net effect of these three distributions is required. At the energies of the median burst sizes evaluated the factor 'j' quoted in the equation will have reached its asymptotic value of 0.33. The values calculated for the most probable energy loss for the protons, pions and muons at the median burst size was 32.0, 34.7 and 37.9 keV respectively.

Symon (1948) has evaluated a complete solution of the Landau distribution for the probable energy loss in a thin absorber and, from this, one may calculate the distributions in energy loss for the three primary components (Fig. 5.2). The net effect of these distributions may be obtained by adding these distributions in terms of their relative contributions once the energy loss is normalised into equivalent particles (Figure 5.3).

However, there is good experimental evidence (Ramana Murthy and G. D. Deemester, 1967) that for very thin absorbers the theoretical distributions of Landau and Symon etc. do not apply. Blunck and Weisegang (1950) and Blunck and Westphal (1951) have modified the Landau distribution to take into account atomic binding effects. The Blunck and Westphal distributions in these conditions are much broader than the Landau distribution and are a better fit to the experimental data. These authors define

$\Delta.\omega$

Ionisation energy loss in 14cm of proportional counter gas.   (keV)
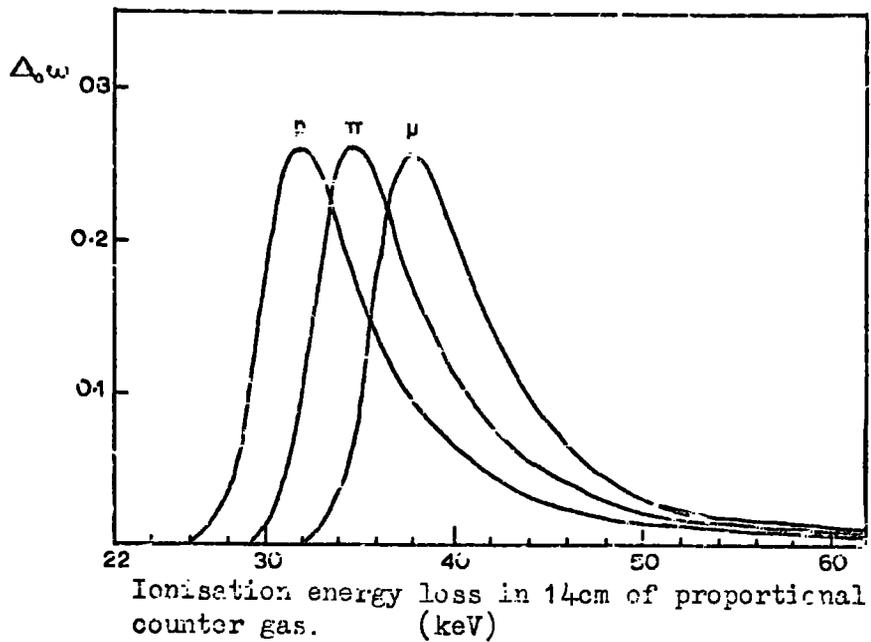
Figure 5.2   Landau distribution of energy loss in 14cm of gas for protons, pions and muons of energy equivalent to a median burst size of 41 equivalent particles.

Ionisation loss for π, p, μ
(equivalent particles)
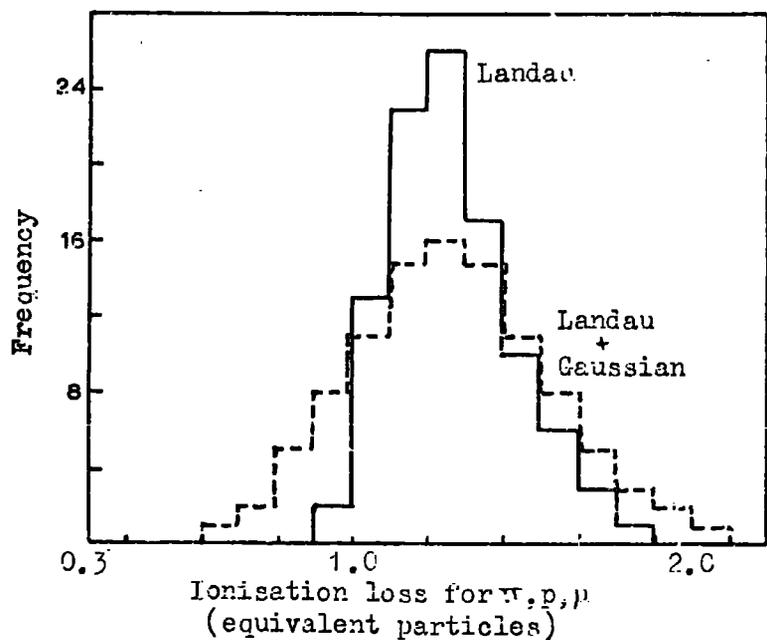
Figure 5.3   Expected total Landau distribution for the energies and rates of π, p, μ calculated for median burst size of 41 equivalent particles. A distribution of track length error, σ=0.21 equivalent particles, has also been folded in.

a parameter, b^2, as:-

$$b^2 = \frac{20 \bar{\Delta}\, z^{4/3}}{\left\{ 0.3\left(\frac{Z}{A}\right)x\left(\frac{m_e c^2}{\beta^2}\right)\right\}^2}$$

where $\bar{\Delta}$ is the average energy loss in traversing the counter in eV.

If $b^2 \gg 3$ then the distribution will be markedly different from the Landau distribution.

Figure 5.4 shows the distributions calculated from this theory for the experimental conditions of protons, pions and muons, $b^2 = 10, 11, 12$ respectively. It can be seen that these distributions are each twice as broad as the original Landau (Figure 5.2). The broadening of the net distribution, as shown in Figure 5.5 is not nearly so large.

The distributions obtained from both the Landau and the Blunck and Westphal theories do not take into account any experimental inaccuracies in the measurement of this ionisation. The most appreciable effect will be produced by inaccuracies in the measurement of track length. This has been calculated above to be represented by a Gaussian of $\sigma = 0.2$ equivalent particles. To obtain a reasonable form for the expected distribution of proportional pulse heights one must fold this Gaussian into the theoretical net distribution loss as given by Symon (Figure 5.3) and Blunck and Westphal (Figure 5.5).

5.5 Other likely effects

5.5.1 Nuclear-interactions in the walls of the counter

One can make an estimate of the contribution to the results from
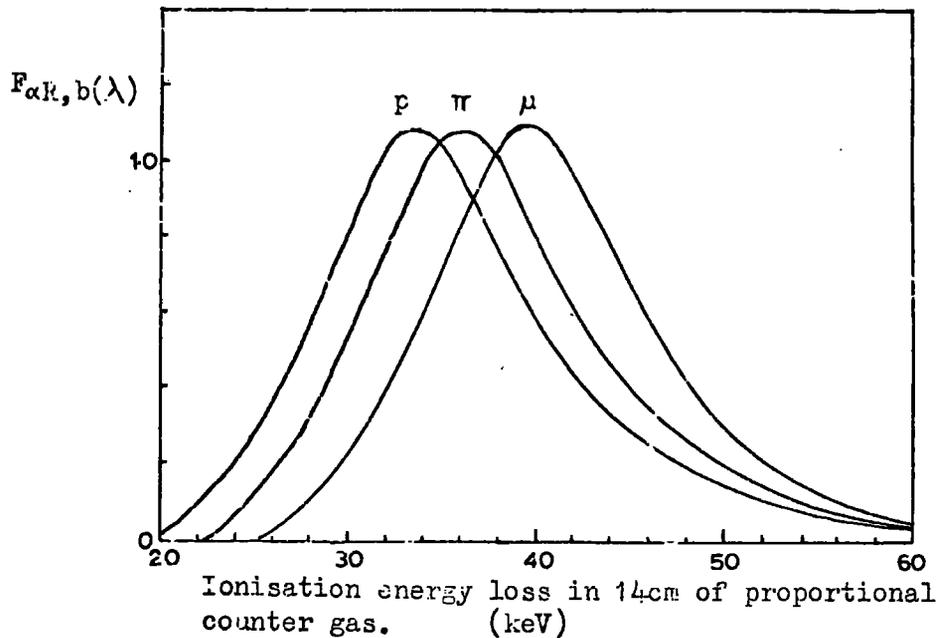
Figure 5.4 Distributions of energy loss according to Blunck et al
in 14cm of counter gas for p,π,μ of median burst size
energy of 41 equivalent particles.
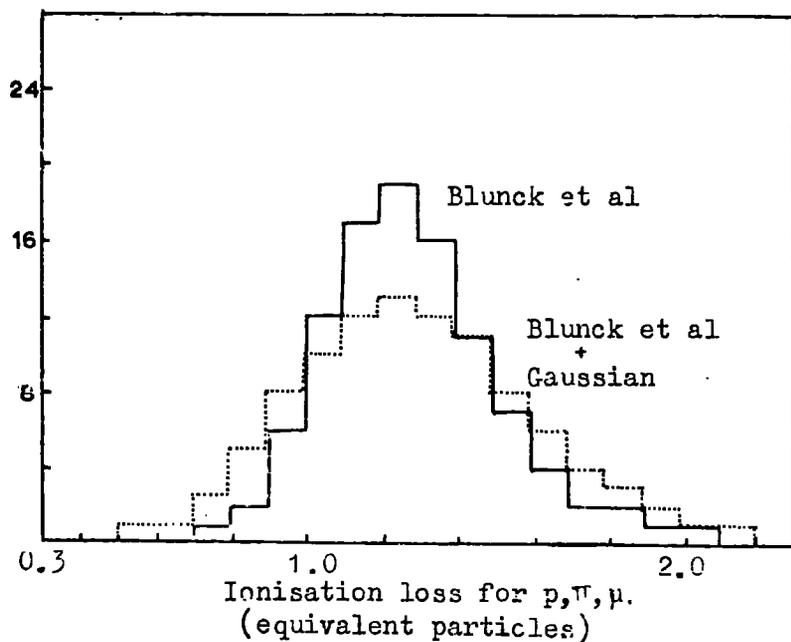
Figure 5.5 Expected total distribution in energy loss for the
energies and rates of p,π,μ calculated from the median
burst size of 41 equivalent particles, A distribution of
track length, σ=0.21 equivalent particles, has also been
folded in.

nuclear interactions in the aluminium walls of the counter by using the geometric cross-section, σ_g. Taking the geometric interaction length L_g to be 87.0 gm cm^{-2} for aluminium one can calculate the fraction of incident particles that would interact from the relation -

$$\left\{ \exp\left(\frac{x}{L_g}\right) - 1 \right\} \quad \text{where } x \text{ is the thickness of the wall.}$$

The expected number of interactions in the wall was calculated to be 2.2%. These would be expected to yield large proportional pulses due to the additional ionisation of the secondaries in the gas.

5.5.2 Knock-on electrons from the wall

Once again one can make an estimate of the percentage of large pulses that would be due to knock-on electrons from the walls entering the gas. The knock-on electrons produced would have to have a minimum energy required to traverse the thickness of the wall, which remains from the point of interaction to the gas. If one takes the knock-on to have occurred at the centre of the wall, then this minimum energy was found to be 2.1 MeV.

With knock-on electrons of this order of energy one can take the simple Rutherford formula for the probability of a particle transferring an energy between E' and $E' + dE'$ to an electron, that is -

$$\Phi_{col}(E')dE'dx = \frac{2Cm_e c^2}{\beta^2} z^2 \frac{dE'}{(E')^2} dx$$

when $E' \ll$ maximum transferrable energy and $C = 0.15 \frac{Z}{A}$

Hence $\phi\,(>E) = 2Cm_ec^2\;z^2\;dx \int_{E'_o}^{\infty} \frac{1}{(E')^2}\;dE'$

and $\phi\,(>2.1\ MeV) = \frac{2.6\ 10^{-2}}{\beta^2}$

The median energies of the primary particles have been stated above and it can be seen from these values that $\beta \simeq 1$. The probability, therefore, of observing events which include knock-on electrons from the walls entering the proportional gas is 2.6%.

5.6 Distributions expected from non-integral charged particles charge 2e/3, 4e/3 etc.

The amount of ionisation produced by a particle traversing the proportional counter is proportional to z^2 and is a function of its Lorentz factor γ. The most probable ionisation for particles of charge 2e/3 etc. is shown in Figure 5.6 as a function of the particles' Lorentz factor. In order, then, to make an estimate of a particular particle's most probable ionisation, one must know the mass and the energy of the particle concerned. Machine experiments in search of sub-integral and integral quarks suggest that the mass is greater than 4 GeV which would mean that except for very high energies the ionisation of the quarks will not be on the plateaux.

If, as Ashton (1965), one takes the model for the production of quarks as -

$$p+N \rightarrow p+n+q+\bar{q}$$
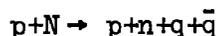
the threshold proton energy for the production of a quark of mass, Mq will be:-

$$Ep = \left\{ 2\left(1 + \frac{Mq}{Mp}\right)^2 - 1 \right\} M_p c^2$$

and then the kinetic energy of quarks in the lab. system will be in the region of the threshold -

$$Eq = \left\{ \frac{1}{2}\left(\frac{Ep}{M_p c^2} + 2 \right)^{\frac{1}{2}} - 1 \right\} M_q c^2 \simeq \frac{M_q c^2}{(2M_p c^2)^{\frac{1}{2}}} Ep^{\frac{1}{2}}$$

In this region the proton spectrum is rapidly falling and therefore one can say that most quarks will be produced near the threshold. If one takes the mass of the quark to be 10 GeV then -

$$E_q = \frac{10}{1.4} (240)^{\frac{1}{2}} \simeq 100 \text{ GeV}$$

$$\gamma_T \simeq 11$$

Therefore the most probable ionisation for a non-integral quark produced by this process would be 2e/3 - 0.36, 4e/3 - 1.43, 5e/3 - 2.26, 7e/3 - 4.27 equivalent particles.

However this can only be taken as a very approximate estimate of the most probable ionisation. The sensitive limits of the experiment for various non-integral charged particles are shown in Figure 5.6.

The distribution in energy loss for a particle of charge z has been discussed in detail for unitary charged particles. The distribution width as a percentage of most probable value will be the same as that of a muon or a proton, as the factor Δ_o in the Landau distribution contains a term of z^2. Figure 5.7 shows the Landau distributions for various most probable pulse heights that could be taken as e/3, 2e/3, 4e/3, 5e/3, of $\gamma > 700$.
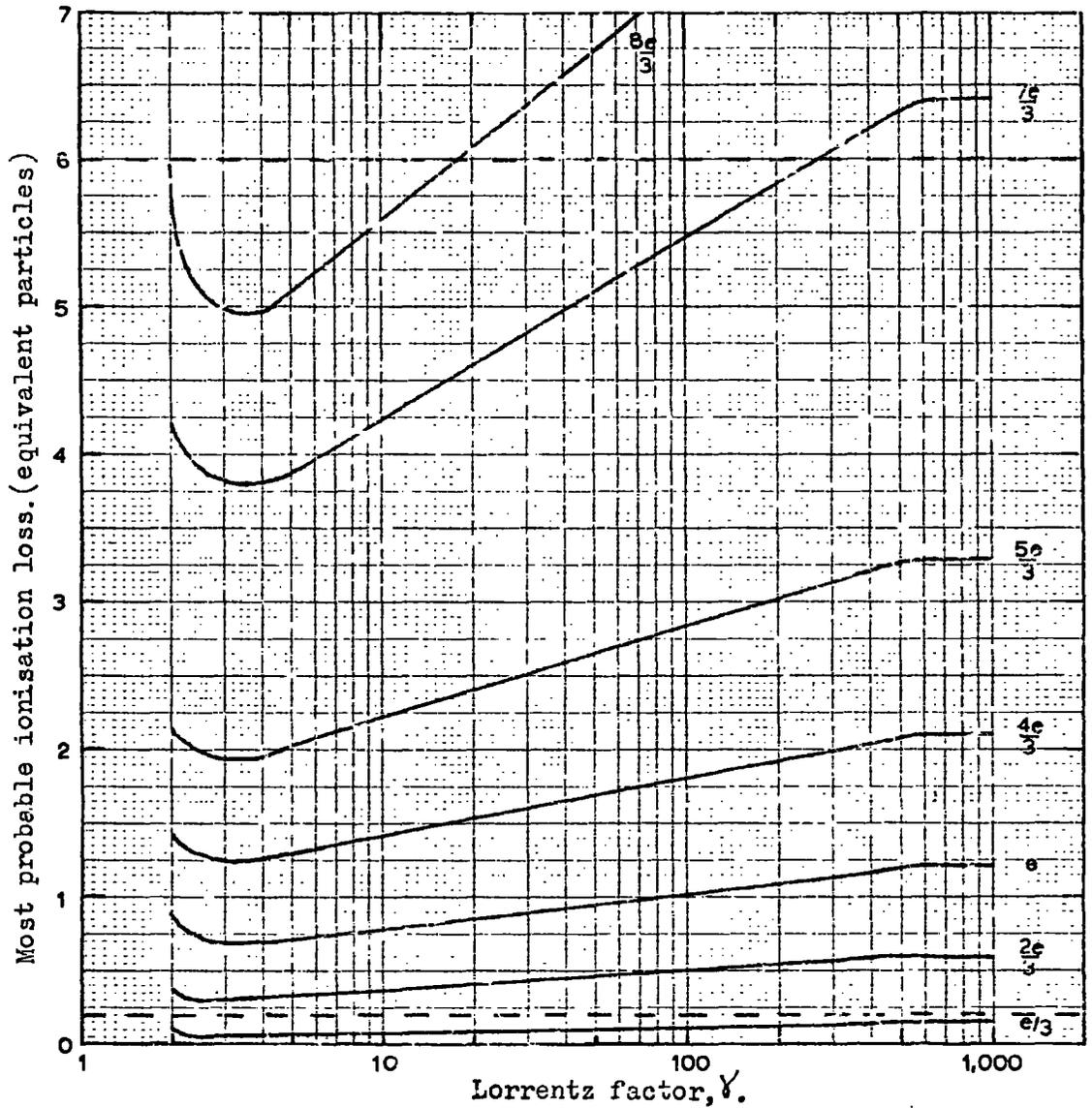
Figure 5.6 The most probable pulse heights produced in the proportional counter by various non-integral charge particles against their γ-factors. The dotted lines show the sensitive limits of the experiment.
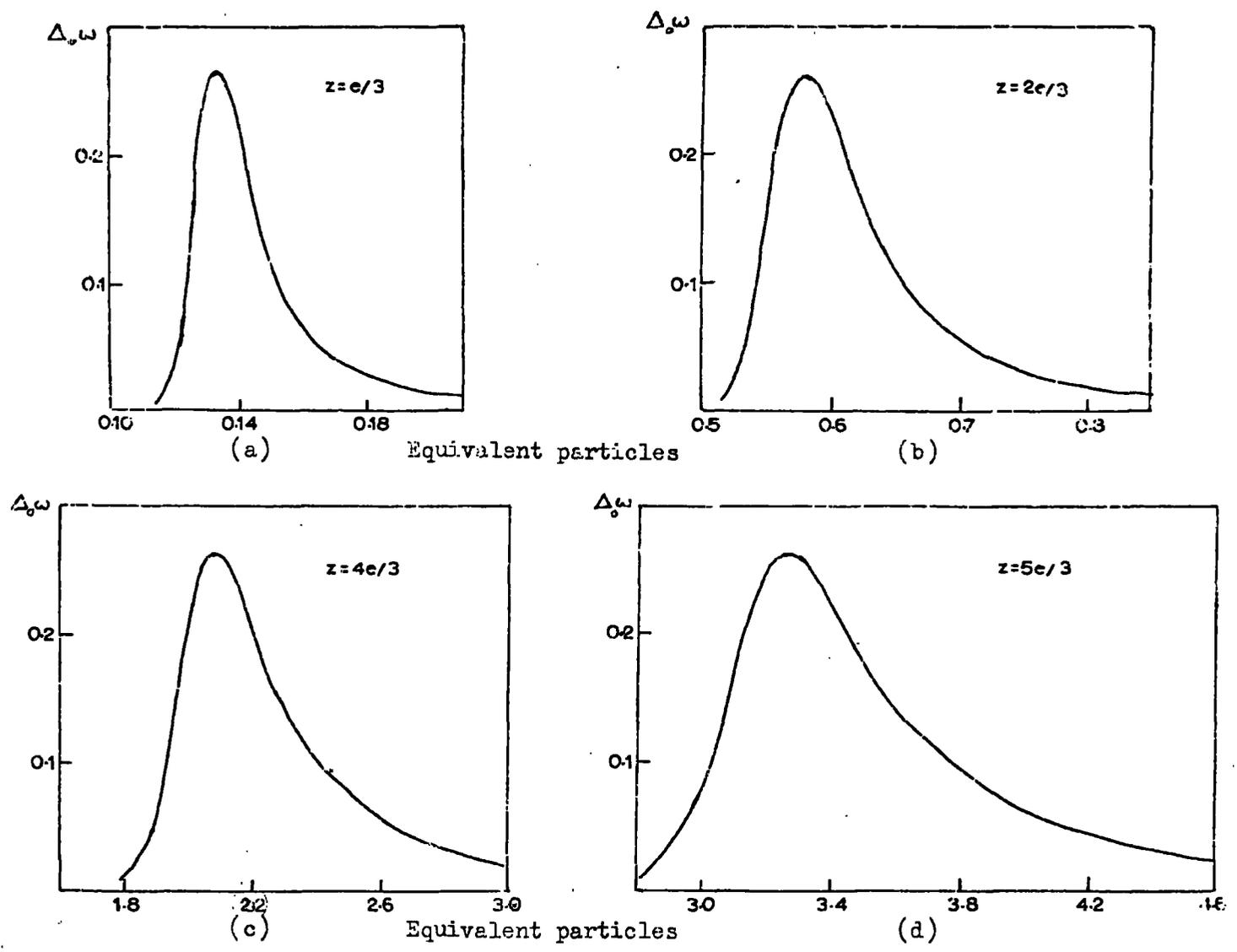
Figure 5.7 The Landau distributions for particles of charge $e/3, 2e/3, 4e/3, 5e/3$ and γ>700.

The error in track length evaluation would also affect these distri-
butions. In order to make a true representation of the experimentally
expected distribution for a non-integral charged particle one must 'fold'
the Gaussian distribution for track length evaluation into these distribu-
tions. Figure 5.8 shows the expected distributions one would obtain in
detecting 50 particles whose most probable pulse height was 0.13, 0.58,
2.10, 3.26 equivalent particles. It must be noted that these distributions
are only meant to give an estimate of what is likely to be observed. The
experimental distributions for high energy non-integral charged particles
are likely to be much broader.

5.7 Conclusion

The results of the experimental run compared with the calculated
expected distribution for the Landau theory and the Blunck and Westphal
modifications are shown in Figure 5.9 and 5.10 respectively. It must be
noted that the experimental results show a long tail to the main distri-
bution, and we must consider the possibility of non-integral charged
particles.

The possibility of 'knock-ons' and nuclear interactions in the wall
has already been discussed. These events would be expected to give large
pulse heights and would probably form a part of all of this tail. It has
been shown that these events would have a frequency of 4.8% and one could
therefore say that there would be a tail to the main distribution of ~ 6
events.

If one assumes that the expected distributions are totally Gaussian
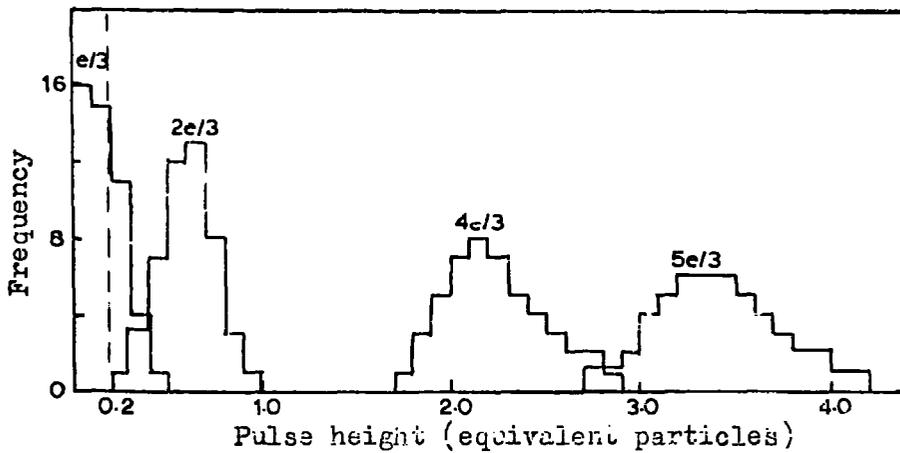
Figure 5.8   Expected distributions in proportional counter pulse
height in observing 50 particles each of charge e/3,
2e/3, 4e/3, and 5e/3 and $\gamma > 700$.
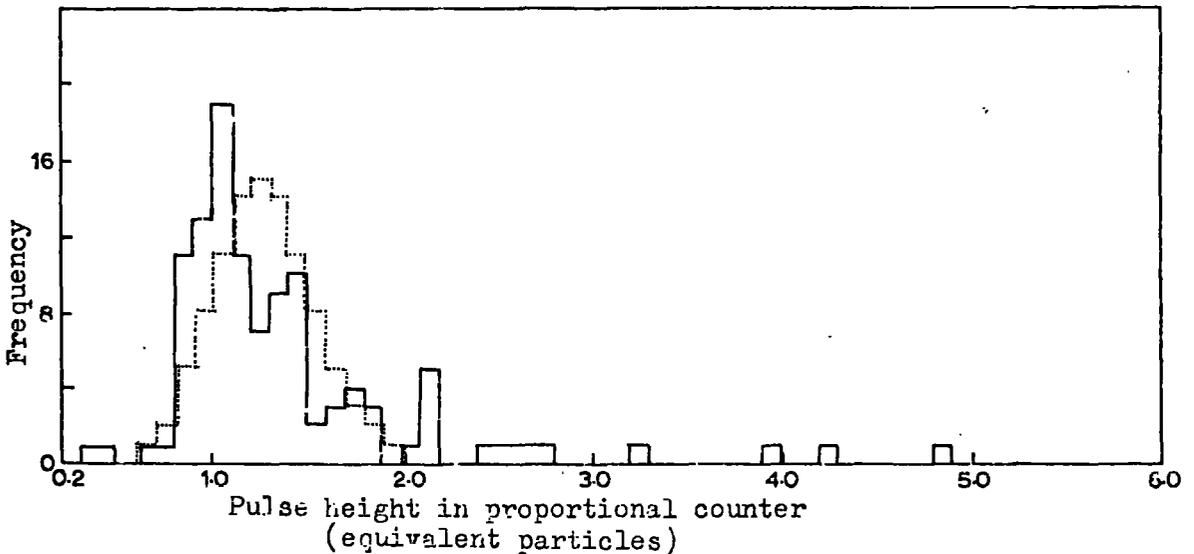
Figure 5.9 The distribution in normalised proportional counter pulse
height obtained compared with the, dotted, expected distribution,
as given by the Landau theory.
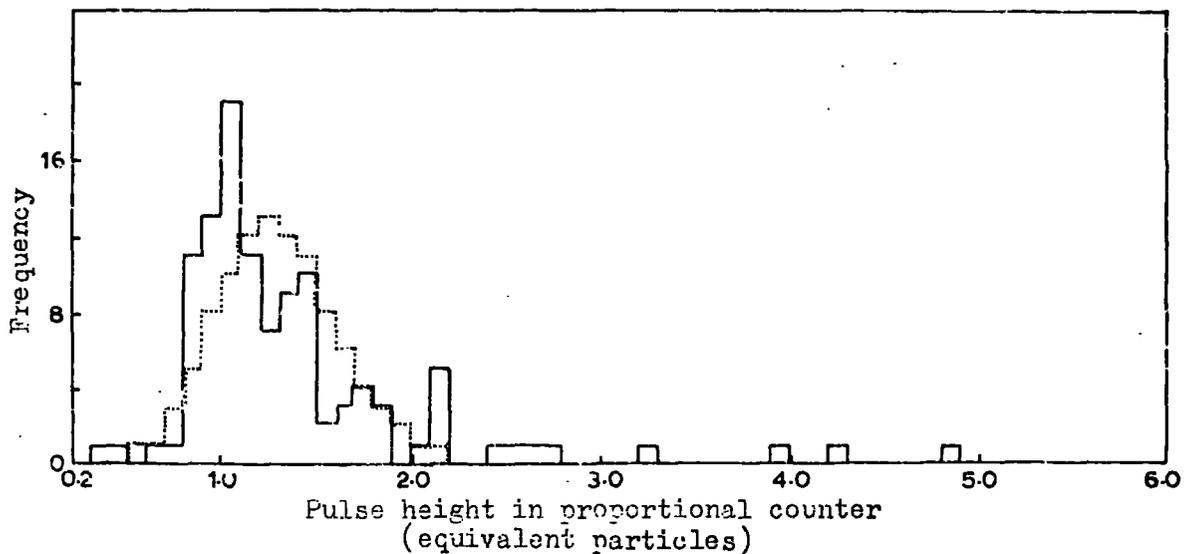
Figure 5.10   The distribution in proportional counter pulse heights
obtained compared with the, dotted, expected distribution
as given by the theory of Blunck et al. All measured
proportional counter pulse height were normalised to a
track length of 14cm.

one can calculate that the Landau and Blunck and Westphal distributions have 'σ's 0.256 and 0.3 respectively. One can therefore say that for each distribution the probability of detecting a particle > 2.0 equivalent particles is 1% for the Landau, and 2% for the Blunck and Westphal. With this reasoning one could therefore say that one would expect to observe a total of seven events and nine events in the tail of the distribution whereas there are fourteen events > 0.2 equivalent particles in the data.

All the events which produced proportional pulses outside the 3 σ limits of the Landau-based expected distribution, underwent careful checking of the selection procedure. No connection could be made with high energy primaries for the events in the tail. There are several possible explanations of these events:

(1) Low energy accompaniment to the primary.

(2) Albedo from the interaction in the steel.

(3) Non-integral charged particles.

(4) Inaccurate evaluation of the expected distribution.

(5) Fluctuations due to the poor statistical sample in this region.

It is very doubtful whether the first two possibilities could cause this surplus of events, as the visual detectors would have shown any accompaniment. Moreover, the selection of the proportional pulse involved agreement with the visual track and therefore these events would be most likely to be selected.

It appears from the pulse height distribution (Figure 5.10) that the surplus of events in the tail could be taken as concentrated at about 2.0

equivalent particles, which is the position one would expect 4e/3 charged particles. Comparing this peak with the calculated distribution (Figure 5.8) one can see that the experimental distribution is much too narrow to be mistaken for a 4e/3 signal.

The expected distribution was calculated using the theory of Blunck and Westphal, which has been shown to be in agreement with experimental evidence at the energies dealt with here. However, the shape of this distribution is largely governed by the error in track length distribution. This was measured as described in Chapter 4 and there is a possibility that this distribution was made too narrow by measurement error. The surplus in the tail of the distribution could easily be incorporated into the main distribution if the standard deviation of the track length evaluation was made larger.

In conclusion, the observed excess in the tail of the distribution compared with the expected excess is not statistically significant. The rate of 4e/3, 5e/3 and 7e/3 non-integral charged particles in cosmic rays can therefore be set only as a limit. Basing the limit on the five 'surplus' events and assuming these particles would interact with the iron target nuclei with the geometric cross section this limit is then -

$$< (4.2 \pm 1.9)10^{-9} cm^{-2} s^{-1} sr^{-1}$$
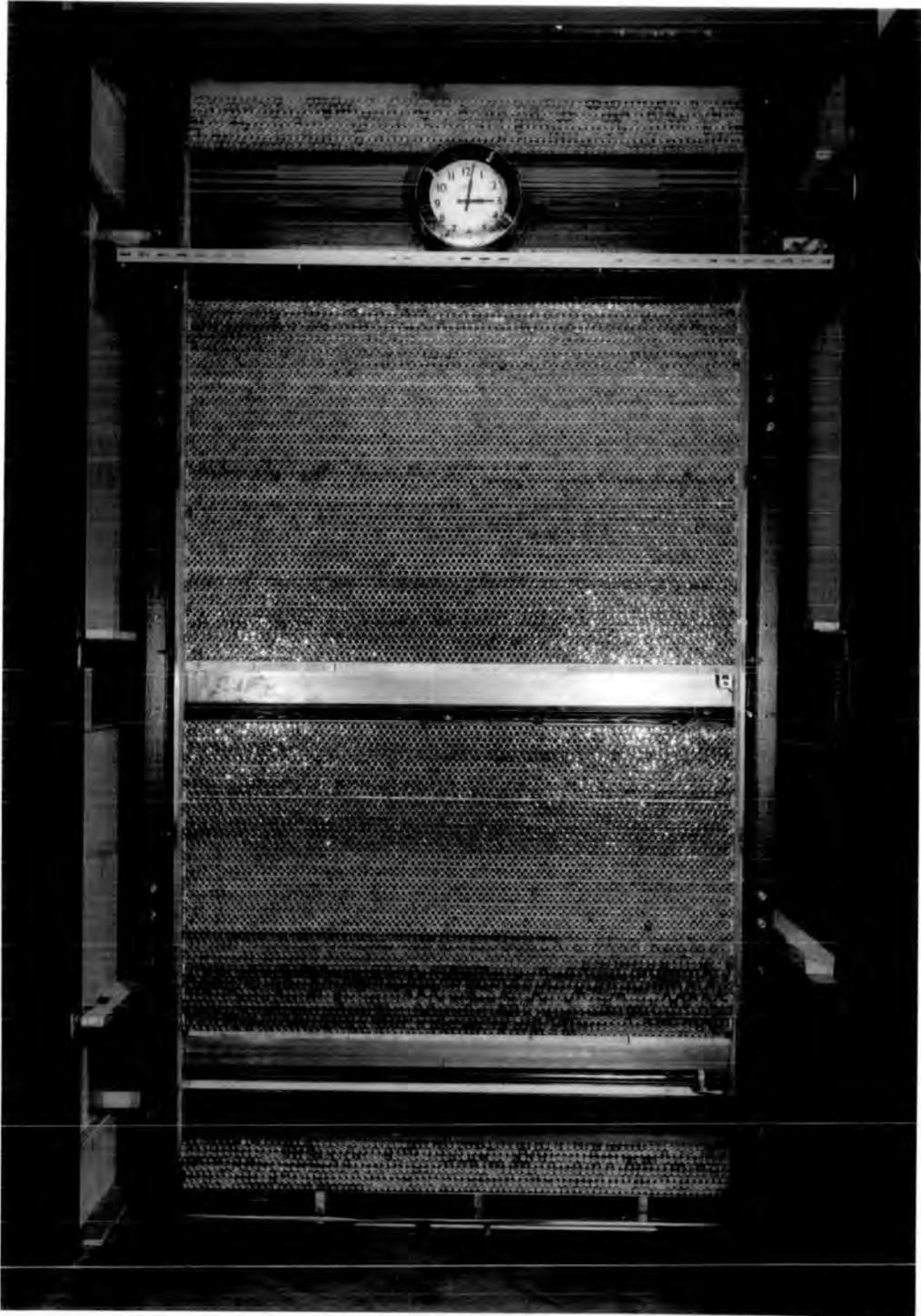
Plate 6.0   The Quark Telescope

CHAPTER 6

AN EXPERIMENT TO SEARCH FOR QUARKS OF CHARGE e/3 CLOSE TO
THE CORE OF EXTENSIVE AIR SHOWERS

6.1 The quark telescope

6.1.1 Design of the experiment

There are three basic requirements for an experiment, which is to
distinguish e/3 charge near an air shower core; one must be able to
select air showers with cores close to the apparatus, the electron
accompaniment must be absorbed out, and the remaining particles must be
examined by some method, which will separate e/3 from e charge, which, in
this case, involves the use of flash tubes.

The telescope consists of 148 layers of neon flash tubes, shielded
above with 15 cm of lead, and along the sides, with 35 cm of barytes
concrete bricks as shown in Fig. 6.1. Two plastic scintillators, A and
B, were positioned in the centre of the telescope and three large liquid
scintillators, North (N), Middle (M) and South (S), were placed above the
lead to act as the air shower detector. In addition, 20 cm. of iron
absorber was placed in the telescope itself.

6.1.2 The flash tube trays

The flash tubes were made of soda glass, 1 mm thick, internal
diameter 1.5 cm filled with commercial grade neon to 60 cm mercury pressure.
Each flash tube was covered with a black polythene sleeve leaving the
viewing end free.

The 11,642 flash tubes were packed glass to glass, with a sheet steel

front elevation

side elevation

NORTH   MIDDLE   SOUTH

LEAD

STEEL

CONCRETE

F1

F2

F3

F4

F5

F6

F7

50 cm

50 cm
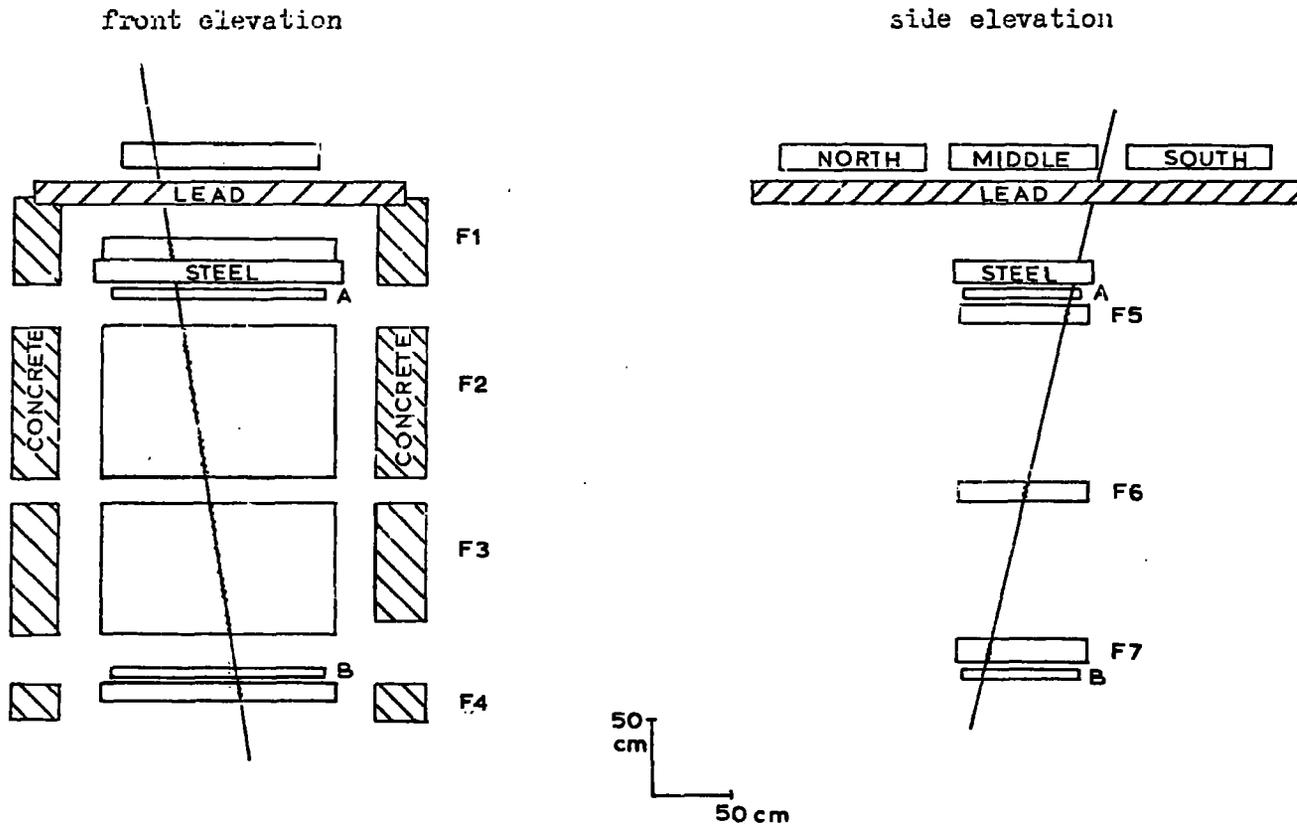
Figure 6.1   The Quark Telescope Experiment

electrode placed between every two layers, in seven trays, each with a
sensitive area of 1.3 m^2. The major measuring trays, F_2 and F_3, contained
58 and 50 layers respectively while the front peripheral trays, F_1 and F_4,
and the side trays, F_5, F_6 and F_7, contained eight layers each. The
electrodes were connected alternately to earth and the high voltage pulsing
unit.

The pulsing unit consisted of a thyristor to trigger one air spark
gap, which in turn discharged a 0.1μF capacitor through a resistor in
parallel with the high voltage electrodes to earth. The capacitance of
the flash tube bank itself was 0.06μF and care had to be taken in
choosing a value for this resistor to give the best high voltage pulse.
By experiment a 100 ohm resistor was used together with a 10 ohm resistor
in series with the flash tubes to reduce 'ringing' on the pulse. The
system gave an easily measurable and reproduceable pulse, a photograph of
which is shown in plate 6.1.

6.1.3 The plastic scintillators

The scintillation counters, A and B, were of the type used by D.A.
Simpson (1968). Each consisted of NE 102A phosphor of dimensions 140 x 75 x
5 cm^3 viewed at each end by three 2 inch photomultipliers through perspex
light guides. The phosphor and the light guides were supported in a light
tight aluminium case, such that a minimum area was in contact with the
supports. This facilitated a more efficient light collection by total
internal reflection.
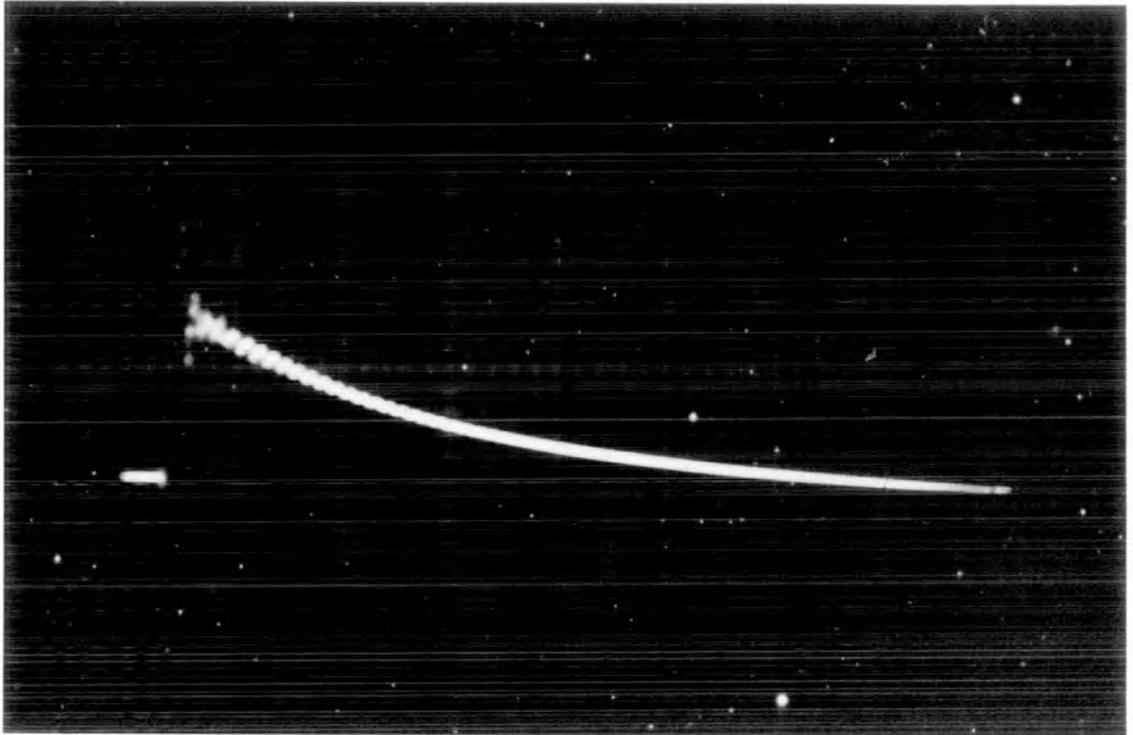
Plate 6.1   The high voltage pulse applied to the flash tube
            electrodes of the Quark Telescope.
            (C.R.O. set at 5kV/cm and 5μs/cm)

Of the six photomultipliers, five were Mullard 53 AVP and one 56 AVP, and resistance values for the dynode had been chosen for high gain. A positive high tension was supplied and negative output pulses of decay time 100 nsecs were taken from the anode. The three output pulses from each side of the scintillator were fed into an emitter follower, the output from which was added to the output from the other side's emitter follower before feeding into the selection electronics. The single particle peaks obtained from scintillators A and B are shown in Figure 6.2 in the form of integral rate-pulse height curves.

6.1.4 The liquid scintillators

The large scintillators used for the air shower trigger were the same counters as used previously with the proportional counter experiment and have been described by Ashton et al (1965). The phosphor in each scintillator was viewed by two photomultipliers (EMI 9583B) which were supplied with a positive H.T. The negative output pulses were taken from the anode and were each fed into a separate emitter follower head unit. The output pulses from these head units were then added for each counter before feeding into the selection electronics.

6.2 The efficiency of flash tubes

6.2.1 Introduction

In an experiment of this type, where one wants to distinguish e/3 charged particles from a multitude of singly charged particles, it is
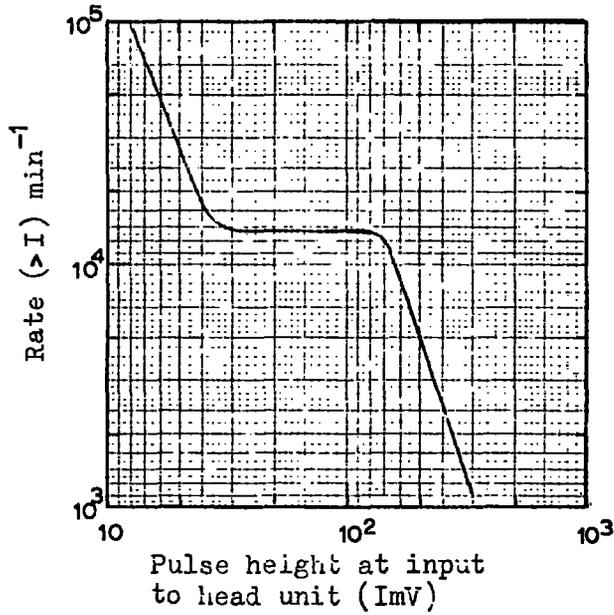
SCINTALLATOR A
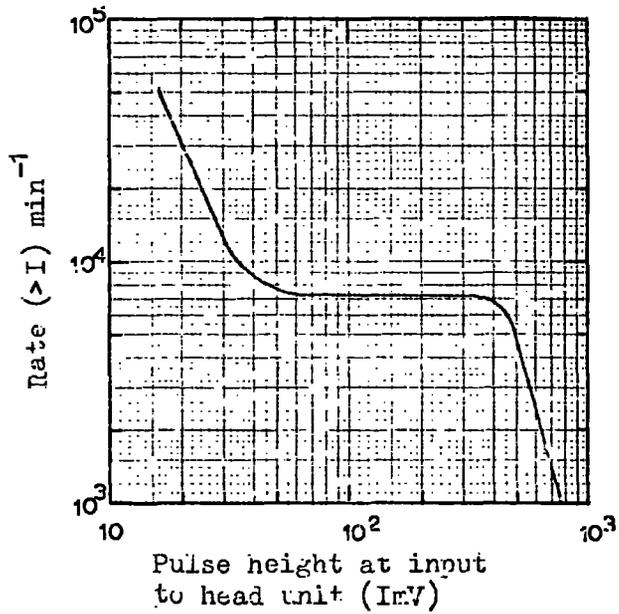
SCINTALLATOR B

Figure 6.2   The single particle peaks obtained from the
plastic scintillators, A and B

imperative that one knows, accurately, the efficiency of the flash tubes for e/3 and e, and moreover, that the width of the distribution for charge e is well defined.

6.2.2 Measurement of the efficiency-time delay curve

By demanding coincident pulses from A and B of size greater than 0.4 times the single particle peak (i.e. in the notation used A(> 0.4), B(> 0.4)) one can select single muons that traverse the stack. The rate of single particles through the telescope was measured to be 10 sec^{-1} compared with 8 sec^{-1} calculated from the 1.05 m^2 scintillator area and the 250 cm telescope arm.

It is imperative at this high rate that no trigger should be allowed to occur with two nontemporal tracks, as the efficiency of flash tubes is markedly dependent on the time interval between the traversal of the particle and the high voltage pulse. One can insure against this by using an anti-coincidence gate, the circuit of which is given in Appendix A. The mode of operation of this type of circuit is described in Section 4.1., but basically, it will paralyse the electronics for 300 msecs. after one particle has traversed the telescope.

The coincident pulse from A and B is thus fed through the anti-coincidence gate before being allowed to trigger the spark gaps or start the cycling system. When the first coincidence is registered this will fire the flash tubes and start the cycling system, which in turn winds on the cameras and allows the high voltage capacitor to recharge, whilst paralysing

the electronics. At the end of this cycle of approximately 7 seconds, the experiment will become sensitive again, but only if there has not been a particle in the previous 300 msecs.

Measurements of the efficiency of the flash tubes were taken for various time delays and the distributions obtained for some of the delays used are shown in Figure 6.3. The means of these efficiencies were plotted on the efficiency-time delay curve (Figure 6.4). It can be seen that the distributions in efficiency get broader for the longer time delays. For theoretical reasons shown below, it was decided that the time delay which appeared to have the best compromise between width and e- e/3 separation was 20 μs.

6.2.3 Single particle calibration run

Having selected 20 μs to be the optimum delay for this experiment, 1,000 tracks were measured at this delay. The distribution in efficiency obtained is shown in Figure 6.5. The mean layer efficiency at this delay for singly charged particles (muons) was found to be $84.4 \pm 0.2\%$ with a standard deviation on the distribution of $\sigma = 0.6$.

Examples of the typical and 'untypical' single particles obtained in this run are shown in Plates 6.2 and 6.3. It must be noted that only tracks with no serious complications, such as that shown on Plate 6.2, were measured. Care had to be taken in cases such as multiple scattering, that the increase in track length through the telescope was taken into account.
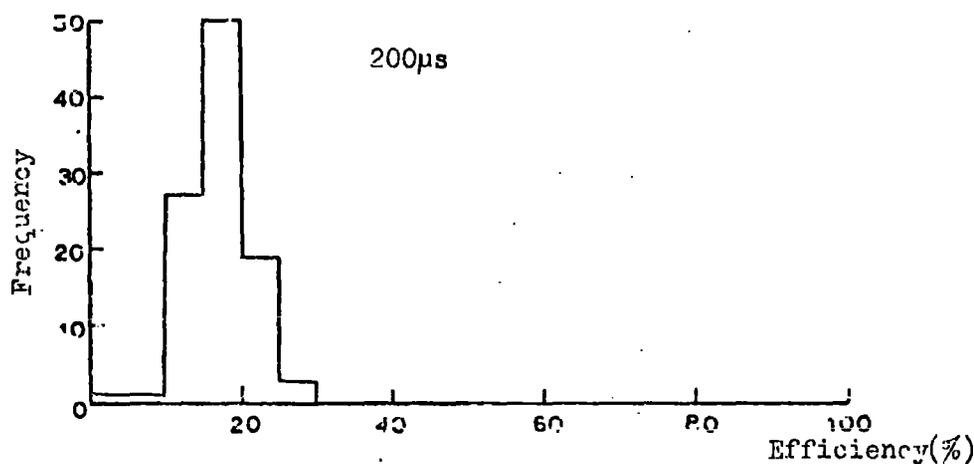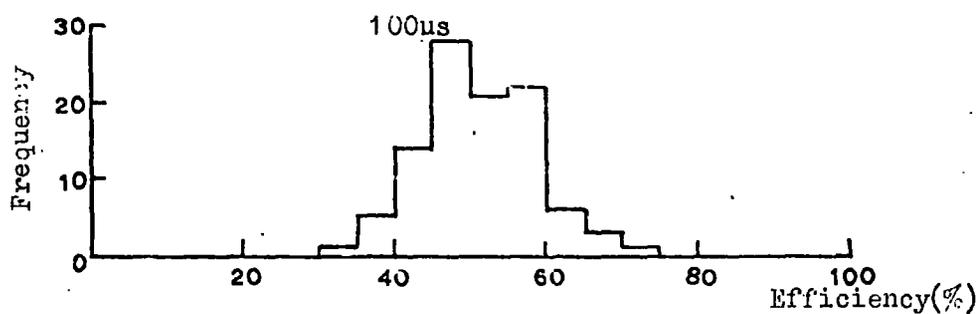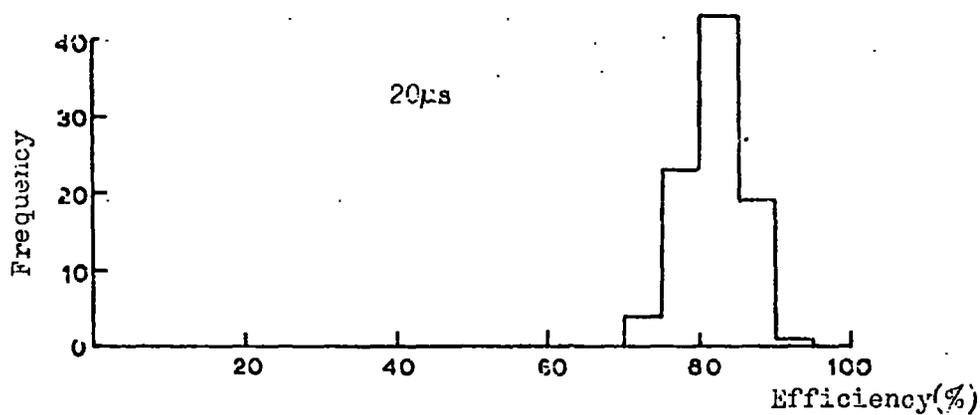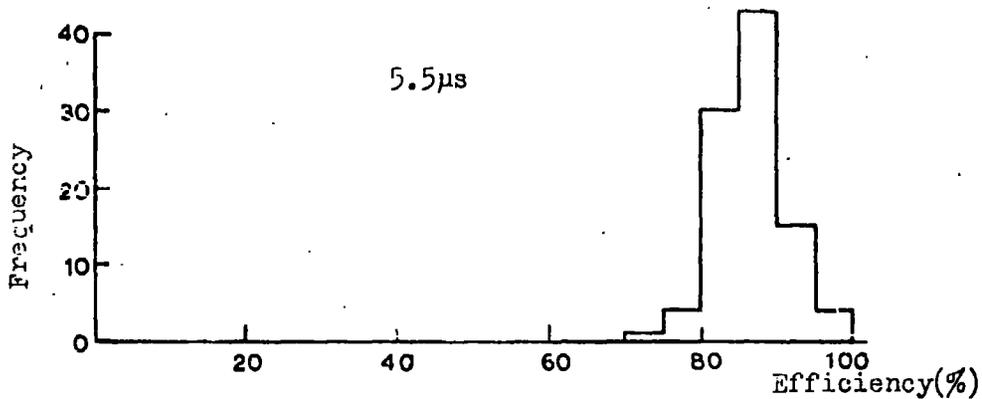
Figure 6.3 The distributions in efficiency of F_2 and F_3 for various
          time delays.

6.2.4 <u>The theory of flash tube efficiency</u>

Lloyd (1960) has applied a rigorous theoretical treatment to the production and recombination of the discharge electrons to explain the efficiency-time delay curves for neon flash tubes. He gives a plot of expected internal efficiency against $\frac{Dt}{a^2}$ for $\frac{Dt}{a^2} < 0.2$ with afQ as a parameter,

where D is the diffusion coefficient for thermal electrons at the

relevant pressure

a is the internal radius of the flash tube

f is the probability of one electron in the tube initiating a

discharge

and Q is the probability of producing a free electron per cm of gas. For $\frac{Dt}{a^2} > 0.2$ he also gives a universal curve of internal efficiency against $afQ \cdot \exp\left(-\beta^2 \frac{Dt}{a^2}\right)$. This curve is the theoretical foundation for the empirical rule found by Coxell and Wolfendale (1960), for if a is a constant and fQ almost so, the efficiency depends only on Dt, i.e. on $\frac{t}{p}$.

From the latter curves, layer efficiency and time delay curves can be derived for the flash tube stacking used here and for various values of afQ. The experimental curve can then be compared with these to find the appropriate value of afQ for the flash tubes used (Figure 6.4). As can be seen from Figure 6.4 there appears to be some inconsistency between the experimental points for layer efficiency and the curves derived from Lloyd's theory. The inconsistency appears to be greatest at short time

delays where Lloyd's theory is the more complex. No precise value of afQ for the flash tubes could be allocated, but a range of values, in which the experimental points lay, was taken. The boundary values for afQ shown in Figure 6.4 were then, afQ = 24 and 12 with the best fit at afQ = 16, which appears as the broken line in the diagram.

In selecting sub-e charged particles, for a given set of flash tubes, the only variable parameter is Q. Since Q is proportional to $(z)^2$, the value for afQ for these flash tubes and for e/3 will be 24/9, 16/9 and 12/9. The efficiency curves produced by these parameters have been included in Figure 6.4. and it can be seen that the optimum time delay is 20 µs.

The values for the expected efficiencies for e/3 on the two boundary conditions and at 20 µs was found to be 54% and 45% compared with the measured layer efficiency of 82% for single charge muons. These boundary conditions are shown on the single particle distribution (Figure 6.5). It can be seen that one would expect to see charge e/3 quarks to a level of greater than 1 in 1,000 charge e.

6.3 The air shower trigger

In an experiment of this type, where one is interested in looking at events close to the core of an air shower, it is advisable to have an array of detectors with which one can locate the position of the core and measure the size of the initiating core. It is possible to select showers using either one or several detectors close together, but this will only give information on the shower density at the specific point.
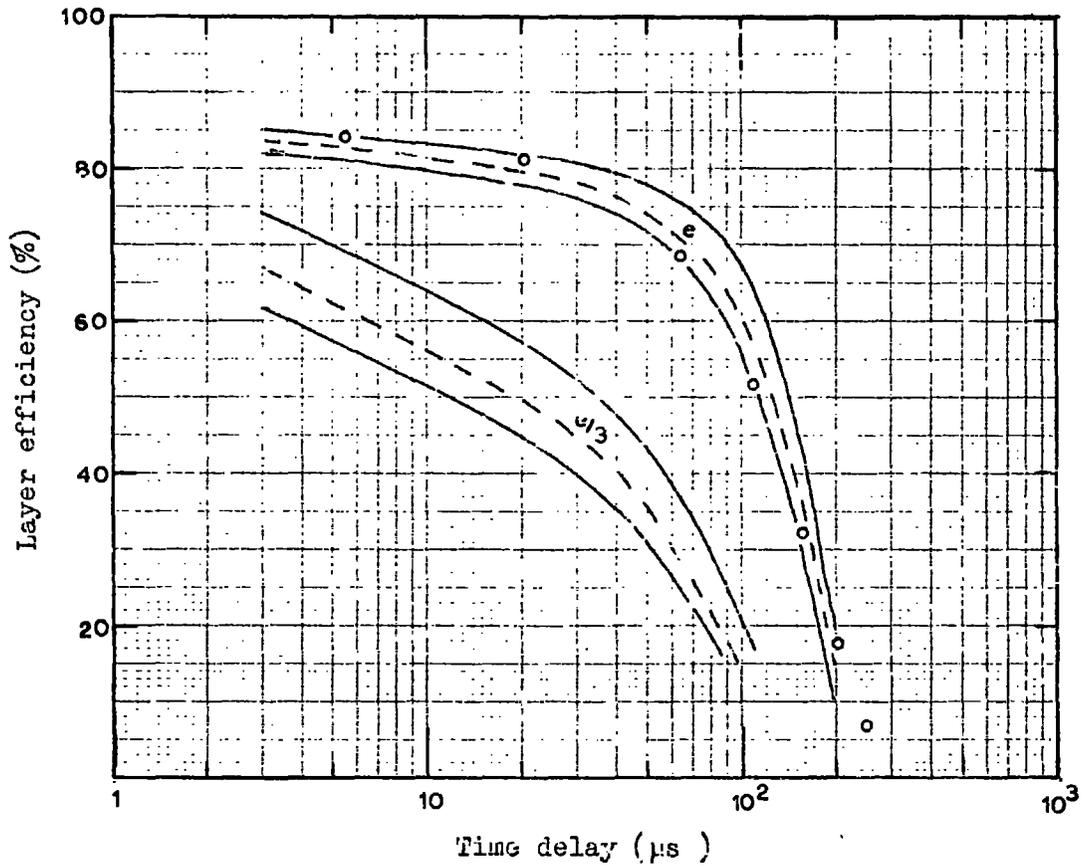
Figure 6.4 The experimental efficiency-time delay curve compared
with the curves of Lloyd for A'q of 24,16 and 12, and
with the expected curves for charge e/3.
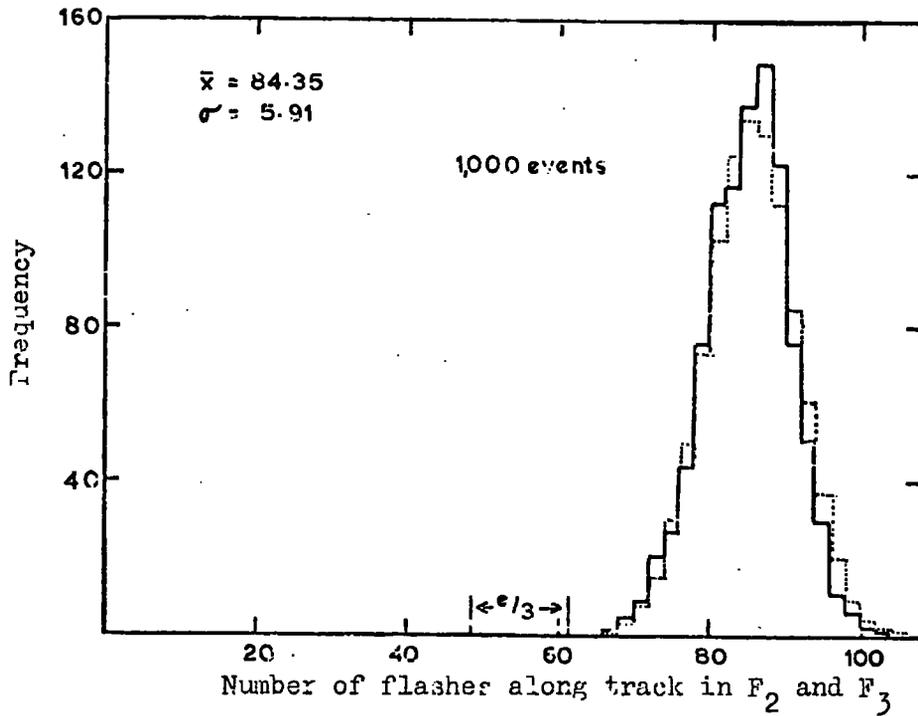
Figure 6.5   The distribution in flash tube efficiency of F_2 and F_3
           for 1,000 single muons of median energy 2.6GeV.

Plate 6.2

1. Single penetrating particle.

2. Multiple scattering.

3. Forward knock-on.
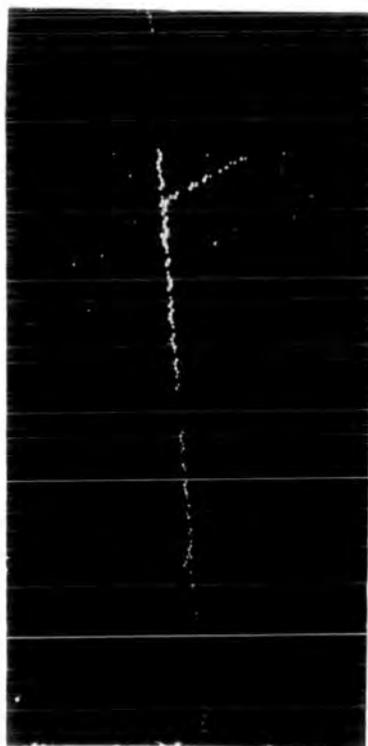
4. Backward knock-on.

Plate 6.3

5. Interaction in iron.

6. Interaction in flash tubes.
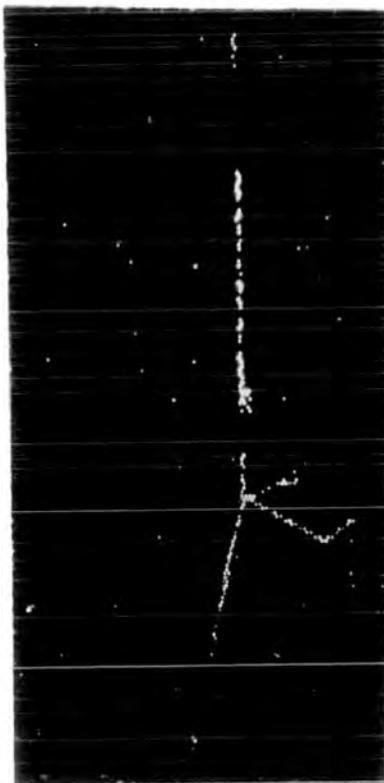
7. Interaction in flash tubes.

8. Interaction in flash tubes.

As can be seen in Figure 6.1 the system used here comprised three large scintillators mounted directly above the flash tube telescope. It was necessary to find out experimentally whether this system would detect showers adequately using one or all three scintillators in coincidence.

6.3.1 The single scintillator run

The response of single scintillators to air showers has been studied by numerous people including Brennan (1957), and Green and Barcus (1959). The density at which the 'single particle' distribution meets the air shower spectrum must be determined.

Pulses were taken from the middle scintillator (M) and selected so that the integral rate distribution could be measured. These pulse sizes could then be expressed in terms of density of particles in the scintillator as it had been previously calibrated using a small scintillator telescope. The integral density spectrum obtained from this scintillator is shown in Figure 6.6. Since the air shower density spectrum is shown by Galbraith (1958) and Cocconi (1961) to have an exponent $\gamma \sim 1.4$ it can be seen that one has to go to very high particle densities (> 300 m^2) in this scintillator before one reaches the air shower spectrum.

6.3.2 The three scintillator run

The integral spectrum obtained, using the three scintillators, N, M and S was found to have an exponent of $\gamma = 1.49$ and is shown in Figure

6.6. This spectrum was derived from data accumulated in two runs in which the selection was greater than 10 particles in each scintillator (N(> 10), M(> 10), S(>10)) and greater than 40 particles in each scintillator (N(> 40), M(> 40), S(> 40)).

This exponent agrees with the air shower data when one considers that the observations probably straddle the 'knee' in the density spectrum at $N = 10^5$ to 10^6 where the slope changes from $\gamma = 1.32$ to 1.58. However, not enough data was obtained to see this change of slope and the best fit through the whole of the data was drawn.

6.3.3 The distribution in density in the three scintillators for an air shower trigger

When the pulse heights in each scintillator were measured for each trigger in the air shower run some very interesting results were found. These pulse heights, in terms of particle density, for each trigger are shown in Figures 6.7 and 6.8 for the two runs (> 10) particles and (> 40) particles respectively. It can be seen that the densities measured in each scintillator in one event can be very unequal.

The air shower triggers can then be classed into 5 types as shown in Figures 6.9 and 6.10 according to the distribution in densities in N, M and S. Events with a slope to the North or a slope to the South can be caused by the position of the core, and one would expect events with a flat distribution. However, events with an excess or a deficiency of particles in the middle would suggest that the air shower has some structure, particularly at the percentage rates seen here. This has not
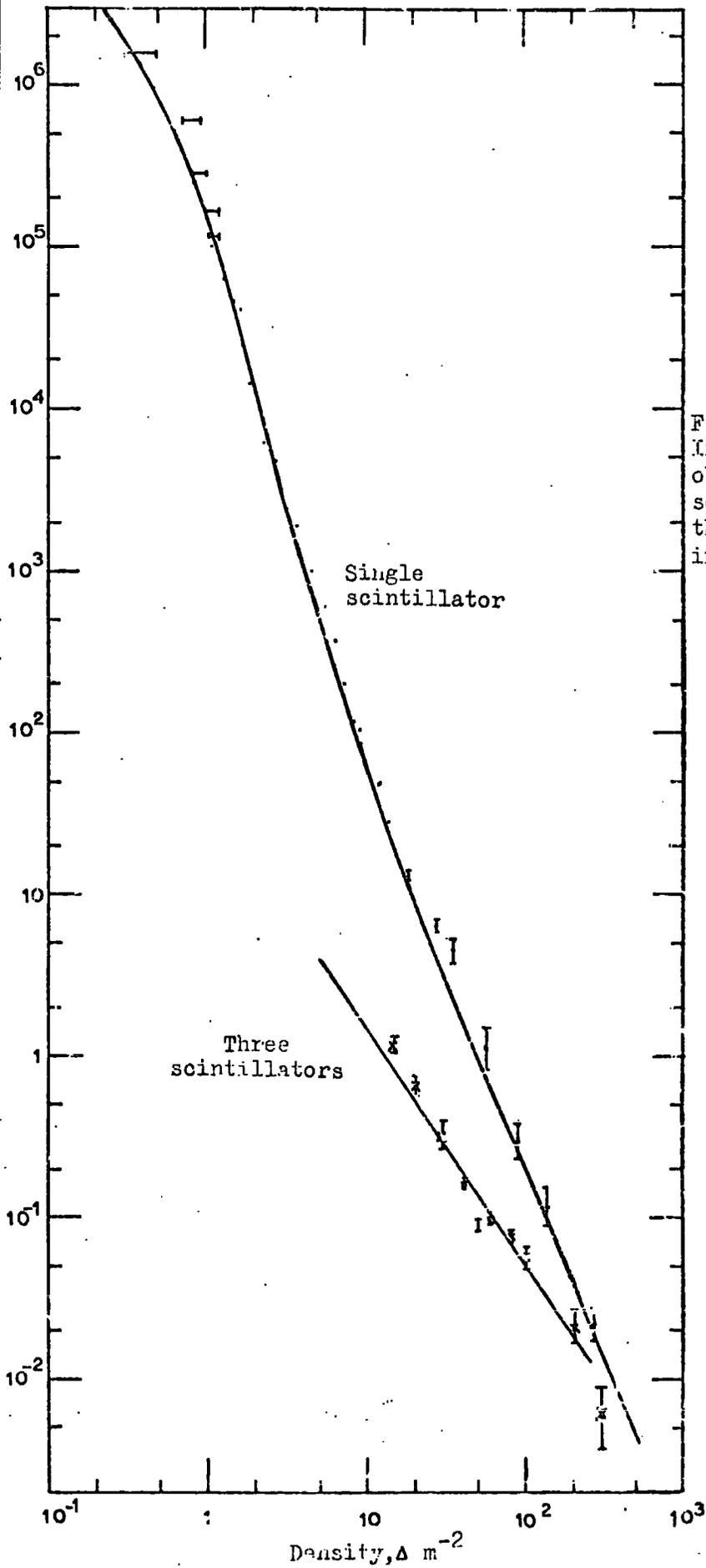
Figure 6.6
Integral density spectra
obtained using a single
scintillator and using
three scintillators, N, M, & S,
in coincidence.

Single
scintillator

Three
scintillators

Density, Δ m^{-2}
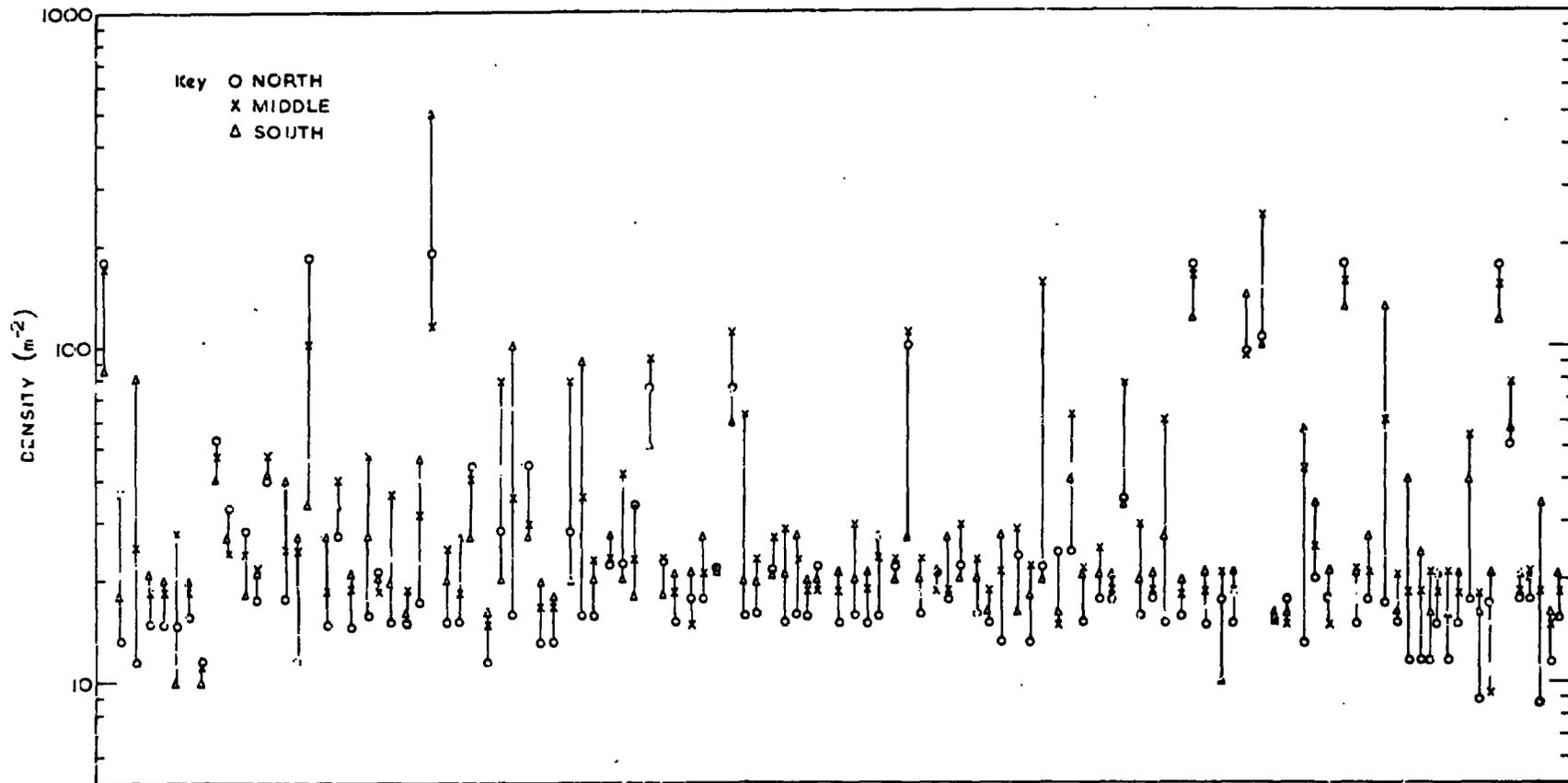
Figure 6.7 The air shower selection system.
The density of particles in scintillators North, Middle
and South for each event of an air shower trigger of
>10 particles in each scintillator,
i.e. $N(>8.8) \cdot M(>9.2) \cdot S(>10)$
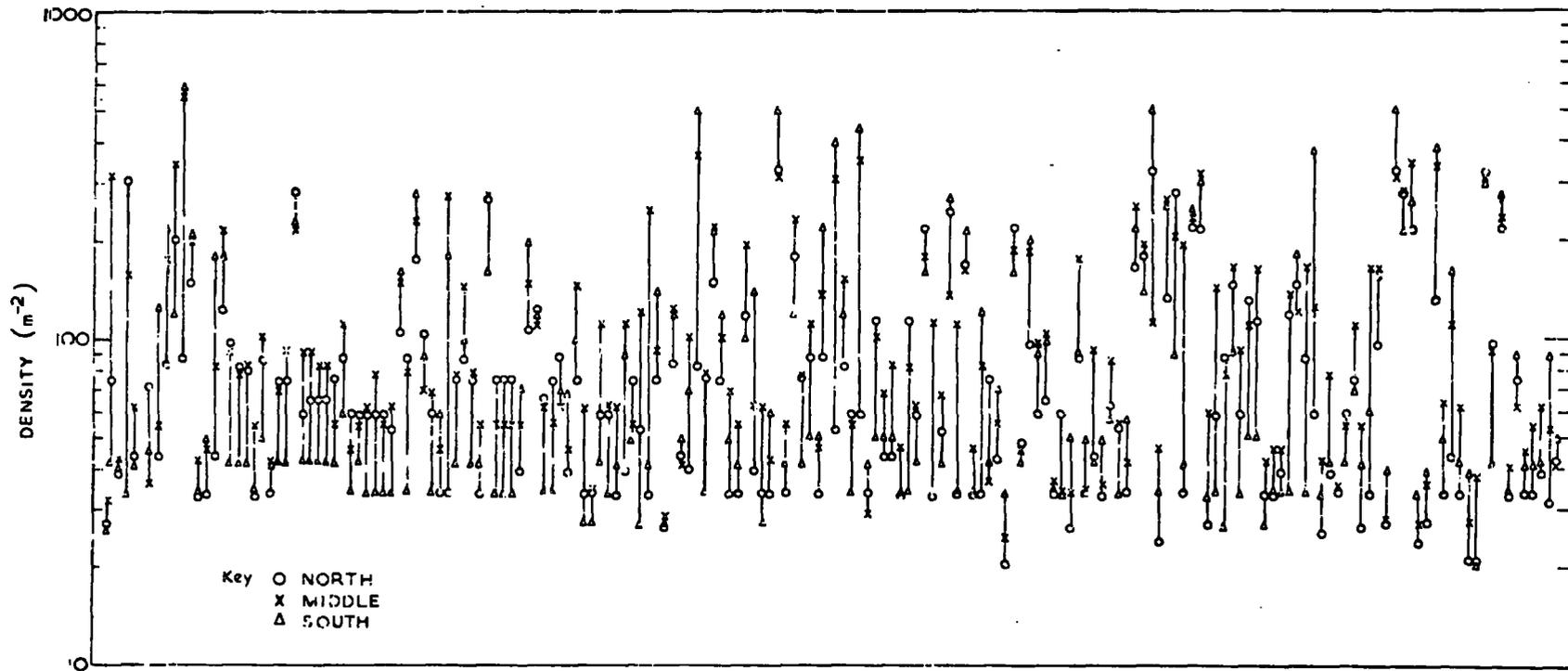
Figure 6.8 The air shower selection system.
The density of particles in scintillators North, Middle
and South for each event of an air shower trigger of
⩾40 particles in each scintillator,
i.e. N(> 35).M(> 37).S(> 40)

been observed by other workers e.g. Heineman (1954) at these high
percentages. One can suggest that this is either due to the 'thick'
scintillator producing bursts in the phosphor, or that the errors in
the density value are much larger than calculated.

6.4 The total experiment

6.4.1 The electronics

A block diagram of the logic system used is shown in Figure 6.11. It
can be seen from this diagram that coincident pulses from the liquid
scintillators, of a level set by the discriminators, will trigger the
oscilloscope, fire the high voltage pulse and start the cycling system.
In addition, there is a proviso, which can be removed, that there must
be coincident pulses in the plastic scintillators A and B.

The pulses from N, M and S were delayed by 3, 6 and 9 µsecs
respectively, and displayed at various amplifications on three beams of
a four beam oscilloscope. This allowed the widest possible range of
densities to be measured. The pulses from A and B were displayed on
the fourth beam together with the coincident pulse after it had negotiated
the previous particle gate. Thus any air shower trigger which was accom-
panied by a previous particle would be marked by the absence of a
coincident pulse from A and B.

6.4.2 Previous particles

From the efficiency-time delay curve (Figure 6.4) the time for the
efficiency to fall to the minimum definition of a track, is approximately
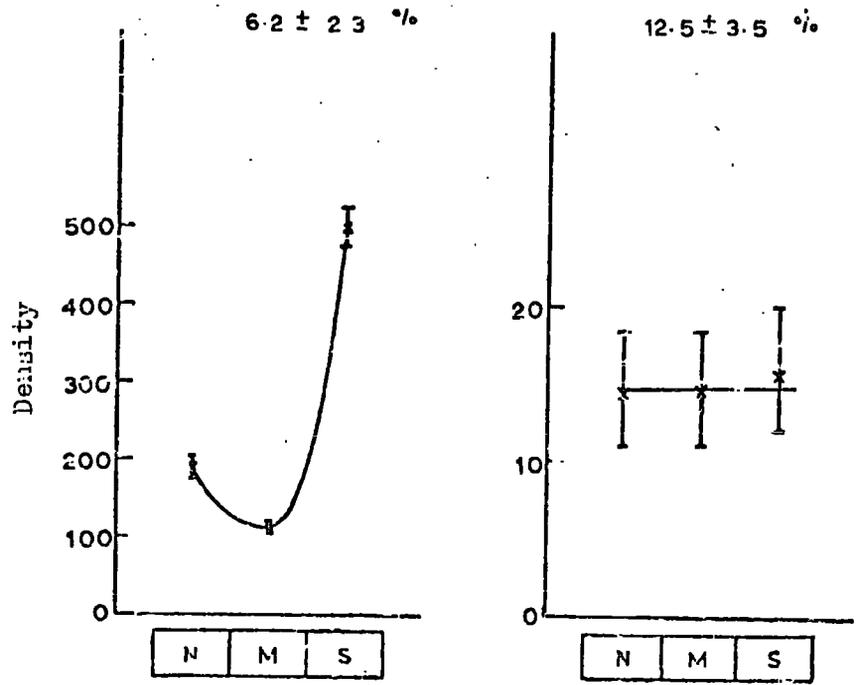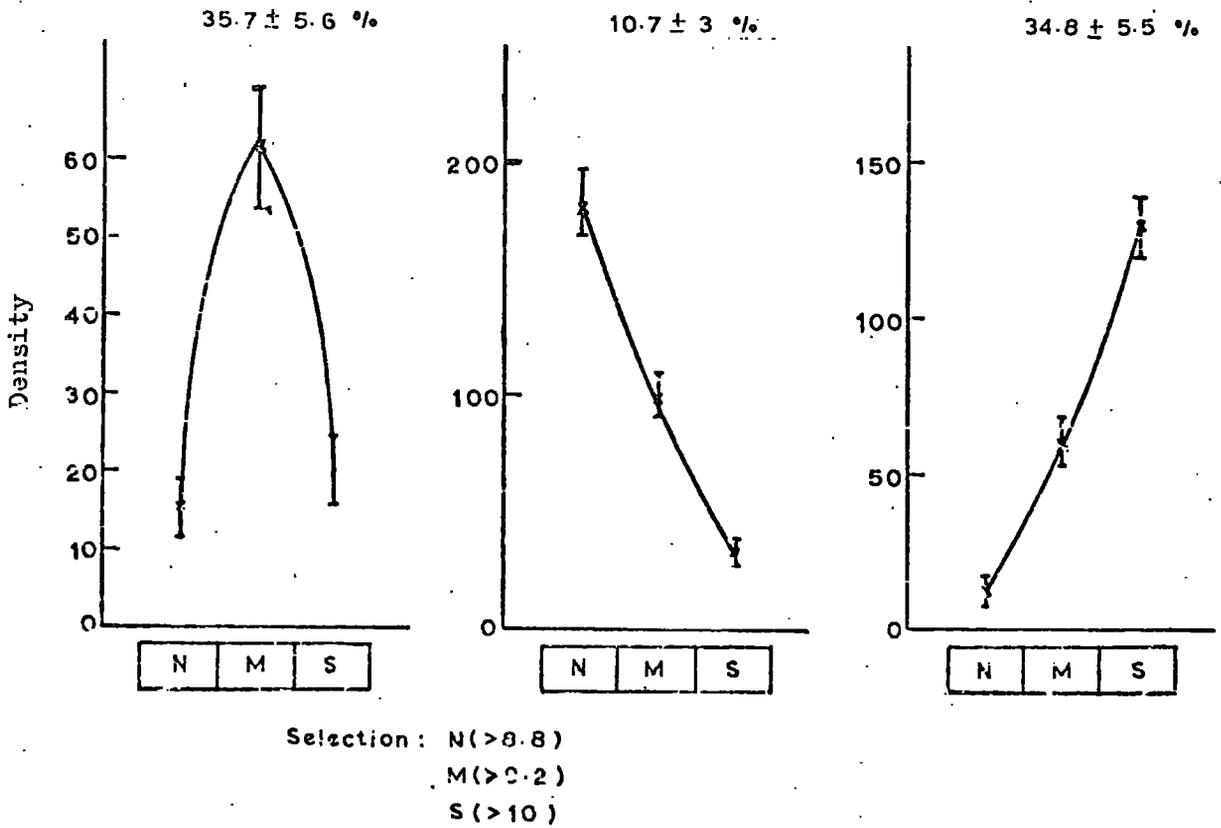
Figure 6.9 Examples of the various types of air shower triggers in the liquid scintillators and their relative frequency.
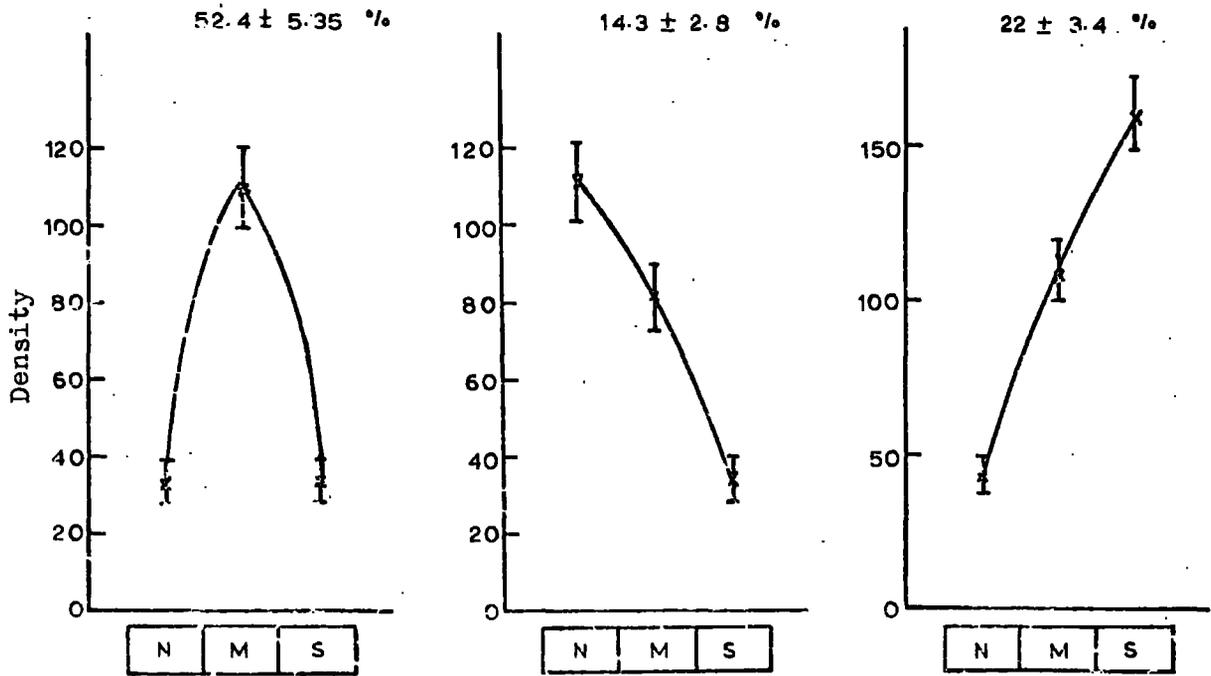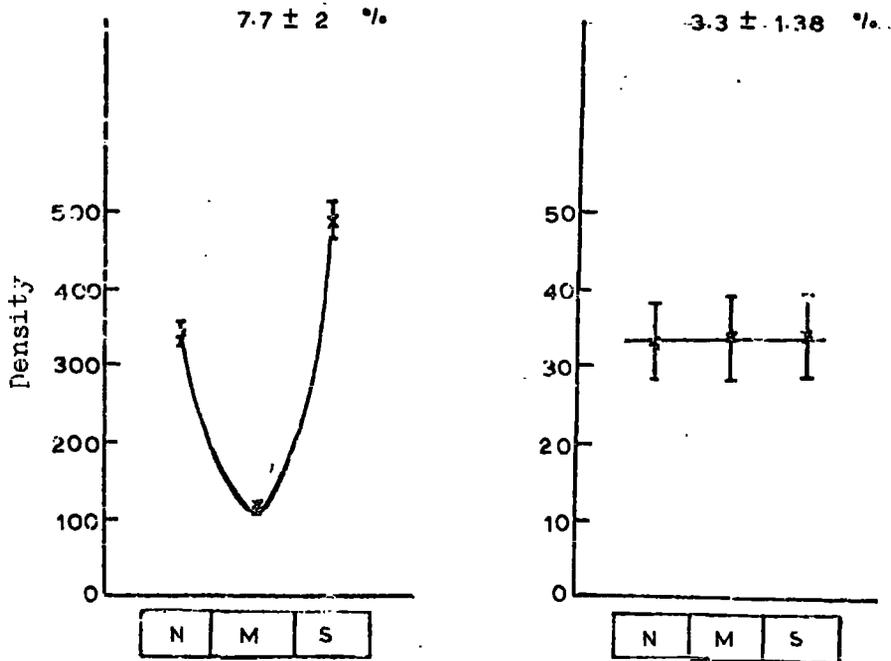
Figure 6.10   Examples of the various types of air shower triggers in
the liquid scintillators and their relative frequency.
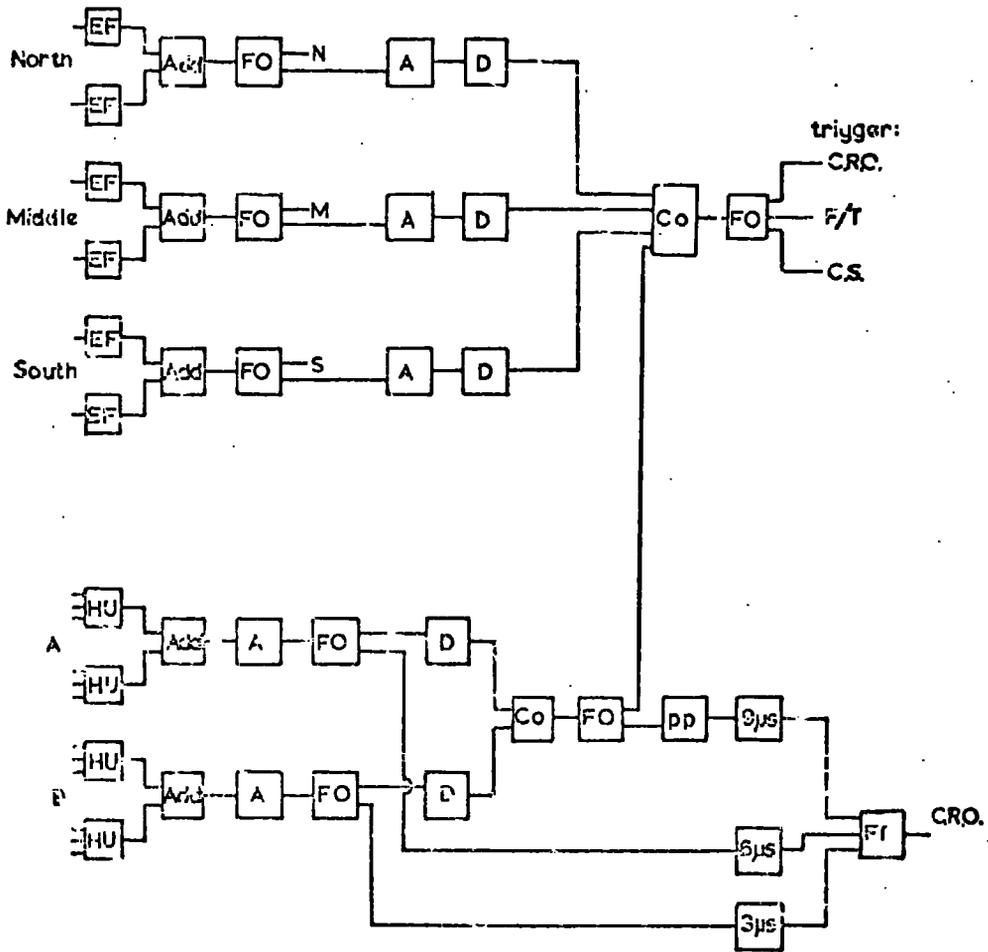
Key:

A   amplifier   FI   fan in
Co coincidence   FO   fan out
D   discriminator   pp   previous particle gate
EF emitter follower
            F/T   flash tube trigger
            C.S. cycling system trigger

Figure 6.11   Block diagram of the electronics used in the
              Quark Telescope air shower run.

200 μs. The number of triggered air shower events for a previous particle to be within this 200 μs., for a rate of muons through the telescope of 10 sec^{-1}, will be 500. It is important, therefore, that these 200 μs are carefully guarded with the previous particle gate.

The circuit used is shown in Appendix A. The coincident pulse from A and B to be displayed on the CRO was gated by a 200 μs pulse, triggered by the same coincidence but delayed by 3 μs. A normal event would therefore display the coincident pulse on the fourth beam of the CRO whereas a previous particle event would have the pulses from A and B alone. It is still possible that a particle will come between the 23 μsecs before and during the high voltage pulse. This cannot be guarded electronically as the noise produced when pulsing the flash tubes requires the electronics to be inoperative. The only possible way to distinguish these tracks is from the angle between the track and the air shower. It is very unlikely that the arrival directions will be the same.

6.4.3 The selection system

Care was taken to achieve the most advantageous selection system in terms of rate of air shower triggers and yield of measurable tracks, through the telescope. Several types of selection were tried, varying the density demanded in the liquid scintillators with, or without a coincidence with A and B. A table of rates and yields obtained is shown in Table 6.12. It must be noted that the figures on the yields of tracks quoted in this table denote the number of observable tracks per trigger,

i.e. the number of tracks per trigger that are well defined and measurable in F_2 and F_3. Tracks that were out of geometry and missed, say, part of F_3, and tracks that were obscured by the density of other tracks could not be included.

As can be seen from this table there is little difference between any of the selection systems, although the yield is increased slightly by demanding a coincidence from A and B. It was decided, therefore, to use the selection of run QT3, which demanded greater than 50 particles in each of N, M and S, in coincidence with a pulse of greater than 1/50th of the single particle ionisation in A and B. With this selection one could choose events which were close to the core and yet be able to fire on the passage of a single quark. However, this event would always be doubtful, as it could be caused by a 'post' particle i.e. a particle on the falling edge of the high voltage pulse.

The expected rates of events would then be one air shower trigger every 10 mins. and an event with an average of 1.7 measurable tracks every hour.

6.4.4 Analysis of data

The data for each event was recorded on three films, two for the flash tube views and one for the CRO. These films were scanned and the events classified.

Normally only the front view and CRO film were analysed due to the difficulty of interpretation of the side view. This view was kept in

reserve for anomalous events. The front view was scanned first, and only events which had observable tracks, as defined above, were subjected to further analysis. The number of flash tubes which fired on each track was counted for trays F_1 to F_4, and the angle of the track to the vertical was measured, and a small scale diagram of the event was drawn. The CRO film was then scanned and the pulse heights in N, M and S and A and B, together with the gate pulse were measured.

It was thought advisable that the information on flash tube efficiency of the tracks should be divided into two categories, namely those tracks which showed evidence of a parallel track, and tracks that were either unaccompanied or definitely not parallel to the main body of muons. The latter class of tracks is likely to be caused by low energy particles, which have suffered serious scattering, or previous particles. In either case the efficiency of the flash tubes to these particles is likely to be different from the norm and might be mistaken for a particle of lower charge.

6.5 The air shower run

The experiment, proper, was run with the selection of QT3 for a total sensitive time of 162 hours. 760 air shower triggers occurred during this time and 240 tracks were measured in the front view. Figures for the rates and yield of the total run are shown in Table 6.12.

Photographs of the various types of events that were observed, as well as some of the more interesting events are shown in plates 6.4, 6.5 and 6.6.

SELECTION		Running time (hrs)	Total no. of triggers	Rate of triggers (hr^{-1})	No of triggers with 'n' observable tracks (Rate hr^{-1})				Rate of measurable tracks (hr^{-1})	Ratio of measurable to total triggers
					1	2	3	4		
QT1	N(>100).M(>100).S(>100)	7.05	29	4.2±0.6	2 (0.3)	1 (0.14)	0 (0)	0 (0)	0.43±0.24	0.1±0.07
QT2	N(>50).M(>50).S(>50)	15.13	113	7.5±0.6	9 (0.6)	10 (0.7)	1 (0.07)	1 (0.07)	1.4±0.3	0.19±0.05
QT3	N(>50).M(>50).S(>50) ·(A(>0.02).B(>0.02))	15.15	94	5.2±0.6	11 (0.7)	4 (0.3)	3 (0.2)	1 (0.07)	1.3±0.2	0.21±0.05
QT5	N(>50).M(>50).S(>50) ×(A(>0.4).B(>0.4))	36	148	4.1±0.3	22 (0.6)	11 (0.3)	7 (0.2)	2 (0.08)	1.2±0.2	0.29±0.07
QT4	N(>20).M(>20).S(>20) ×(A(>0.02).B(>0.02))	5.05	73	14.5±1.7	13 (2.6)	3 (0.6)	0 (0)	0 (0)	3.2±0.8	0.22±0.08
QT6	N(>20).M(>20).S(>20) ×(A(>0.4).B(>0.4))	3.83	27	7.0±1.4	6 (1.5)	1 (0.3)	0 (0)	0 (0)	1.8±0.7	0.26±0.15
A.S. run QT3,7,8,9	N(>50).M(>50).S(>50) ×(A(>0.02).B(>0.02))	162.36	750	4.68±0.17	128 (0.78)	29 (0.18)	14 (0.09)	3 (0.02)	1.07±0.08	0.23±0.02

Table 6.12   Comparison of the rate of triggers and yield of measurable tracks for various selection systems, including the final air shower run.

Plate 6.4
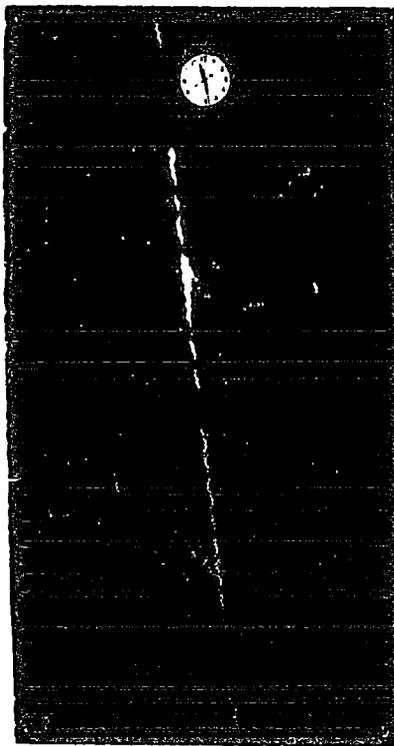
9. 1 penetrating particle
   traversing all telescope.
   $N=60m^{-2}, M=74m^{-2}, S=120m^{-2}$.
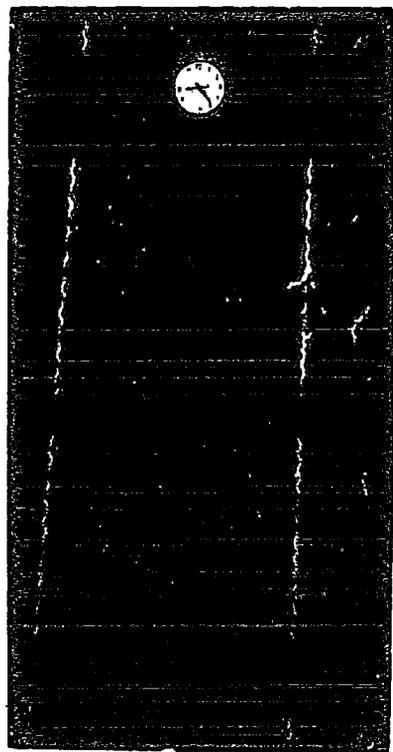
10. 2 penetrating particles
    traversing all telescope.
    $N=160m^{-2}, M=270m^{-2}, S=490m^{-2}$.
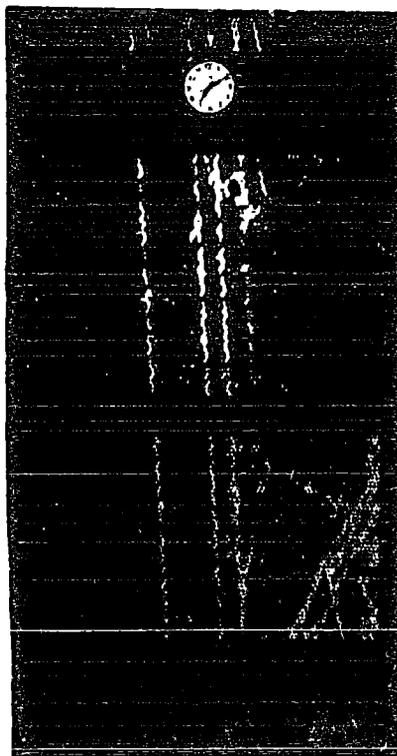
11. 3 penetrating particles
    traversing all telescope.
    $N=150m^{-2}, M=150m^{-2}, S=190m^{-2}$.
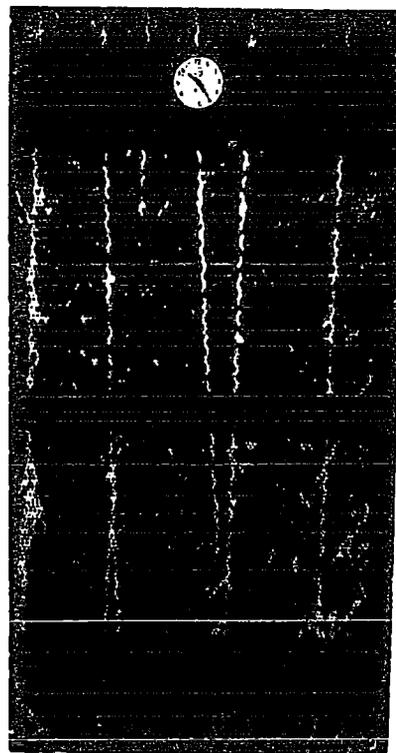
12. 4 penetrating particles
    traversing all telescope.
    $N=73m^{-2}, M=76m^{-2}, S=55m^{-2}$.

Plate 6.5

13. Low energy interaction
in lead shield.
N=50m^{-2}, M=120m^{-2}, S=60m^{-2}.

14. High energy interaction
in lead shield.
N=60m^{-2}, M=80m^{-2}, S=70m^{-2}.
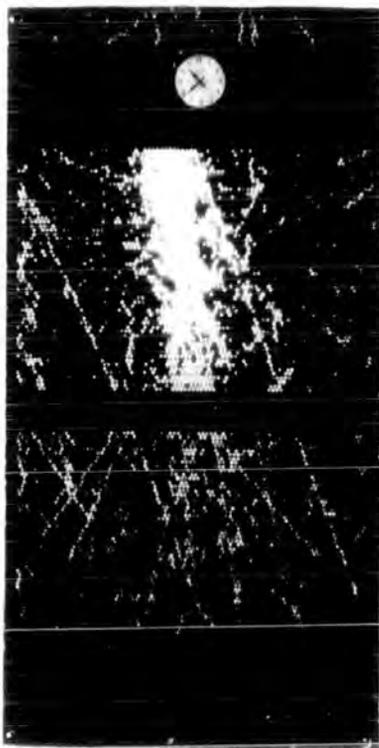
15. Interaction in iron.
N=37m^{-2}, M=37m^{-2}, S=160m^{-2}.

16. Interaction in flash tubes
with backward secindary or decay
of heavy mass particle.
N>350m^{-2}, M>370m^{-2}, S>400m^{-2}.

Plate 6.6
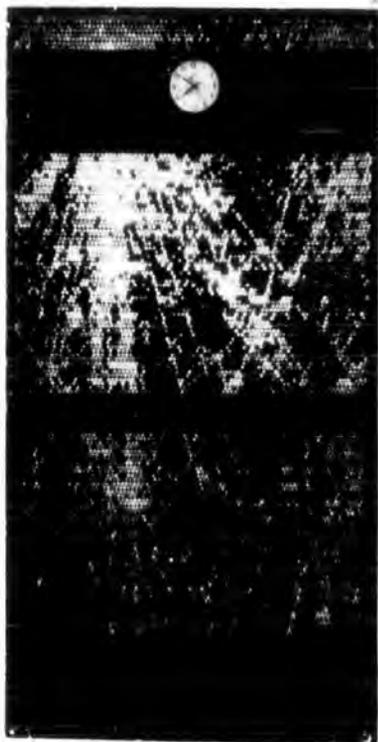
17. Low energy hadron with
    electron accompaniment.
    $N > 300m^{-2}, M > 170m^{-2}, S > 150m^{-2}$.
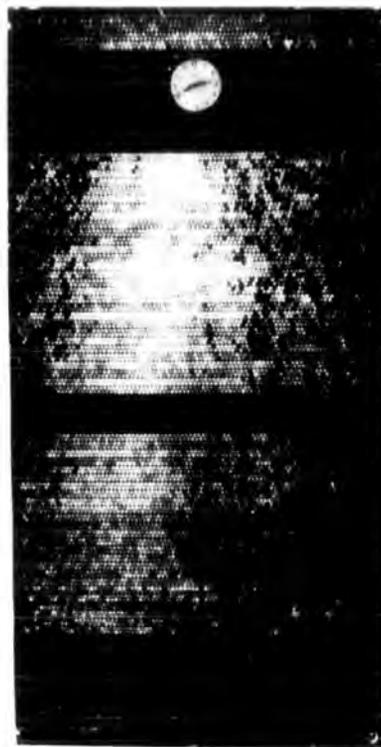
18. High energy hadron with
    electron accompaniment.
    $N = 260m^{-2}, M = 400m^{-2}, S = 420m^{-2}$.
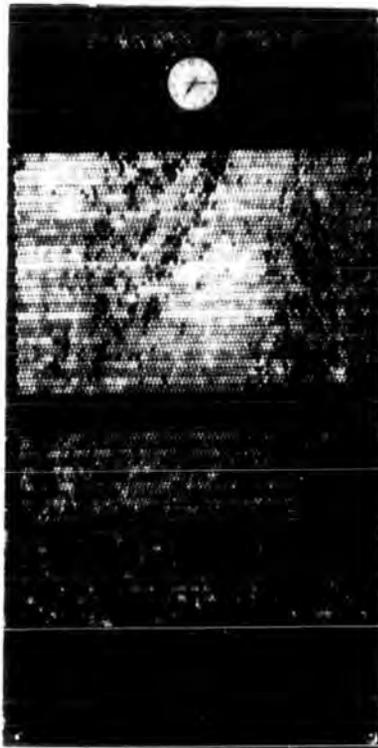
19. Two high energy hadrons
    with electron accompaniment.
    $N = 70m^{-2}, M = 300m^{-2}, S = 380m^{-2}$.

20. Several penetrating
    particles.
    $N = 228m^{-2}, M = 460m^{-2}, S = 450m^{-2}$.

The interpretation of the results obtained is dealt with in Chapter 7, but the distributions in efficiency obtained for all tracks and for parallel tracks only are shown in Figure 6.13 and 6.14. No evidence was found for a difference in efficiency between single and parallel tracks; the medians of these distributions were 91.6 ± 0.4 and 91.25 ± 0.5 respectively. Neither was there any evidence of fractionally charged particles, and the expected efficiency for e/3 charge was well separated from the main distribution i.e. by 6σ.
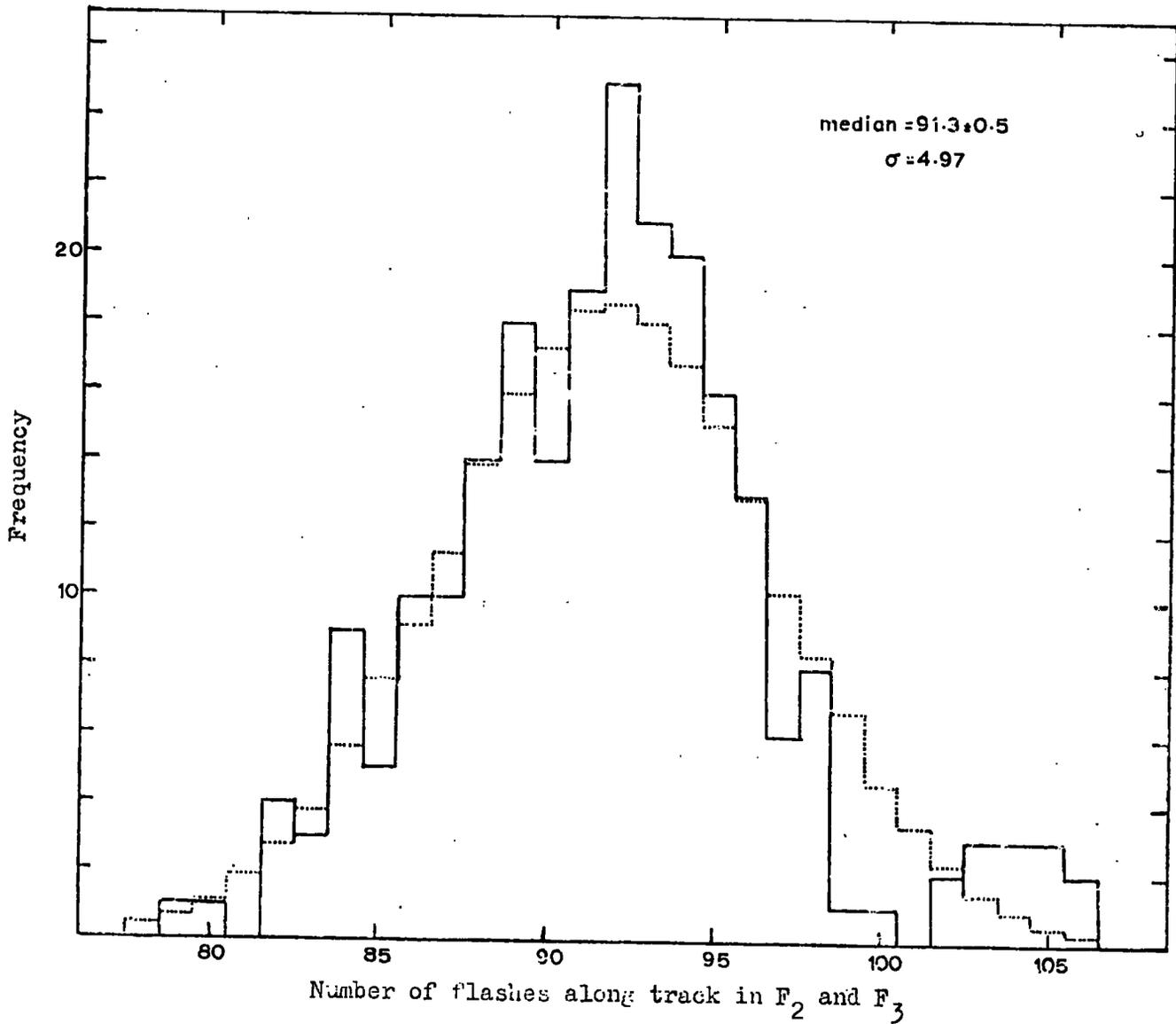
Figure 6.13 The distribution of flash tube efficiency of F_2 and F_3 for all the tracks measured in the air shower trigger. (The dotted curve represents a Gaussian fit)
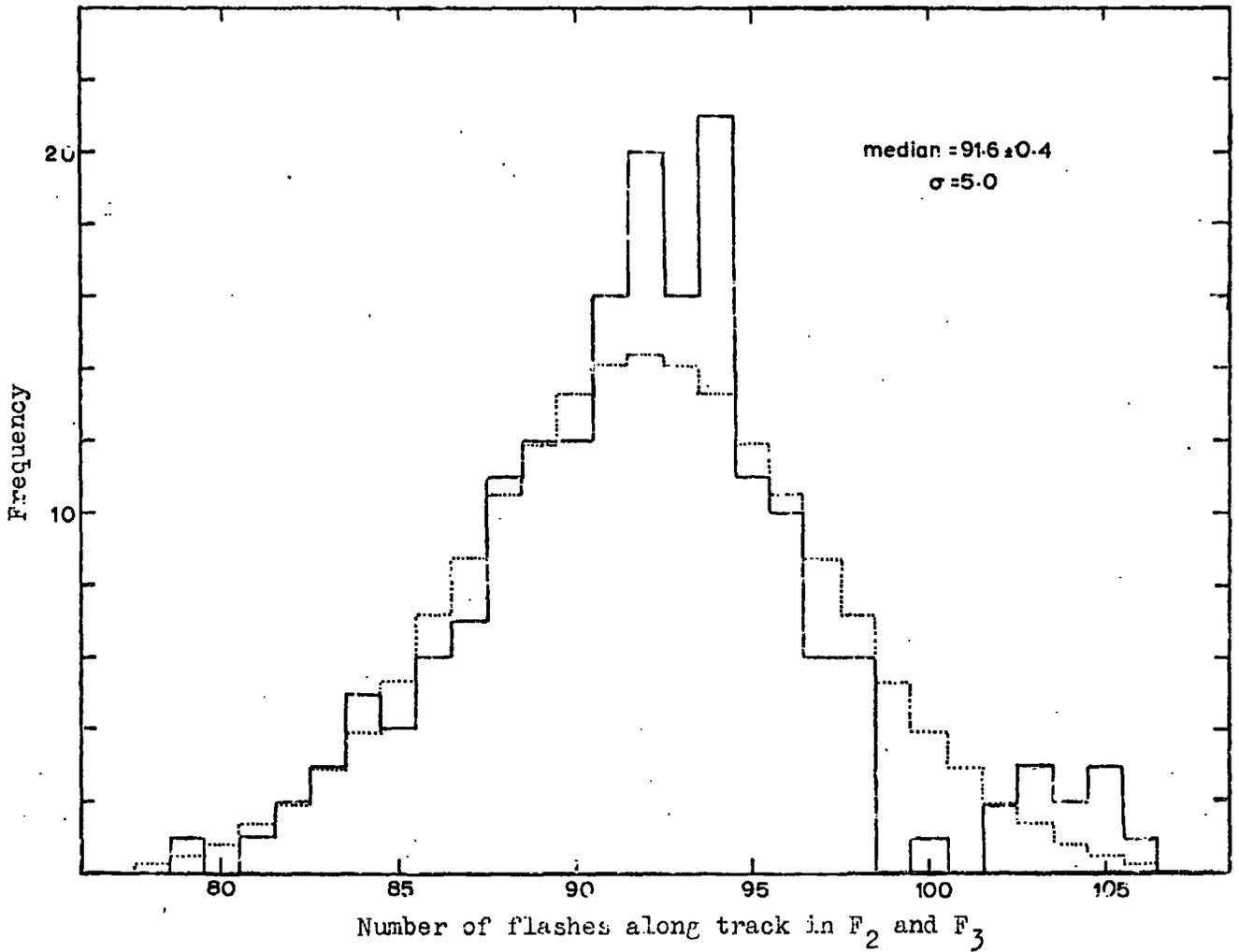
Figure 6.14   The distribution of flash tube efficiency of F_2 and F_3 for
all measured tracks in the air shower trigger which have
evidence of a parallel track.
(The dotted curve represents a Gaussian fit)

CHAPTER 7

THE RESULTS OF THE AIR SHOWER EXPERIMENT AND THEIR
INTERPRETATION

7.1 General

The distributions in efficiency obtained from the air shower run

and the two calibration runs, which were performed before and after the

air shower run, are shown in Figure 7.1. The expected position for

e/3 charged particles of the same γ as the calibration muons, $(e/3)_{min}$,

and for quarks of the same γ as the air shower muons, as calculated

below, $(e/3)_{plat.}$, is also shown in this figure. As can be seen, in the

174 air shower triggers examined, there is no evidence for an e/3

charged particle. However, there is a marked increase in efficiency for

the air shower tracks, 7.1 + 0.6% in the median value and 5.5 + 0.6%

in the mole. This increase is a real effect because the two calibration

efficiencies 'straddle' the air shower run and have the same efficiency

within experimental errors.

There are several effects that could cause a difference in efficiency

between the calibration and air shower tracks. If the calibration energy

was such that it was on the minimum of the Landau curve for Neon, and

the air shower energy was on the plateau one would expect a 40% difference

in ionisation. Moreover, one would expect to find more 'knock-on'

electrons for the higher energy, which at the lower angles could be

mistaken for the track and hence increase the measured efficiency. The

difference in angular distribution of single muons and air showers could
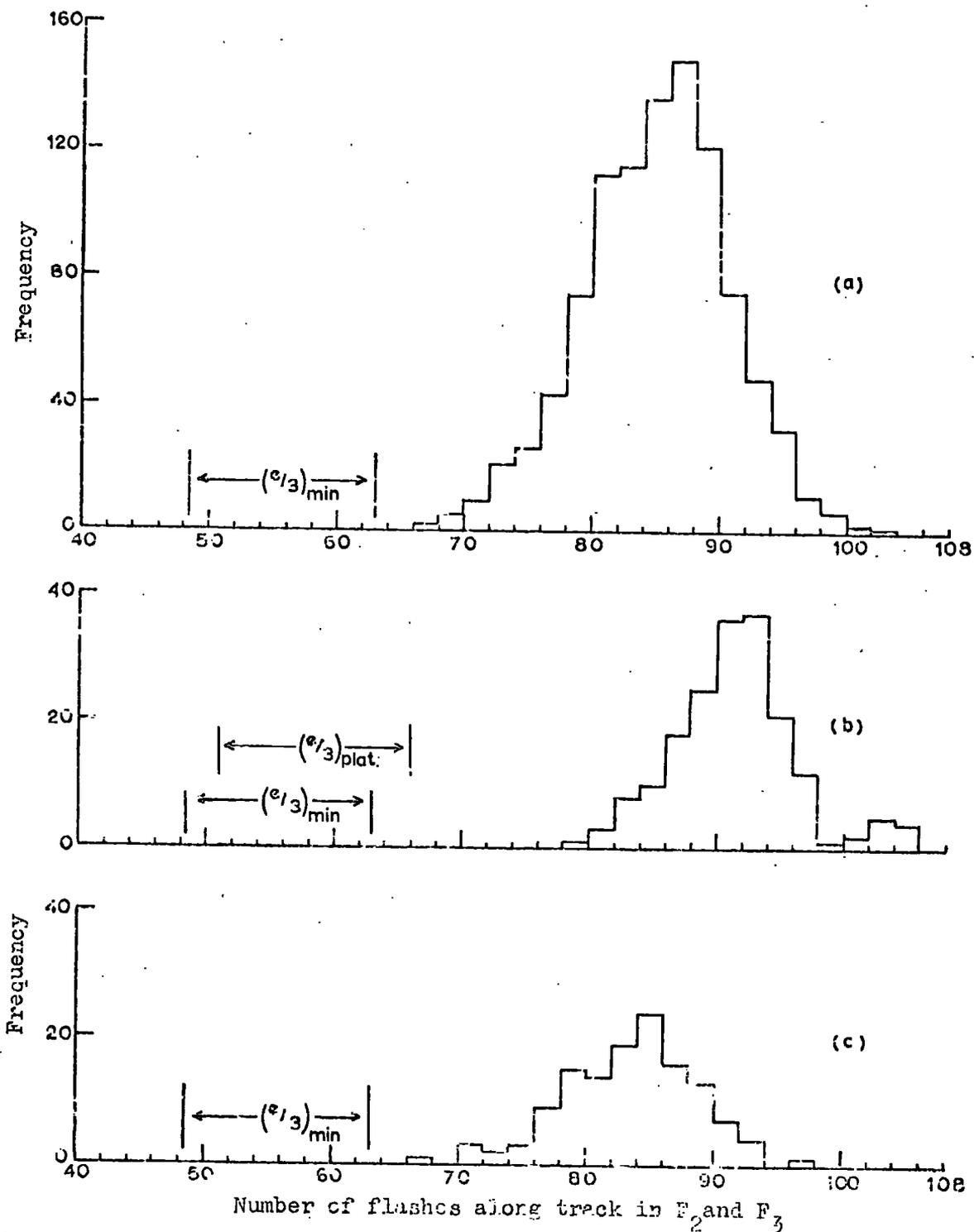
Figure 7.1   Comparison of the efficiency of the flash tubes:
(a) The 1,000 event calibration run, median 84.3 ± 0.2
(b) The air shower events, median 92.0 ± 0.6
(c) The calibration run after the a.s. run, median 83.9 ± 0.5

also have an effect on the efficiency. The mean zenith angle of air showers is greater than single muons, and hence air shower particles are likely to have a greater track length in the flash tubes.

All these factors of the experiment are dealt with below, and the total effect on the efficiency is, where possible, assessed.

7.2 The energy of the calibration muons

A particle must traverse 516 gm cm^{-2} or 433 gm cm^{-2} water equivalent in order to pass through the telescope, and 329 gm cm^{-2} water equivalent to reach the middle of the flash tube trays. To obtain a value for the calibration energy the median of the muon energy spectrum at the centre of the stack was taken with the primary energy cut-off at 516 gm cm^{-2}.

Serre (1967) has produced a comprehensive set of results for his range-energy calculations, which include values for muons. This work was used to determine that the minimum energy to traverse the stack was 940 MeV, and to convert the muon differential energy spectrum of Fazzini et al (1968) to the centre of the telescope. The differential energy spectrum both above and at the centre of the telescope is shown in Figure 7.2, curves a and b respectively. The integral energy spectrum at the centre of the stack is also shown, curve c. From this curve one can see that the median muon energy for the calibration is 2.4 GeV.

7.3 The air shower trigger
7.3.1 The position of core and size of shower from this selection

If one assumes a constant distribution of air showers, regardless of
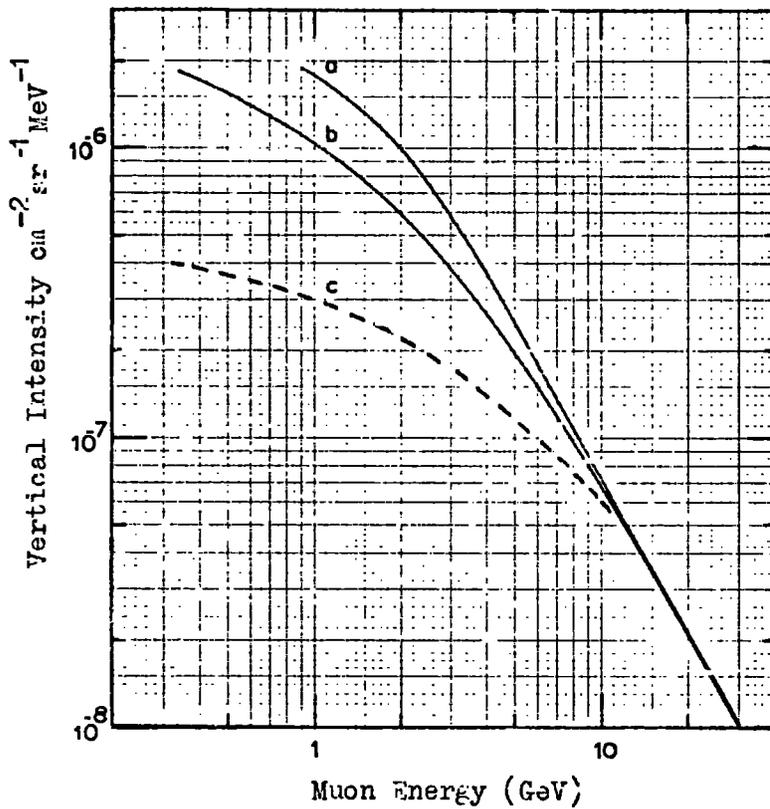
Figure 7.2   The differential muon energy spectrum:
            a.   Above the telescope
            b.   At the centre of the telescope
         (c.   represents the integral muon energy
               spectrum at the centre of the telescope)

size, one can quite easily calculate the expected distribution of core

distance and shower size for a selection of, say, $> \Delta m^{-2}$.

Cocconi (1968) plots a function of probability, $P(r)$ against r, that

one electron in a shower at sea level will land on 1 m^2 at a distance r

from the core. Since the density $\Delta(r)$ is related to the shower size by

the expression

$$\Delta(r) \;=\; NP(r)$$

one can obtain a value for the most probable shower size of a shower at a

distance, r, for the density Δ. Knowing the size of the shower, one can

then refer to the size spectrum (Cocconi, 1968), and convert this to the

rate to obtain the differential distribution in core distance.

In fact we are dealing here with a density $\Delta > 50m^{-2}$ and hence the

integral rate of showers falling in an area $2\pi r \delta r$ for the range of

distance $r - \delta r$ to $r + \delta r$ is

$$F(> N) \text{ x } 2\pi r \delta r \text{ sec}^{-1} sr^{-1}$$

where $\qquad F(> N) \;=\; \dfrac{\Delta(r)}{P(r)}$

The integral size distribution can be found from the rates and sizes

calculated. Figures 7.3 and 7.4 show the integral size distribution and

the integral distribution in core distance respectively. The median size

and distance calculated for densities $> 50 \ m^{-2}$ was $N = 1.8.10^5$ and

$r = 13.6 \ m.$

However, in scanning the film an extra selection, of demanding a track

in F_2 and F_3, has been added. This might affect the values of size and
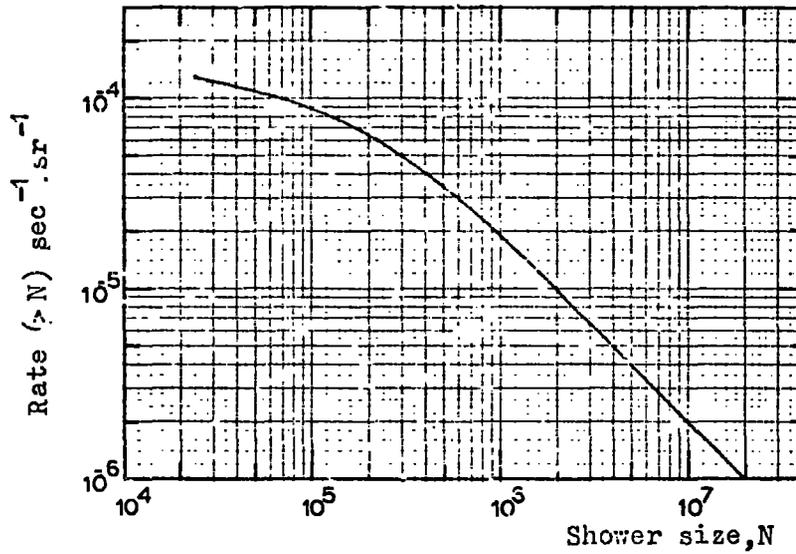
Figure 7.3   Integral distribution of shower size, N,
             producing a density $\Delta > 50m^{-2}$.
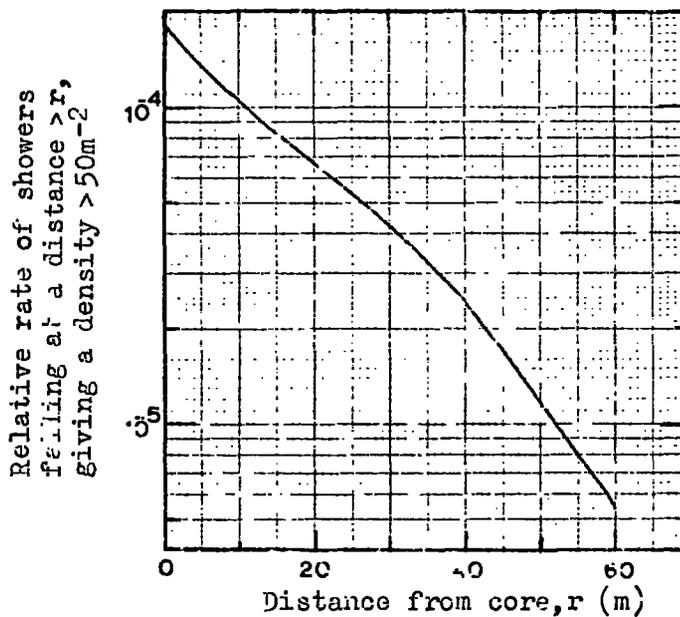
Figure 7.4   Integral distribution of core distance
             of showers giving a density $\Delta > 50m^{-2}$
             at $r=0$.

distance and it is necessary to calculate this effect.

7.3.2 Position of the core, etc. for the measured events

If the distribution in density in the middle scintillator is plotted (Figure 7.5), one finds that the median density for the measured events is 131 m^{-2}. Now from Cocconi (1968) the total number of particles present in a shower that contributes most to the densities around Δ is found to be:-

$$N \approx \Delta(r_2)^2$$

where r_2 is defined as the unit lateral displacement and is equal to 84 m at sea level. The shower size corresponding to the median of the density distribution in M is therefore $N \approx 9.10^5$.

De Beer et al. (1966) plots the lateral distribution of muons for a constant shower size of 10^6. Thus if the muon density can be measured, then the corresponding distance from the core can be obtained for the shower size $\sim 9.10^5$. The distribution in muon density was obtained by taking all the tracks that passed through the area of flash tubes at the top of F_2. All the tracks that passed through this area of 1.3 m^2, regardless of geometry were taken to be muons. The distribution obtained, whose median value was 2.0 m^{-2}, is shown in Figure 7.6. The value of core distance obtained from de Beer was then $\sim$ 14 m.

Turver (1969) has quoted figures for the muon energy related to core distance, which are based on data provided by Orford (1968). From this one can say that the average muon energy in the measured air shower events is of the order of 30 GeV, compared with 2.6 GeV for the calibration.
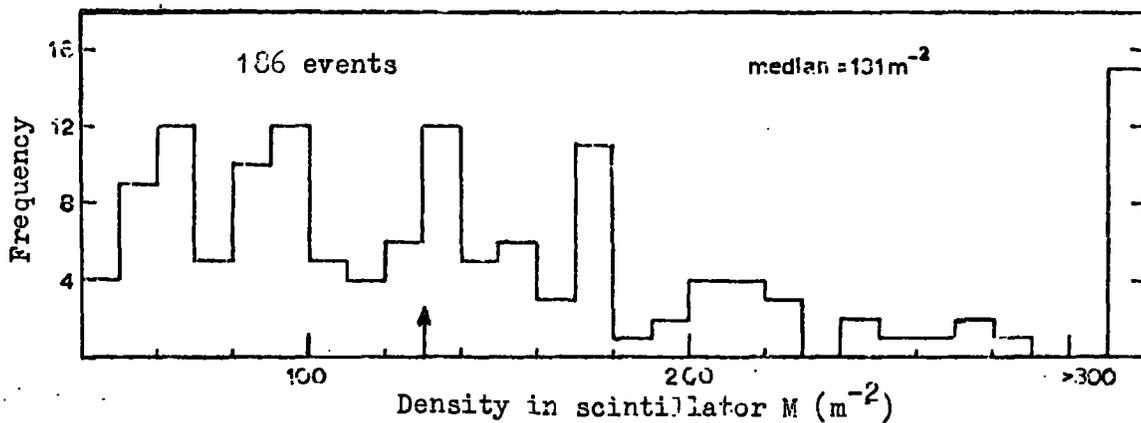
Figure 7.5   Distribution in air shower density in M for all
             events with at least one measurable track.

Number of muons through the flash
tube area $(1.3m^2)$ for each measured
event.
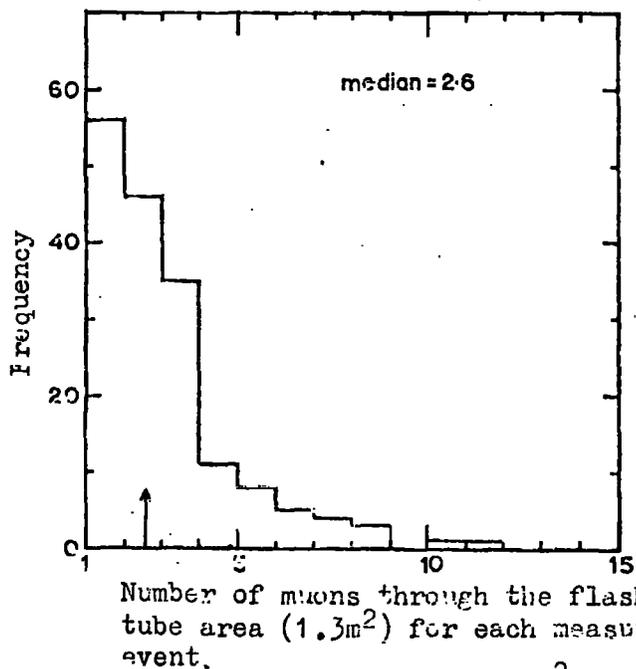
Figure 7.6   Distribution in muon density (in $1.3m^2$) for the
             measured events in the air shower run.

7.4 The ionisation loss in neon

The most probable ionisation loss, as a function of muon energy, in neon, at 60 cm of mercury pressure can be calculated using, as before, the expression:-

$$Ep = \frac{2Cm_e c^2}{\beta^2} \; z^2 \; x \left(\ln \left\{ \frac{4C(m_e c^2)^2 \; x}{(1-\beta^2)I^2(Z)} \right\} - \beta^2 + j \right)$$

where all the symbols have the expressions assigned to them above. When the density effect as attributed to Fermi (1939) or Sternheimer (1956) is brought into effect, one is left with the curve for the most probable ionisation loss shown in Figure 7.7.

7.5 Calculated differences in efficiencies due to ionisation loss

The difference in ionisation between the calibration muon track and the air shower track will be, from Figure 7.7., 0.76 KeV to 1.05 KeV. The efficiency parameter, afQ, will vary linearly with this increase in ionisation, and since the best fit of afQ to the calibration muons was 16, one can say that the best fit of afQ for the air shower muons is 22.1. Unfortunately this is not a precise value as it was found that calibration data did not fit Lloyd's curves exactly. However, when Lloyd's curves are studied, the difference in layer efficiencies between these two 'best fit' values for afQ was 2.7%.

7.6 Knock-on electrons

One must now consider the possibility of the primary muon undergoing
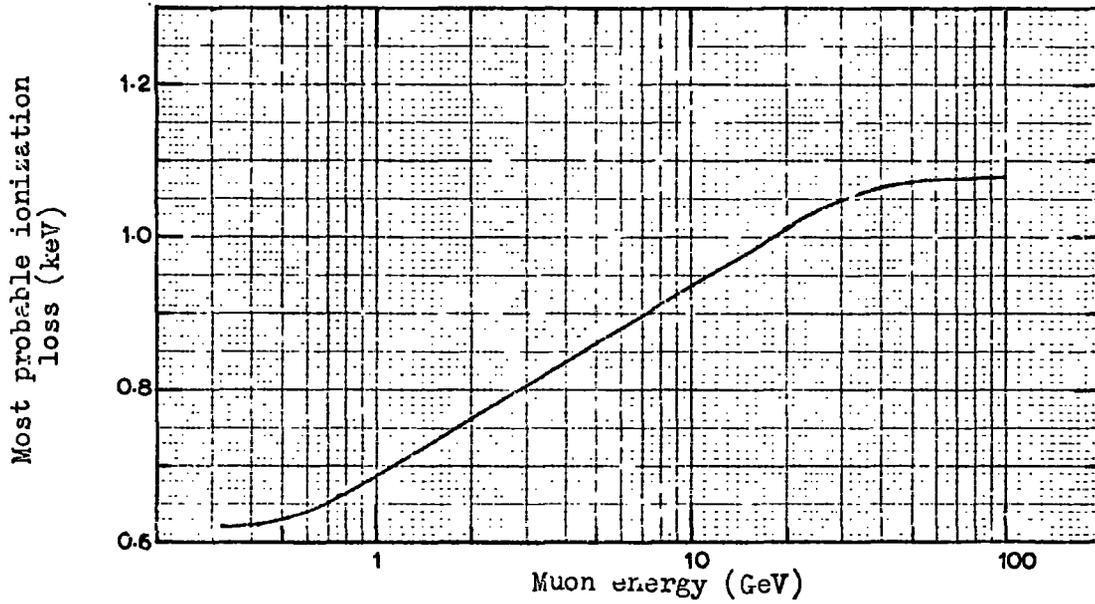
Figure 7.7   The variation with energy of the most probable
energy loss for muons traversing a flash tube
filled with neon at 60 cm Hg.

a collision in the glass of a flash tube and producing a knock-on electron with sufficient energy to traverse into the gas of the flash tube, and increasing its probability of flashing. For simplicity, take the case where the collision takes place at the centre of the glass, i.e. after approximately 0.5 mm, 0.211 gm cm^{-2}. From the Feather rule, the minimum energy required for an electron to traverse the remainder of the glass will be

$$E_{min} = \frac{R+0.16}{0.54} \quad \text{i.e. } 0.618 \text{ MeV}$$

The differential collision probability for particles of mass, m, and spin $\frac{1}{2}$ has been calculated by Bhabha (1938) and by Massey and Corben (1939) and is

$$\phi_{col}(E,E')dE' = \frac{2Cm_ec^2}{\beta^2} \frac{dE'}{(E')^2} \left(1 - \frac{\beta^2 E'}{E'_m} + \frac{1}{2}\left\{\frac{E}{E+mc^2}\right\}^2 \right) gm^{-1}cm^2$$

where $C = 0.15 \frac{Z}{A}$

m_ec^2 is the rest mass of the electron

β is the velocity of the incident particle of energy E

E' is the energy of the knock-on electron

E'_m is the maximum transferable energy and is given by:-

$$E'_m = 2m_ec^2 \frac{(E^2 - m^2c^4)}{(2Em_ec^2 + m^2c^4 + m_e^2c^4)}$$

Here one wants the probability of producing a knock-on of energy from E_{min} to E'_m. This will be given by -

$$\phi_{col}(E, > E'_{min}) = \int_{E_{min}}^{E'_m} \left\{ \frac{2Cm_ec^2}{\beta^2} \frac{1}{(E')^2} \left(1 - \frac{\beta^2 E'}{E'_m} + \frac{1}{2}\left[\frac{E'}{(E+mc^2)}\right]^2 \right) \right\} dE'$$

This function was evaluated for the air shower muons of energy 30 GeV and the calibration muons of median energy 2.6 GeV. The values for E'_m for these primaries was found to be 22.2 GeV and 500 MeV respectively, A 1.46% difference was found between the two values of probability.

It is difficult to predict what effect this increase in probability of knock-ons would have on the measurement of efficiency. Only the small angle knock-ons would be likely to have an effect, as the large angles would be seen in scanning. The actual difference in probability of knock-ons would occur for the higher energies, which would affect the efficiency more, because of the greater probability of small angles. One can therefore say that the increase in efficiency due to knock-ons is likely to be in the order of 1.46%, which assumes that the knock-ons will affect one flash tube only.

7.7 The angular distributions

One can expect an increase in efficiency for tracks of increasing zenith angle, because of the track length of the particle in the flash tubes. This effect is likely to be very small and, as can be seen in Section 7.5, a large increase in ionisation produces a very small increase in efficiency.

A more serious effect, which is likely to be observed at specific angles, is an increase or decrease in efficiency due to the stacking of the flash tubes. For example, in the extreme cases it is possible for a vertical particle to traverse a minimum of half the flash tubes, where a particle

at 30° to the vertical has a minimum of no flash tubes, and a maximum of all the flash tubes along its line of flight.

If there was a marked difference in the mean zenith angles of the calibration and the air shower muons, this could produce a difference in the layer efficiencies obtained. However, the geometry of the telescope is such that it would tend to accept only those events with low zenith angles, which would bring the two means closer together and nullify this effect. Since it was not possible to obtain information from the side view for the air shower data, the angular distribution could only be studied by taking the projected zenith angles in the front and side views.

7.7.1 The front view

A scatter plot of layer efficiency to projected zenith angle in the front view, was drawn for all the measured events in the air shower run (Figure 7.8). No strong angular dependence in efficiency was seen although the efficiency did increase by 2.5% in moving from 5.4° to 15.9°.

When one compares the frequency distribution in θ_F for the calibration and the air shower muons, as shown in Figure 7.9, one can see that the median angles are 9.7 ± 0.5 and 10.7 ± 0.6 respectively. One can estimate that the difference in efficiencies for the two runs will be in the order of 0.3 ± 0.3 in F_2 and F_3.

7.7.2 The side view

Unfortunately only the calibration muons could be measured in the side view. The scatter plot and angular distribution obtained from these muons
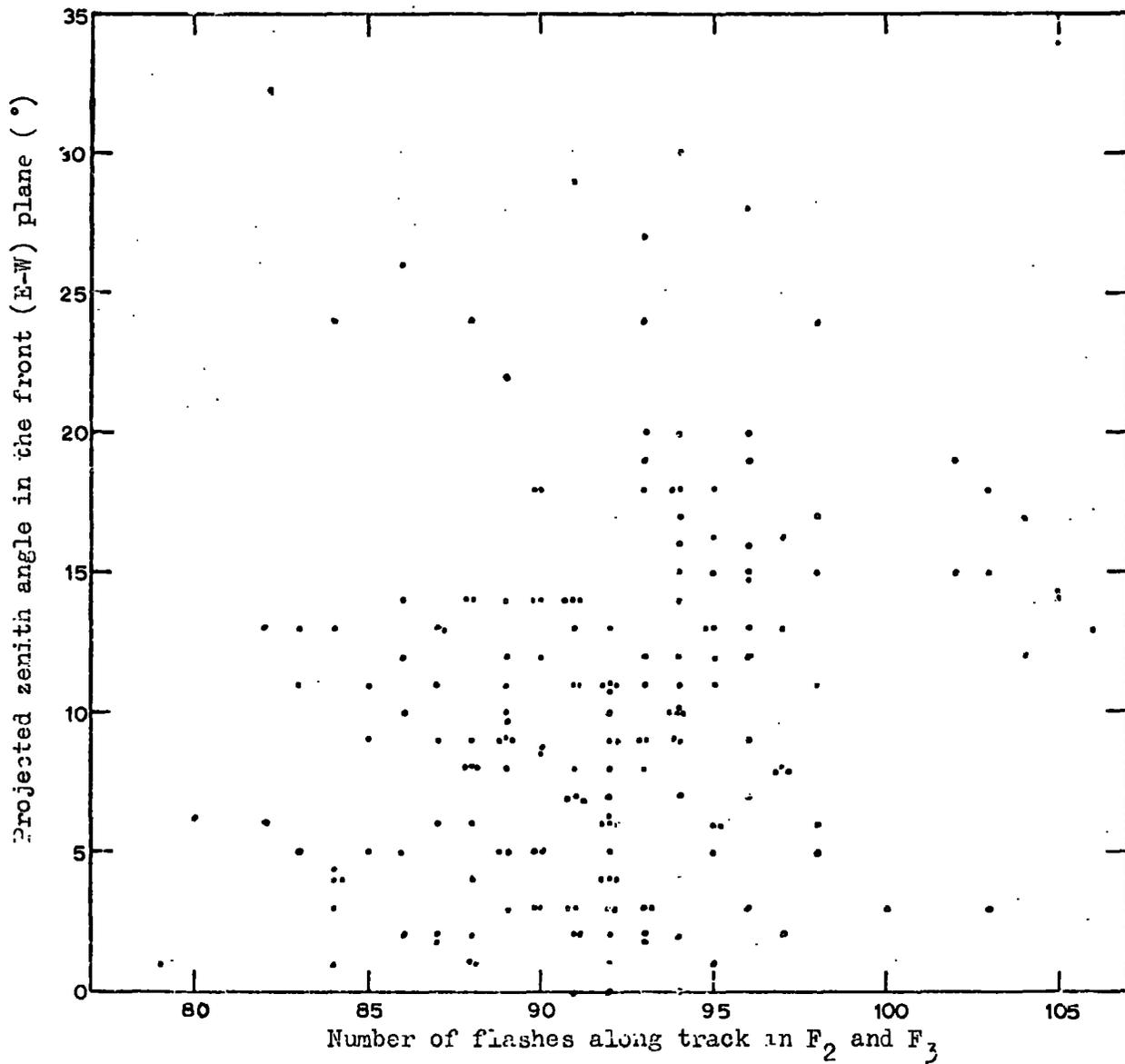
Figure 7.8   Scatter plot of the projected zenith angle in the front
plane to the number of flashes along the track for all
measured tracks in the air shower run.
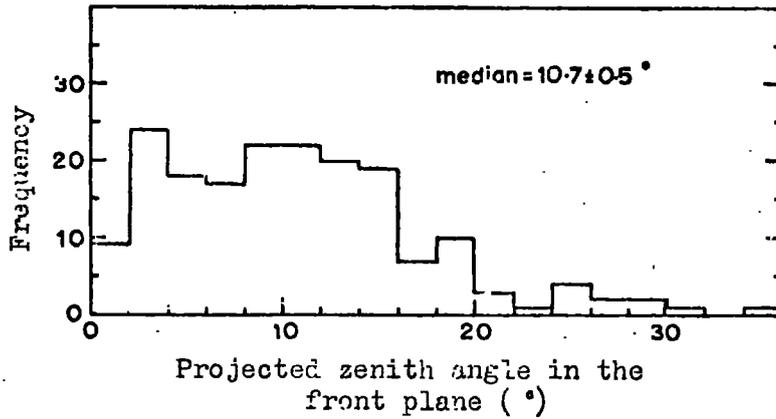
a. air shower events.
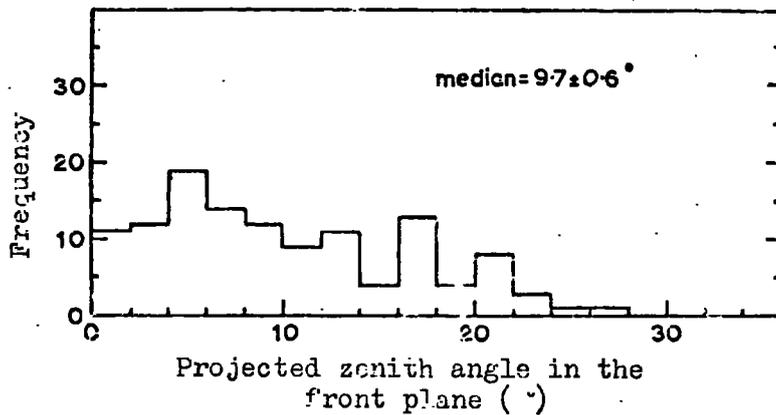
b. calibration events

Figure 7.9 The distribution in projected zenith angle for:
a. All measured air shower tracks.
b. The calibration tracks.

is shown in Figures 7.10 and 7.11. Again there is a slight dependence of efficiency on zenith angle, as is expected. In moving from 2^O to 10° the efficiency moved by 2.2 flashes in F_2 and F_3.

If one takes the increase in the median of θ_s for the air shower events to be proportional to the increase in θ_F then one can say that the expected median θ_s for the air shower muons was 5.8^O. This would indicate an expected increase in efficiency for the events to be of the order 0.1 flashes in F_2 and F_3.

7.8 Summary of results

No low ionising particles have been measured in a total of 174 measurable air shower events, which were taken from 760 showers of size, $N \sim 10^6$. However, there was a shift of 7.1% in the layer efficiency for the calibration and the air shower tracks, which if due to an error in Lloyd's theory could shift the expected efficiency for $e/3$ quarks to an immeasurable size. It was found that a shift of approximately 4.5% could be explained by the differences in ionisation, knock-on electrons, and angular distribution of the two types of muons. When one observes that the shift in moles of the calibration and the air shower events is in fact 5.5% it can be seen that this effect is probably not real and is within the errors of observation.

The experiment has thus proved itself capable of detecting a 40% shift in ionisation, the results of which, within the errors of observation hold to Lloyd's theory of flash tube efficiency. This experiment is therefore
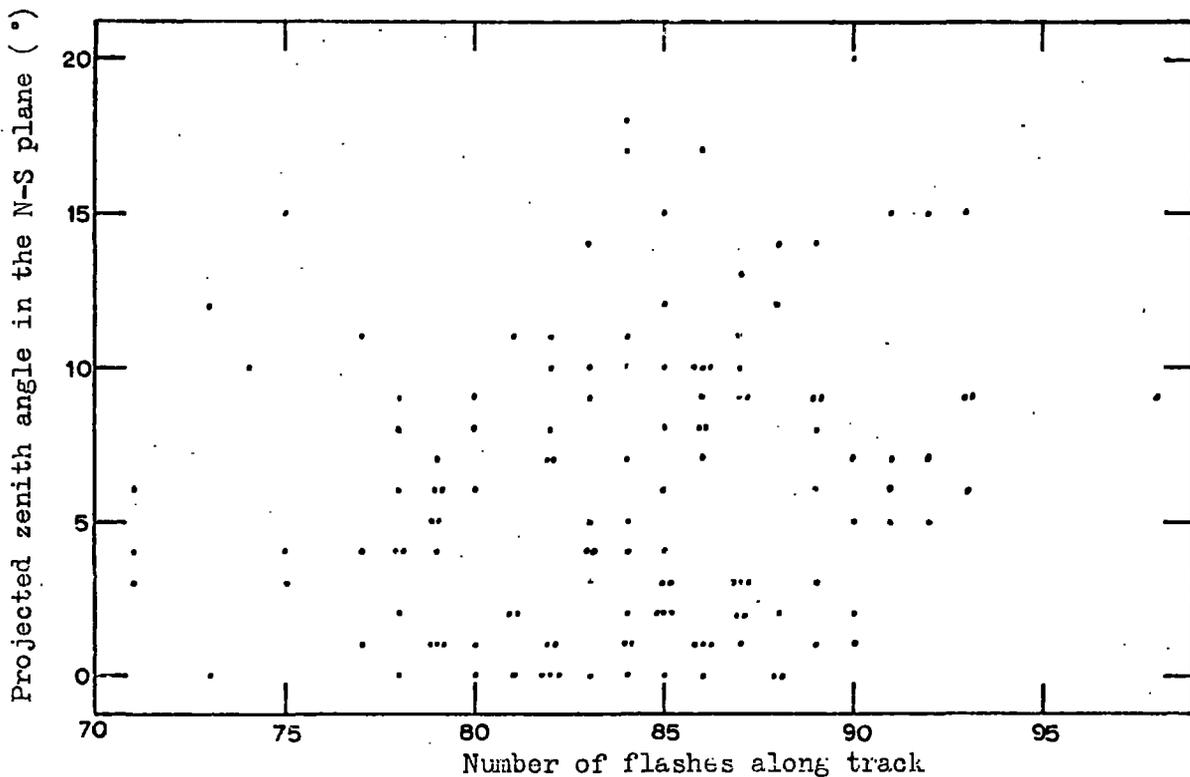
Figure 7.10   Scatter plot of the projected zenith angle in the side
plane to the number of flashes along the track for the
calibration run.
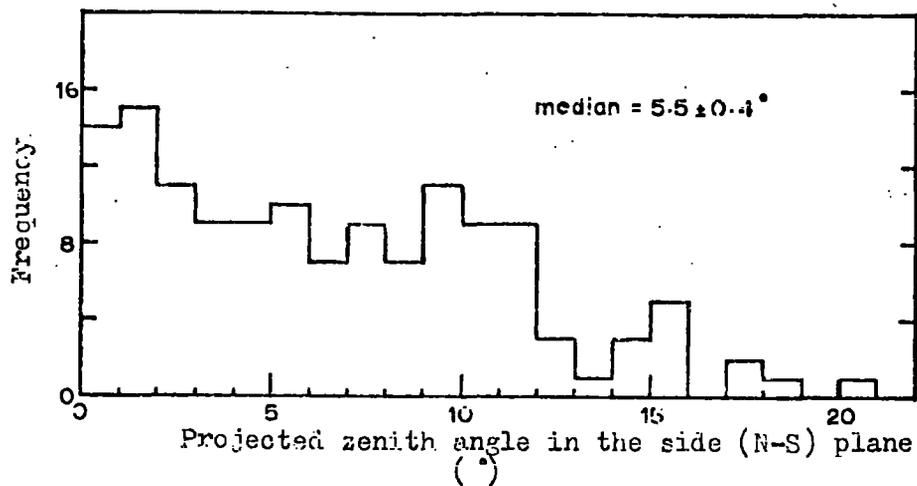
Figure 7.11   The frequency distribution in projected zenith angle
in the side plane for the calibration events.

quite capable of detecting e/3 charged particles close to air shower cores and, in observing 174 of these showers, has detected no quarks.

CHAPTER 8

CONCLUSION

Although the quark model has proved a useful tool in the understand-
ing of elementary particles no strong evidence of their existence has
been found experimentally. This suggests that either they are just a
useful mathematical model or the researchers have been looking in the
wrong place.

The charge distribution of interacting particles in cosmic rays
was measured in the search for non-integral charged particles of the
type suggested by de Swart (1967). No strong 'signal' was obtained
and the limit for the rates was given by the 'noise' of the experiment.
Because of this noise the limit obtained was very much greater than
that obtained by Adair et al. (1968).

The proportional counter proved to be a useful instrument for the
measurement of ionisation of cosmic ray particles, although the distri-
bution in ionisation loss was broad and, for 4e/3, one is limited by
the long tail, and the errors in track length. This could be deviated
by using several layers of proportional counters, Ramana Murthy (1967).

All previous searches for quarks have not been able to identify a
low ionizing particle in the presence of another particle. One therefore
has to assume that, in production, the quark will be given enough trans-
verse momentum to 'clear' the other components of the interaction.
McCusker (1969) has looked at penetrating particles near the air shower
core and, in one years running, has observed four lightly ionising

events through his cloud chamber. These events would be taken as 2e/3 charged particles; the apparatus was unable to detect e/3. Unfortunately, no previous particle indicator was used and, although by suitable analysis, ,ne should be able to estimate the age of the track, there is still some doubt of the validity of these events,

Flash tubes have been used for several years as visual detectors of cosmic rays. However, as the efficiency is dependent on the amount of ionization, they can provide a large volume detector which will distinguish the charge on a particle and yet be able to accept multiple tracks in one event. A large bank of flash tubes, suitably shielded, was used to observe tracks close to the air shower core. It was found that the detector would distinguish between e/3 and e charged particles to a level of greater than 1 in 1,000. The results obtained from the low energy muon calibration and the high energy air shower muons agreed, within experimental errors, with the expected relativistic logarithmic rise in ionisation. No confusion could be expected from minimum ionising events. The experiment was run for 162 hours and no e/3 particles were observed. It is hoped that it will continue operating for ,several months once an air shower array for core positioning has been added.

ACKNOWLEDGEMENTS

REFERENCES

Adair, R.K., Kasha, H., Larsen, R.C., and Leipuner, L.B., (1968), Phys. Rev. Letters, 20, 217.

Ashton, F., (1965), Proc. Int. Conf. Cosmic Rays, London, 2, 1108.

Ashton, F., Coats, R.B., Kelly, G.N., Simpson, D.A., Smith, N.I., and Takahashi, T., (1968), Canadian Journal of Physics, 46, S1125.

Ashton, F., Coats, R.B., Kelly, G.N., Simpson, D.A., Smith, N.I., and Takahashi, T., (1968a), Proc. Phys. Soc., 1, 569.

Ashton, F., Coats, R.B., and Simpson, D.A., (1965), Proc. Int. Conf. Cosmic Rays, London, 1078.

Ashton, F., Burchaladze, A.A., King, J., Smith, N.I., Mamidzhanian, E.A., (1969a), Izvestia Academy Nauk, SSSR, Ser. Fiz., 33, 1818.

Ashton, F., Smith, N.I., King, J., Mamidzhanian, E.A., (1969), Izvestia Academy Nauk, SSSR, Ser. Fiz., 33, 1557.

Axford, I., (1968), J. Geophys. Res., 73, 6855.

Bhabha, H. J., (1938), Proc. Roy. Soc., A164, 257.

Blunck, O., and Leisegang, S., (1950), Z. Physik, 128, 500.

Blunck, O., and Westphal, K., (1951), Z. Physik, 130, 641.

Brennan, M.H., (1957), Il Nuovo Cimento, Series X, 6, 216.

Buhler-Broglin, A., Dalpiaz, P., Massam, T., and Zichichi, A., (1967), Il Nuovo Cimento, Series X, 51, 837.

Buhler-Broglin, A., Fortunato, G., Massam, T., and Zichichi, A., (1967), Il Nuovo Cimento, Series X, 49, 209.

Burcham, W. E., (1963), 'Nuclear Physics, An Introduction', published by Longmans.

Cairns, I., McCusker, C.B.A., Peak, L.S., and Woolcott, R.L.S., (1969),
Phys. Rev., 186, 1394.

Coats, R.B., (1967), A Ph.D. Thesis, Durham University.

Cocconi, G., (1961), Handbuch der Physik, edited by S. Flugge, 215-271.

Coxell, H., and Wolfendale, A.W., (1960), Proc. Phys. Soc., 75, 378.

Curran, S.C., Cockroft, A.L., and Angus, J., (1949), Phil. Mag., 40, 929.

De Beer, J.F., Holyoak, B., Wdowczyk, J., and Wolfendale, A.W., (1966),
Proc. Phys. Soc., 89, 567.

Fano, V., (1947), Phys. Rev., 72, 26.

Fazzini, M.C., Galli, M., Guidi, I., and Randi, P., (1968), Canadian
Journal of Physics, 46, part 4, S1077.

Fermi, E., (1939), Phys. Rev., 56, 1242.

Fermi, E., (1940), Phys. Rev., 57, 485.

Galbraith, W., (1958), 'Extensive Air Showers', published by Butterworths.

Gell-Mann, M., (1964), Phys. Letters, 8, 214.

Green, J.R., and Barcus, J.R., (1959), Il Nuovo Cimento, Series X, 14,
1356.

Hanna, G.C., Kirkwood, D.H.W., and Pontecorvo, B., (1949), Phys. Rev.,
75, 985.

Heineman, R.E., (1954), Phys. Rev., 96, 161.

Heineman, R.E., and Hazen, W.E., (1953), Phys. Rev., 90, 496.

Kerns, Q.A., Kirsten, F.A., and Cox, G.C., (1959), Review Sci. Instrum.,
30, 34.

Kokkede, J.J.J., (1969), 'The Quark Model', published by Benjamin.

Landau, L., (1944), J. Exp. Phys. USSR, $\underline{8}$, 201.

Lloyd, J.L., (1960), Proc. Phys. Soc., $\underline{75}$, 387.

Massam, T., (1968), CERN report 68-24, unpublished.

Massey, H.J., and Corben, H.C., (1939), Proc. Camb. Phil. Soc., $\underline{35}$, 463.

McCusker, C.B.A., and Cairns, I., (1969), Phys. Rev. Letters, $\underline{23}$, 658.

McDowell, M.R.C., and Hasted, J.B., (1967), Nature, $\underline{214}$, 235.

Melton, C.E., Hurst, G.S., and Burtner, T.E., (1954), Phys. Rev., $\underline{96}$, 643.

Nir, A., (1967), Phys. Rev. Letters, $\underline{19}$, 336.

Orford, K., (1968), Ph.D. Thesis, Durham University.

Ramana Murthy, P.V., (1968), Nuclear Instruments and Methods, $\underline{63}$, 77.

Ramana Murthy, P.V., and Demeester, G.D., (1967), Nuclear Instruments and Methods, $\underline{56}$, 93.

Rossi, B., (1952), 'High Energy Particles', published by Prentice Hall.

Schmeider, K., (1939), Annalen d. Phys., $\underline{35}$, 445.

Serre, C., (1967), CERN report 67-5, unpublished.

Simpson, D.A., (1967), Ph.D. Thesis, Durham University.

Singer, S.F., (1951), Phys. Rev., $\underline{81}$, 579.

Smith, N.I., (1969), Ph.D. Thesis, Durham University.

Sternheimer, R.M., (1952), Phys. Rev., $\underline{88}$, 851.

Sternheimer, R.M., (1953), Phys. Rev., $\underline{91}$, 256.

Sternheimer, R.M., (1956), Phys. Rev., $\underline{103}$, 511.

Swart, J. J. de., (1967), Phys. Rev. Letters, $\underline{18}$, 157.

Symon, K. R., (1948), Ph.D. Thesis, Harvard University.

Turver, K.E., (1969), Information on H.E.A.S., Informal Meeting on Quarks, Rutherford High Energy Lab., not published.

Vavilov, P.V., (1957), Soviet Physics, JETP (Engl.), $\underline{5}$, 749.

Wilkinson, D.H., (1950), 'Ionization Chambers and Counters', published by Cambridge U.P.

Yukawa, H., (1935), Proc. Phys. Math. Soc., Japan, $\underline{17}$, 48.

Zweig, G., (1964), CERN reports TH401 and TH402, unpublished.

APPENDIX A

ELECTRONICS

The circuit diagrams for the electronics which were developed for the experiments above are shown in this appendix. Unless otherwise stated all values of resistance are quoted in $k\Omega$ ($10^3\Omega$), all values of capacitance are quoted in μF ($10^{-6}F$), and all transistors used were of the type OC171.

The circuit for the previous particle gate described in Chapter 7, together with a block diagram explaining its operation, is shown in Figure A.10.
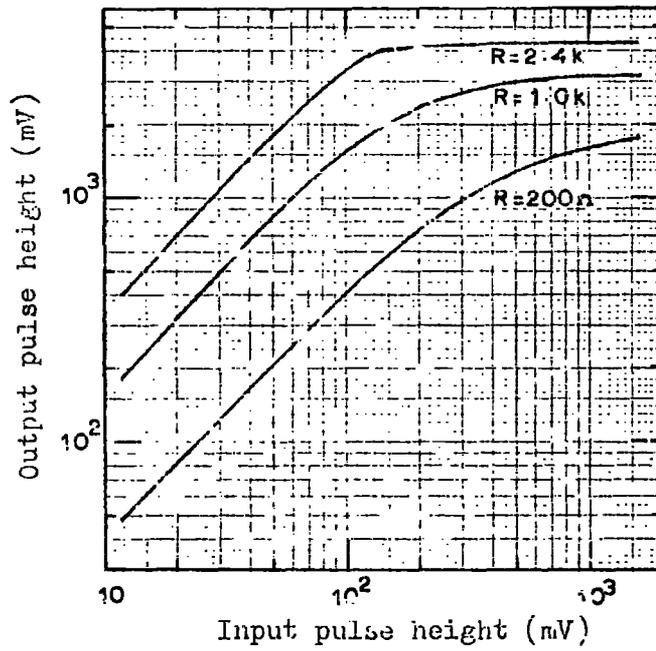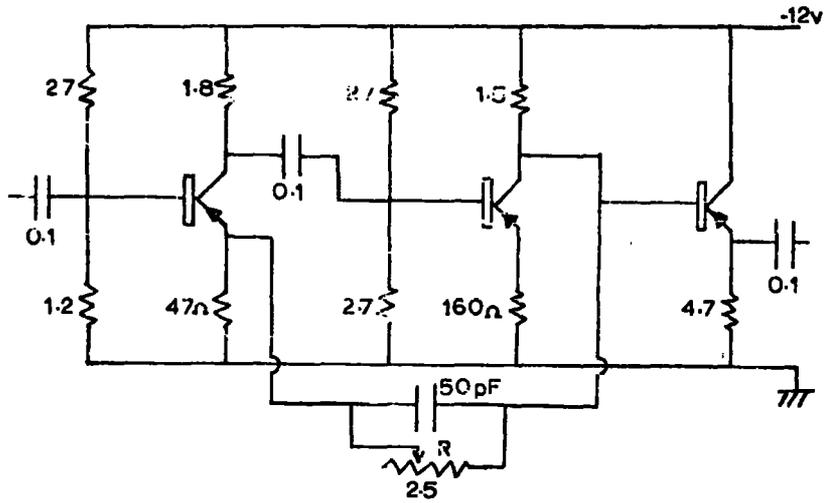
Figure A1 The voltage amplifier and its characteristics for various values of feedback resistance, R.
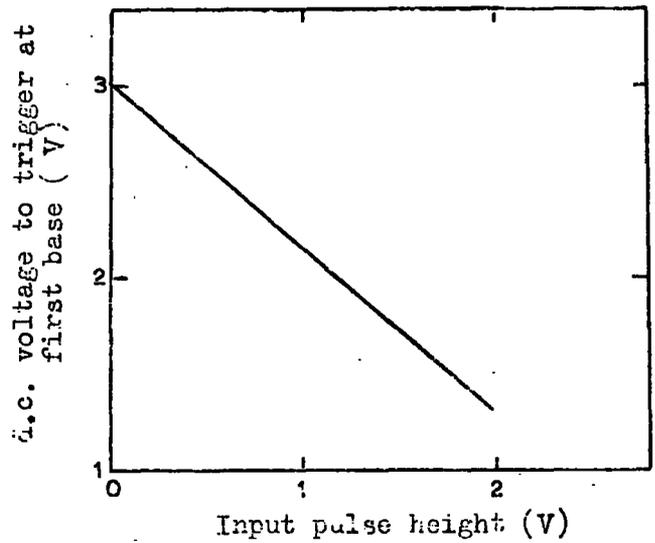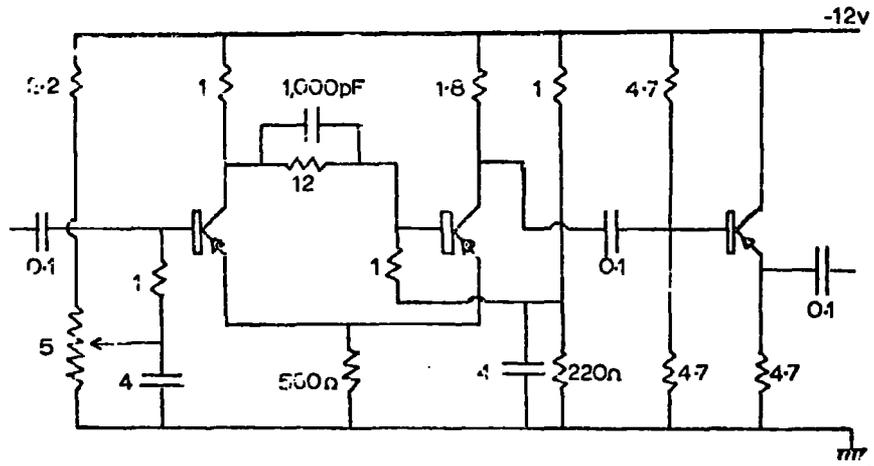
Figure A2   The discriminator circuit and the relationship
between the d.c. level on the base of the first
transistor and the minimum input pulse height
required to trigger the circuit.
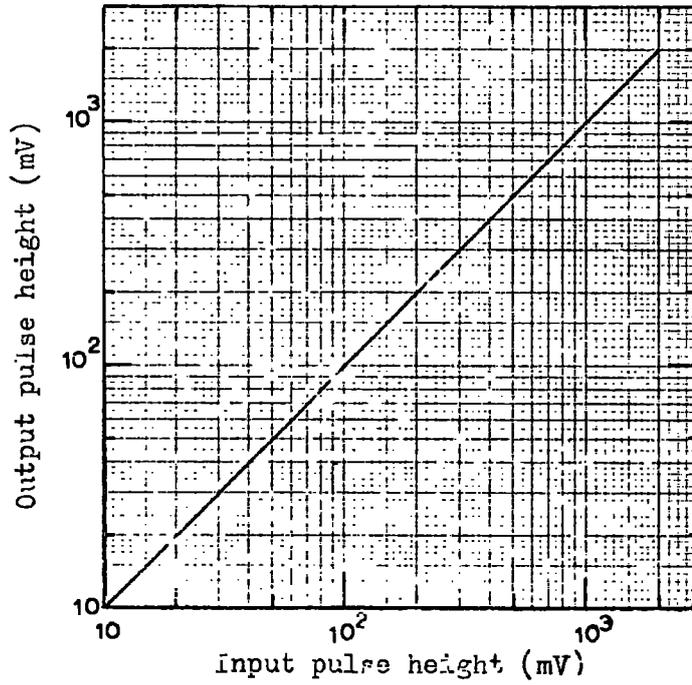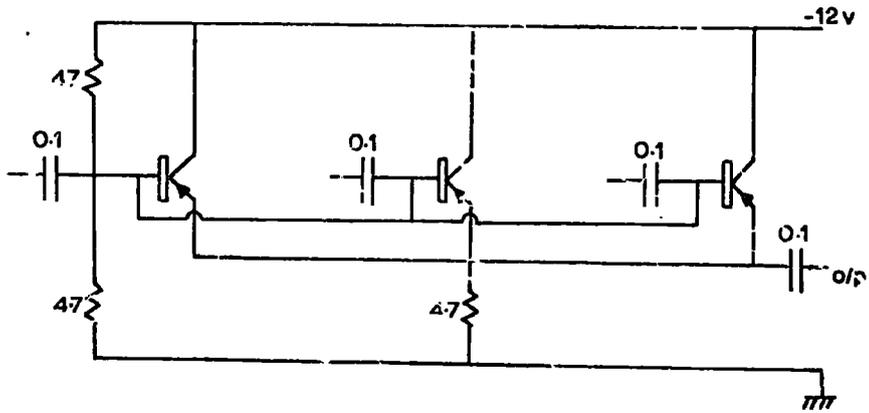
Figure A3   The fan-in and its input-output characteristics.
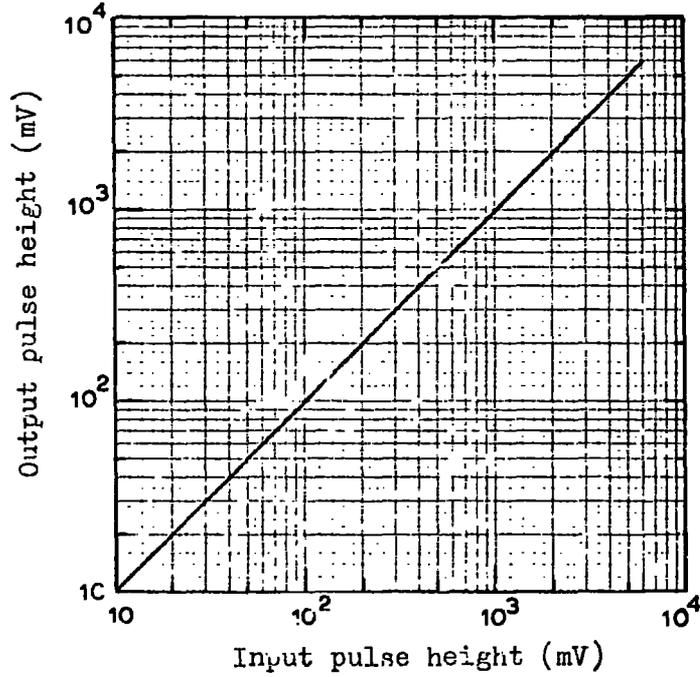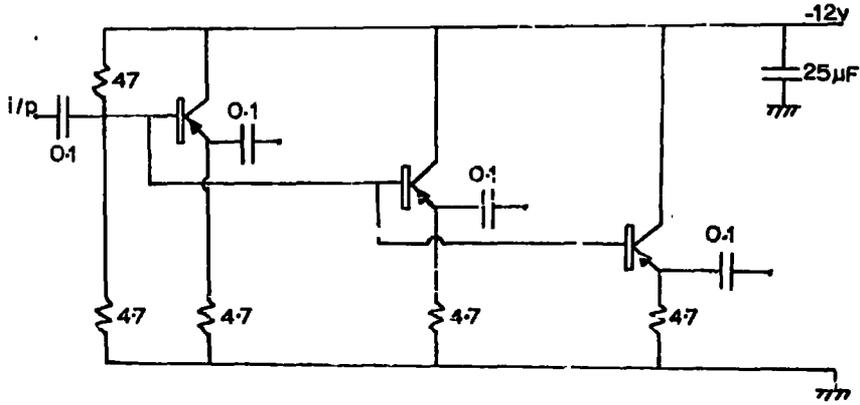
Figure A4   The fan-out and its input-output characteristics.
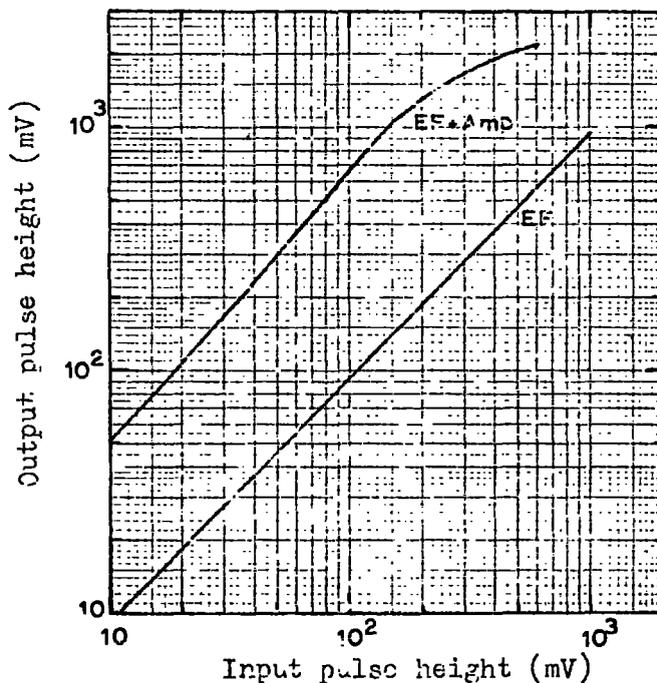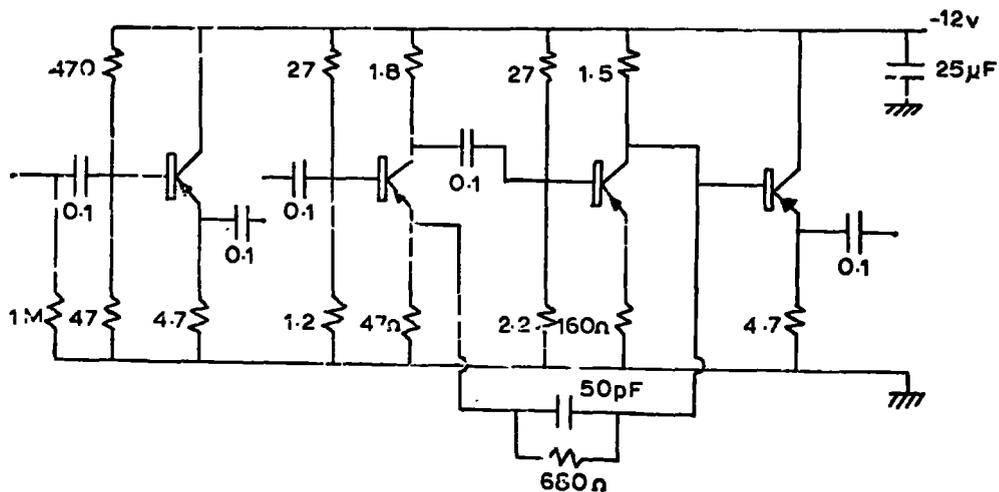
Figure A5   The anode head unit used on the large liquid scintillators.
The input-output characteristics are given for emitter-
follower alone (EF) and for the whole circuit which includes
a ×10 amplifier (EF+Amp).
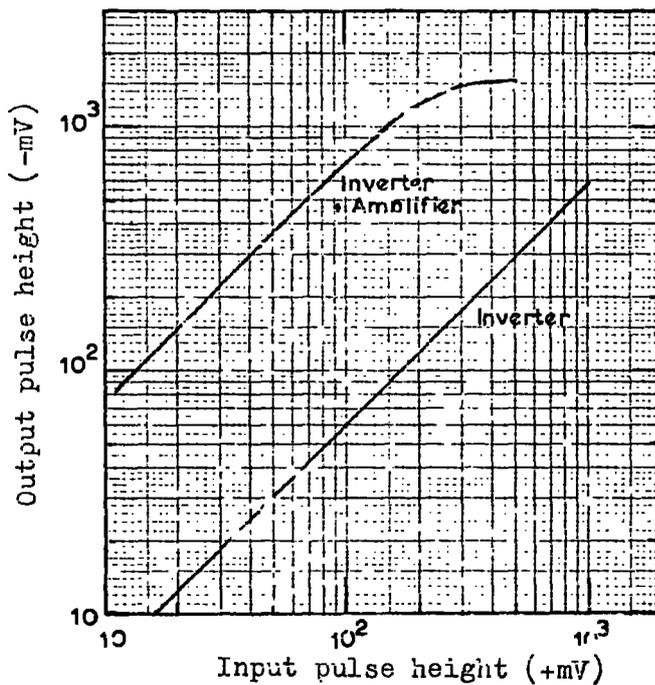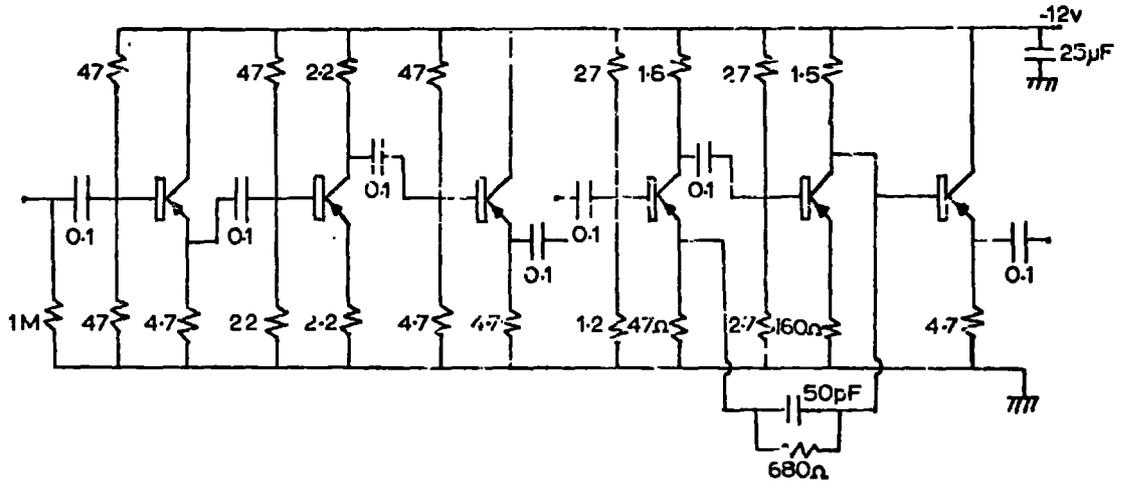
Figure A6   The dynode head unit used on the large liquid scintillator.
The positive input pulses are inverted and the characteristics
are given for the inverter stage and for the whole circuit
which includes a ×10 amplifier.

a)

b)

c)

d)
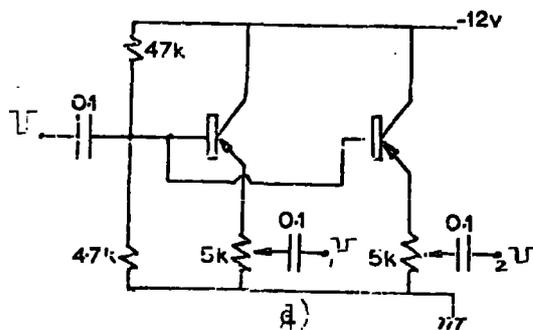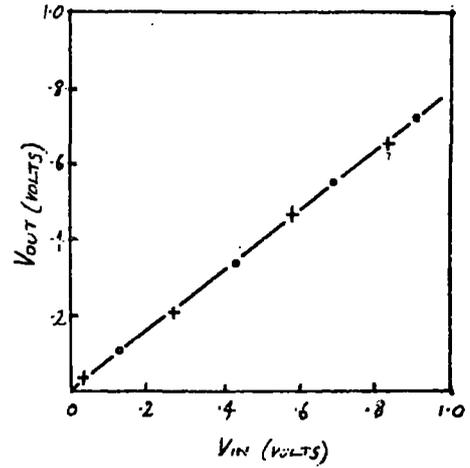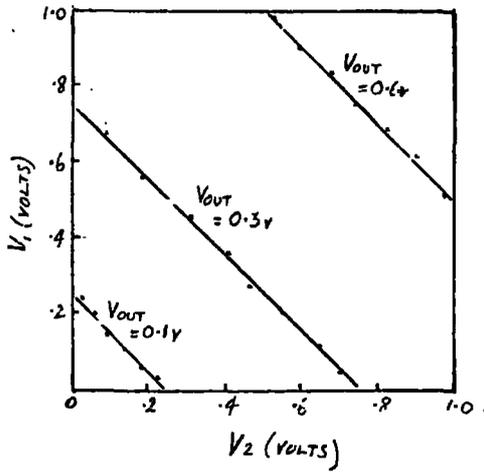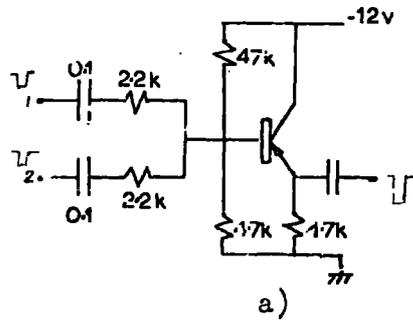
Figure A7 a) The adder circuit.
b) A plot of the input pulse height, V_1 & V_2 for a constant output pulse height, V_{out} ,
c) A plot of input pulse in one channel, V ,against output pulse height.
d) The splitter circuit used to test the adder.
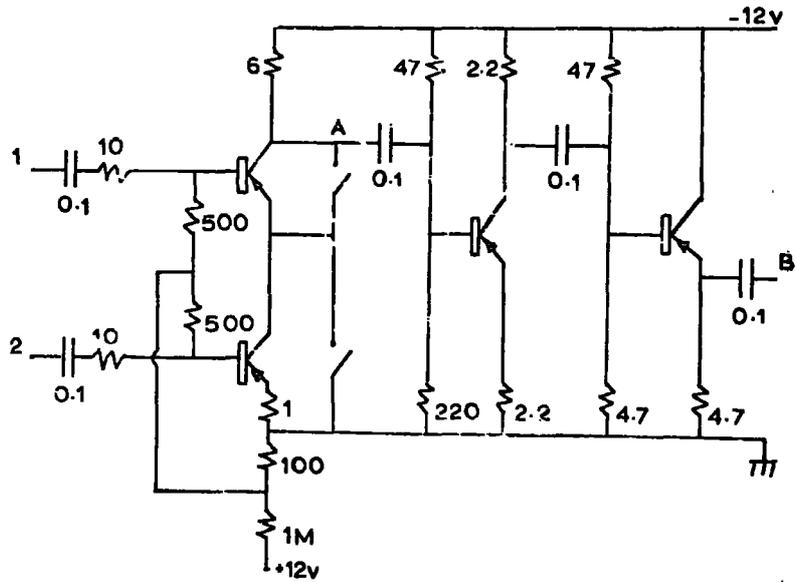
	Input from Discriminator	Output at A		Output at B		
		1 fold	2 fold	1 fold	2 fold	pulse width
Channel 1	-5v	+0.15 v	+ 5.4 v	- 0.05 v	-4.1v	1us
Channel 2	-5v	+0.02		-0.04		1us

Figure A8 A two-fold coincidence unit.
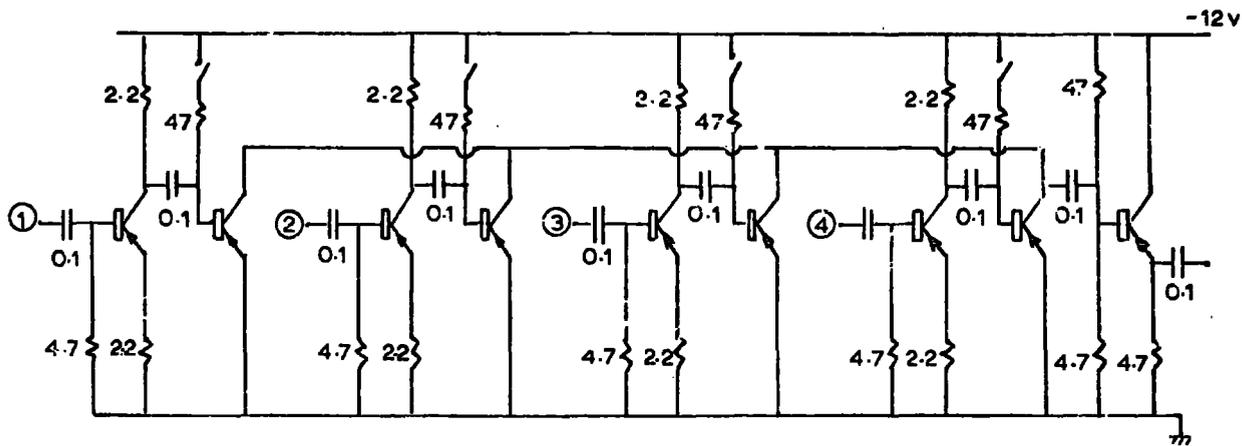
No. of coincident i/p pulses	Output pulse height
4 (-5V)	-4V
3 (-5V)	-0.1V
2 (-5V)	-0.07V
1 (-5V)	-0.06V

Figure A9   The four-fold coincidence used on the air shower experiment.
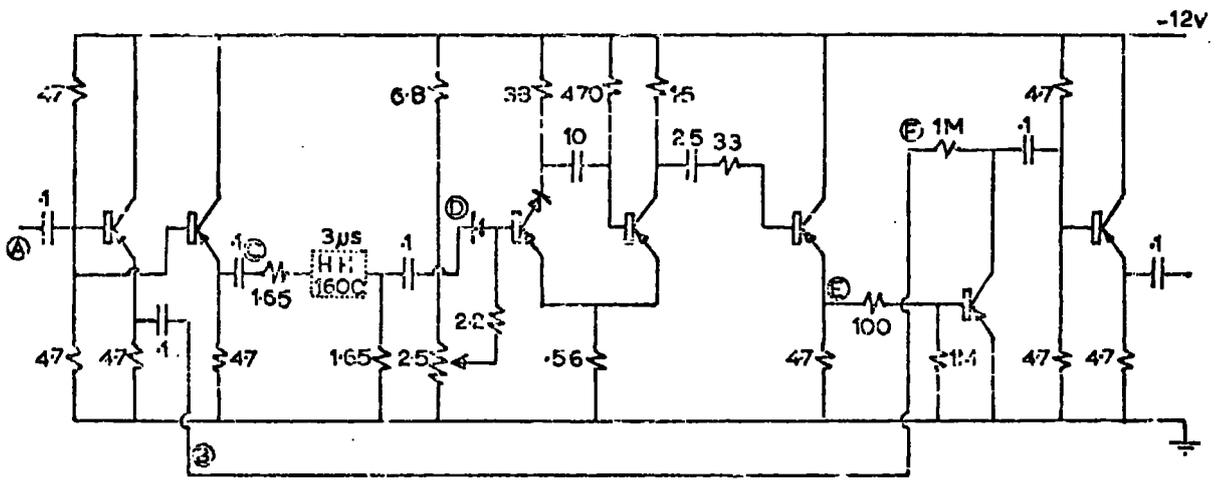
a)
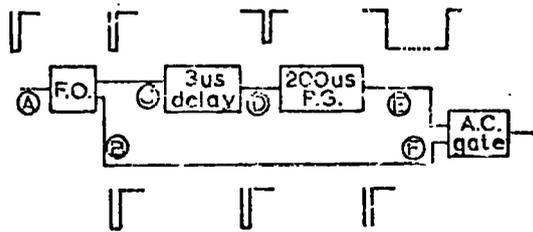
b)

Figure A10 a) The previous particle gate..
         b) A block diagram of this circuit.
             No pulse will traverse the A.C. gate while
             there is a pulse at (E).
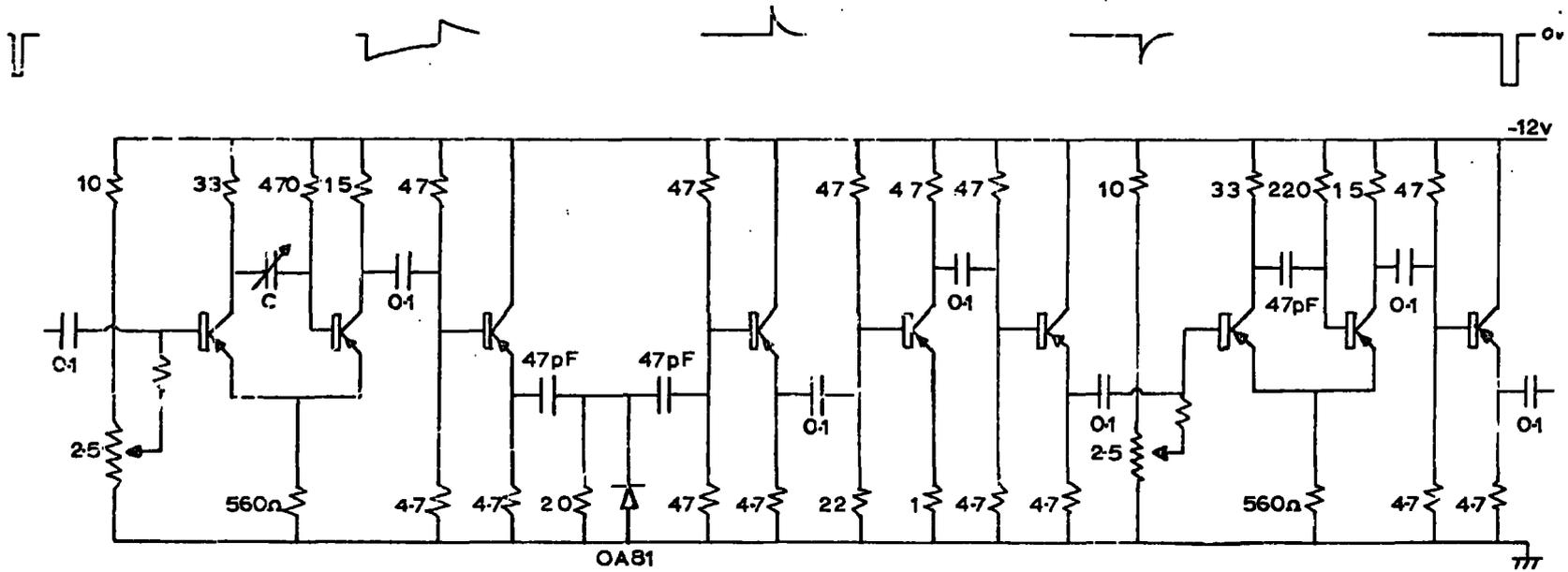
Figure A11 The variable-delay pulse generator.
The delay is governed by the capacitance, C.
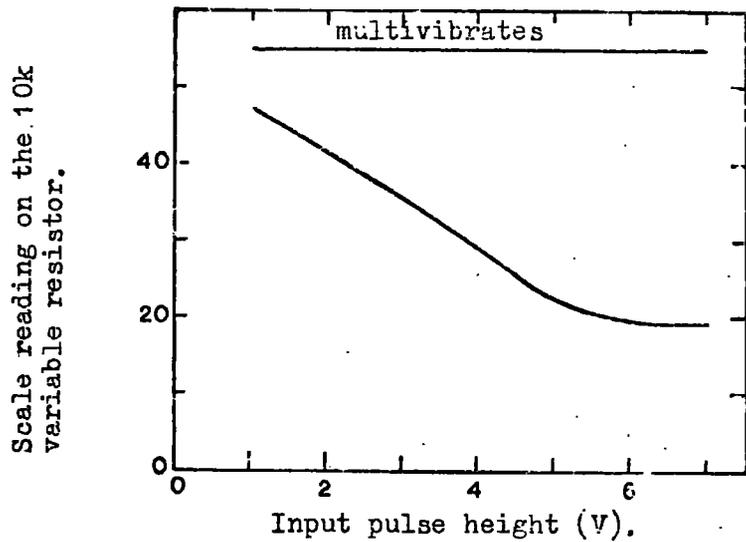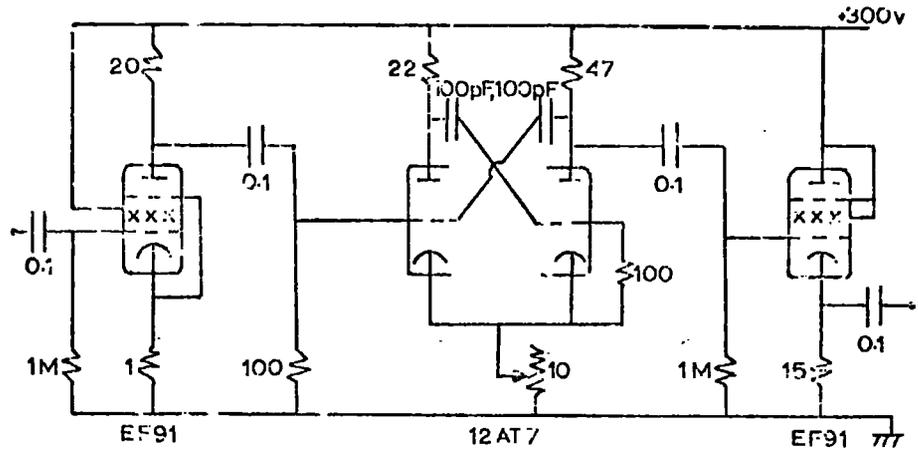
Figure A12   The valve monostable used to trigger the thyristor.
The input pulse height required to fire the
monostable at a specific scale reading is shown in
the graph. At a setting above 55 the circuit
multivibrates.
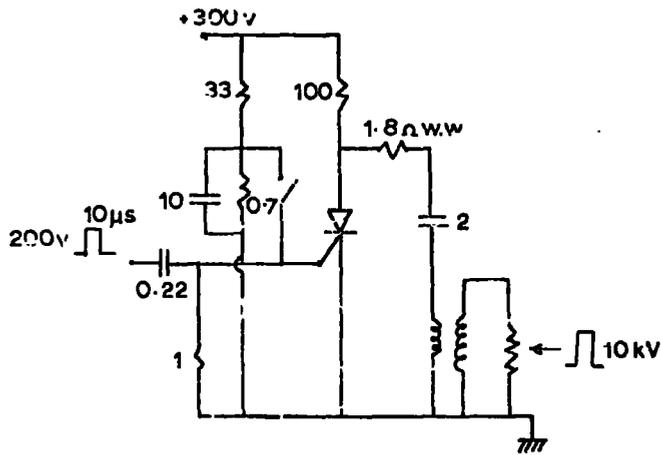
Figure A13   The thyristor unit.
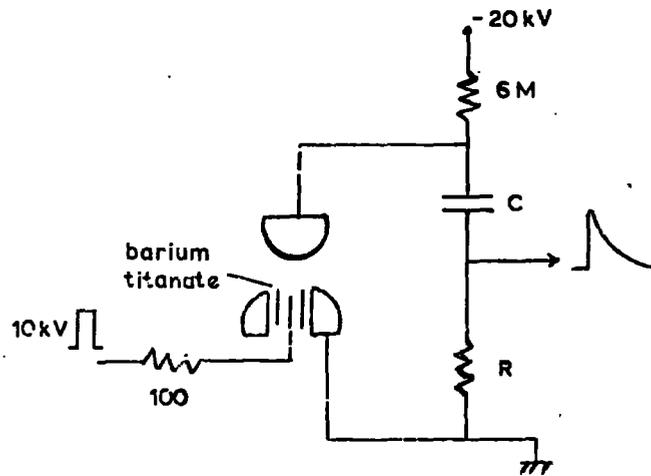
Figure A14   An air spark gap which is triggered by the
thyristor unit. Values of C and R are determined
by the experimental conditions.
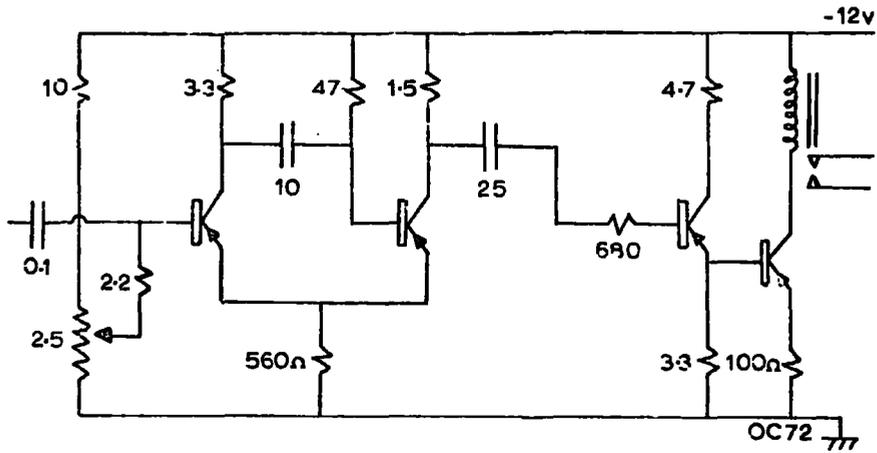
Figure A15 The cycling system trigger.
A −5V, us, pulse at the input will close the
relay and start the cycling system.
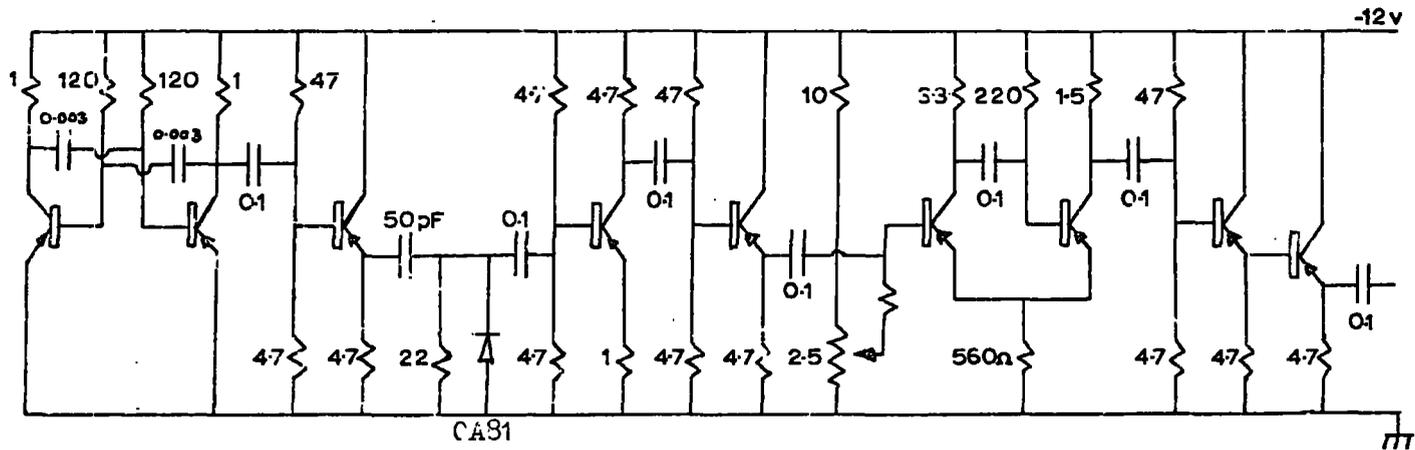
Figure A16 A 10 kiloHertz, 1 us, pulse generator.
The width of the pulse may be varied from 0.9
to 4us by the 2.5k potentiometer.
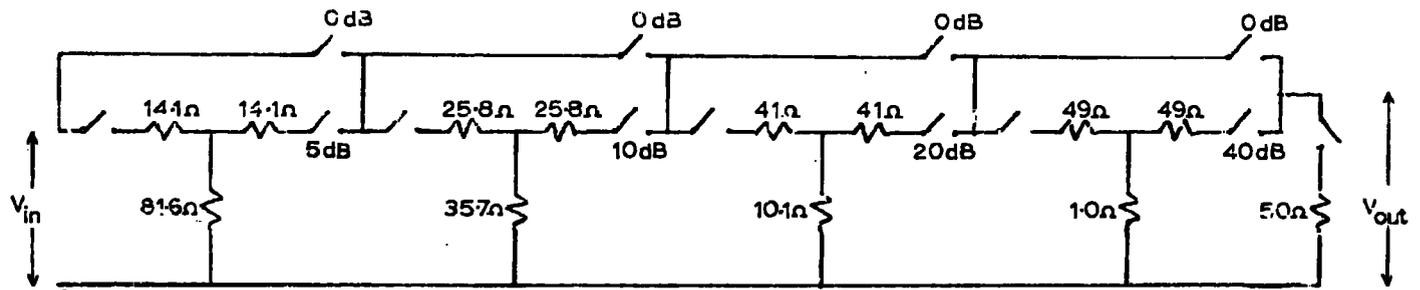
BASIC T-SECTION ELEMENT
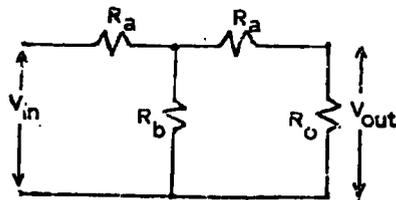
$$R_o = \sqrt{R_a^2 + 2R_a R_b}$$

$$\frac{V_{out}}{V_{in}} = \frac{R_b}{R_a + R_b + R_o}$$

REQUIRE $R_o = 50\Omega$

Figure A17 A 0-75dB attenuator of characteristic impedance, 50Ω.

APPENDIX B

COSMIC RAY TELESCOPES

B.1 Scintillator telescope

A small scintillator telescope was used to calibrate the large liquid scintillators in both main experiments described in this thesis. The telescope was made up of two plastic scintillators, dimensions 15.24 x 10.16 x 2.54 cm^3 of NE109A phosphor, each viewed by one 1 inch photomultiplier in optical contact with one end of the phosphor. The resistor chain used on the base of each photomultiplier is shown in Figure B.1 and a block diagram of the electronics is shown in Figure B.2. All the circuitry used for the telescope has been shown in Appendix A. The amplifier developed for the telescope, unlike the voltage amplifier shown in Appendix A, did not require an emitter follower being used at the photomultiplier base. This circuit was designed for its low input impedance and its ability to deal with short pulse lengths.

The single particle peaks obtained from each scintillator are shown in Figure B.4 as the plot of the differential rate against pulse height. It can be seen that these peaks are quite well separated from noise. The coincidence rate is shown as a function of the rate from each scintillator in Figure B.5 for a separation of 60 cm. It can be seen that the plateau for single particle detection is very wide so that the telescope is not dependent on the discriminator setting.
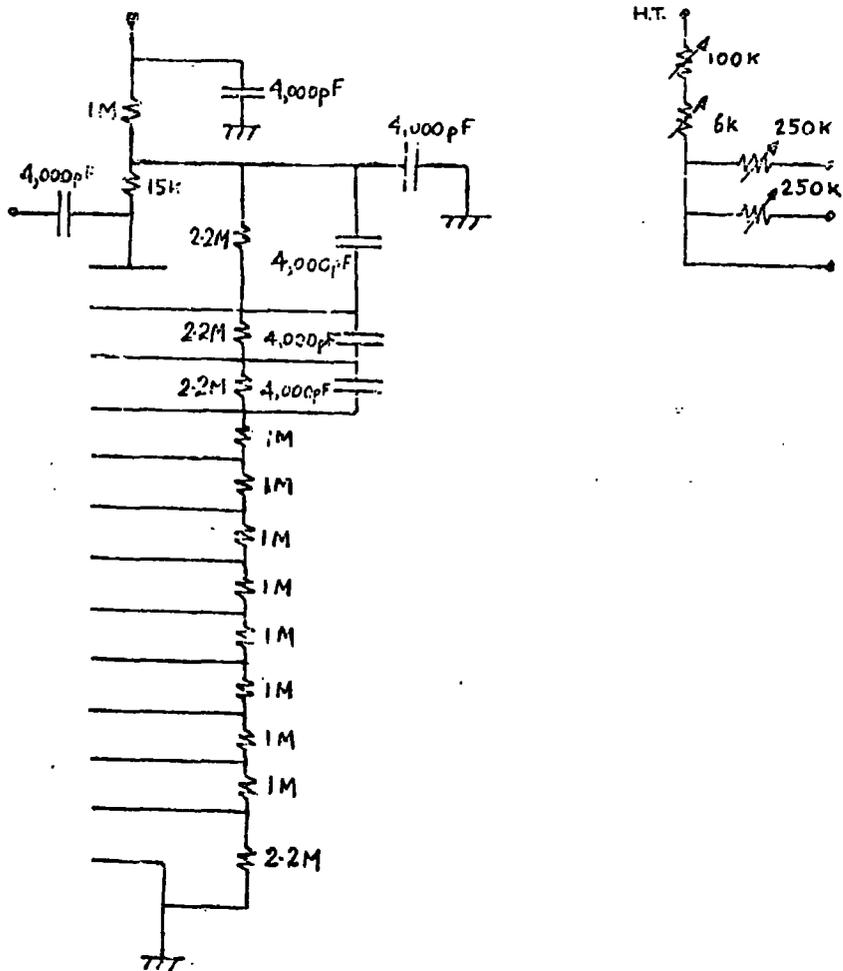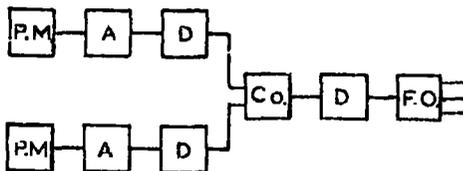
Figure B1   Photomultiplier base connections.

Key;   P.M.   photomultiplier   Co.   coincidence
        A   amplifier   F.O   fan out
        D   discriminator
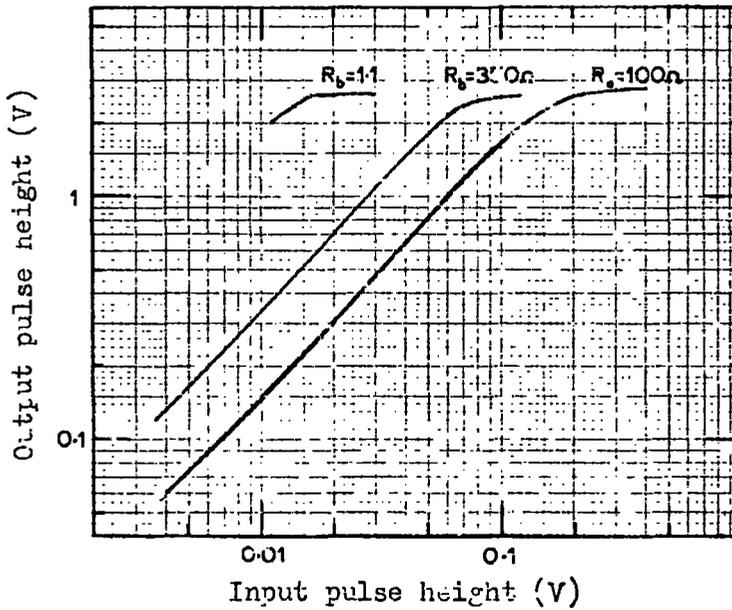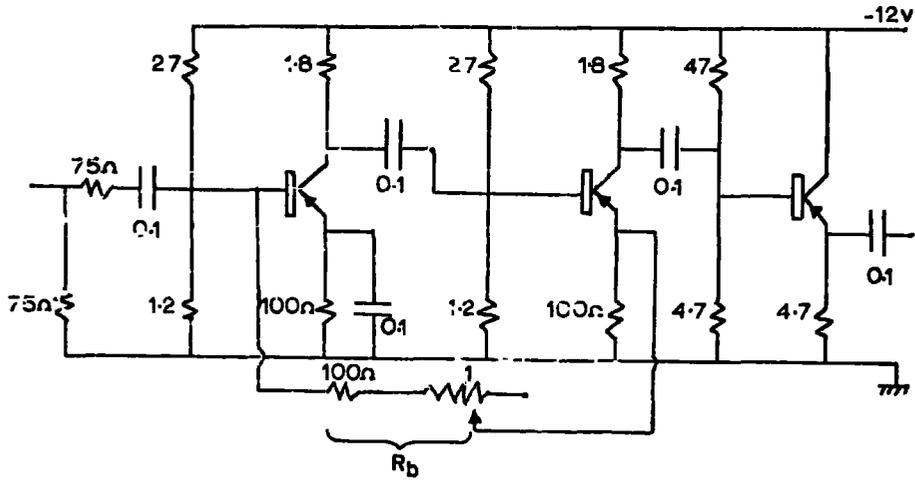
Figure B2   The electronics of the scintillator telescope.

Figure B3   The scintillation amplifier and its input-output
characteristics at various values of feedback
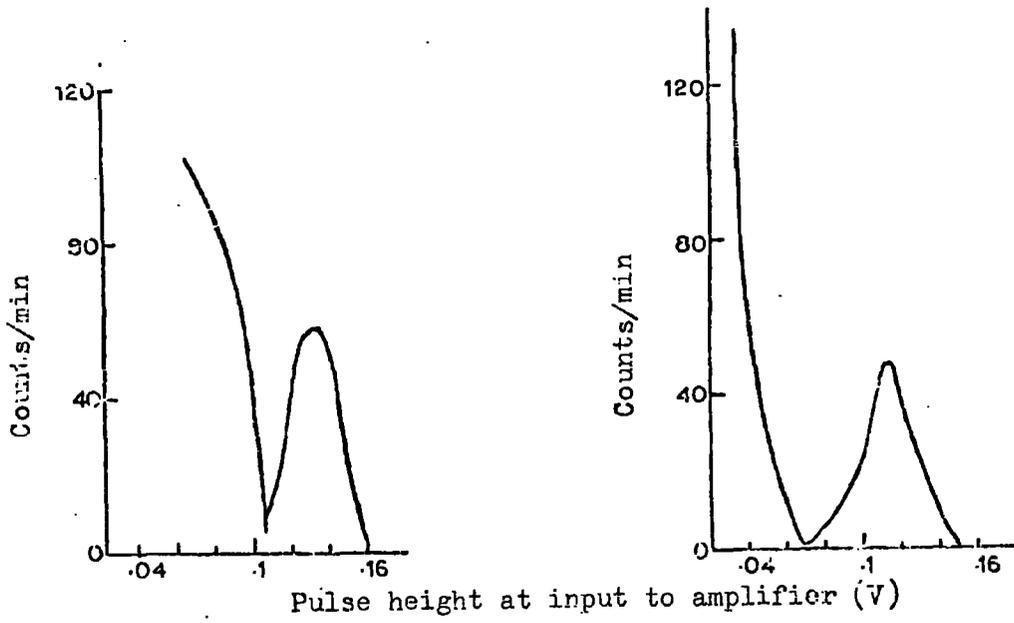resistance, R_b.

Figure B4   The differential rate-pulse height response obtained
             from each of the small plastic scintillators.
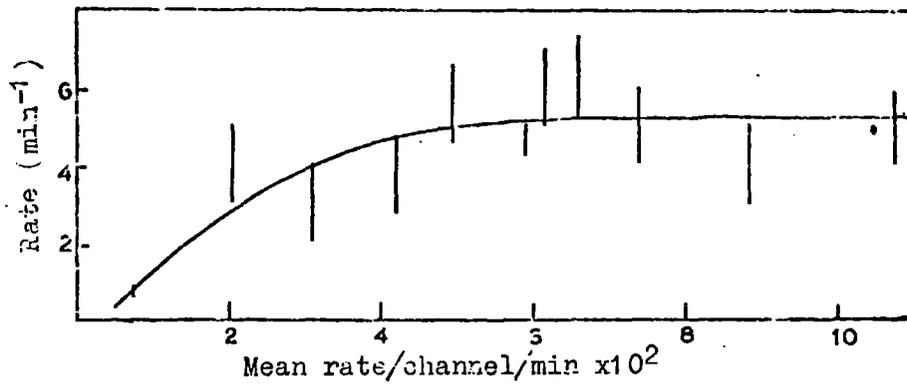

Figure B5   The rate of coincidences between the two scintillators
             as a function of the rate in each scintillator.
             (Scintillators separated by 60cm)

B.2 Geiger Telescope

The geiger telescope has been described in Chapter 2.6. The telescope consisted of three trays of Geiger tubes, each tube having dimensions 30 cm long and 3.5 cm diameter. The upper tray was made up of 3 tubes and the two lower trays each had 4 tubes. The outputs from the tubes in each tray were connected together and led into the input of a quenching unit (Figure B.6). The positive output pulses (~ 130v) from each of the three quenching units were lead, via coaxial cable, to a three-fold coincidence unit (Figure B.7). Each Geiger tube had to be calibrated separately to ensure that its operating voltage was at the centre of the Geiger plateau.
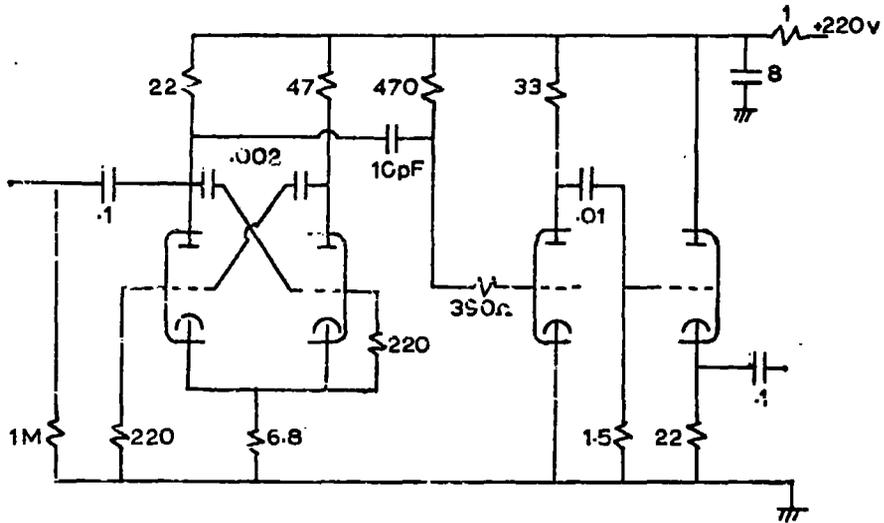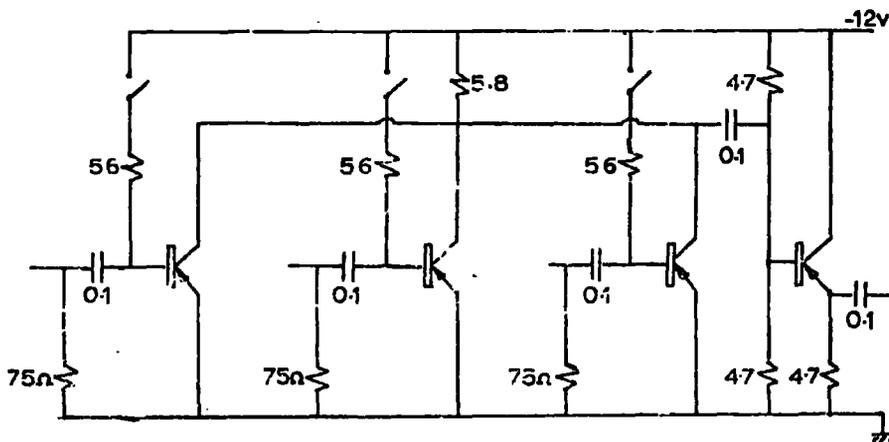
Figure 36   The Geiger quenching unit.

Figure 37   The Geiger coincidence unit.
(This circuit operates on input pulses of
+100V from the quenching unit.)

APPENDIX   C

COMPARISON OF THE SCINTILIATION COUNTERS

All the scintillators used in the experiments have been described previously.   The integral rate - output pulse height curves obtained for each type of scintillator are shown in Figure C.1.   The rates have not been normalised so that the largest area counter, the liquid scintillator, has the largest rate.

The liquid scintillator has been described in Chapter 4.3.   The scintillation material was medicinal paraffin plus 0.5 gm per litre p-terphenyl and 0.005 gm per litre POPOP, dimensions 130 x 90 x 17.8cm^3. The phosphor was viewed by two 5" photomultipliers positioned at the centre of the 90 cm sides.

The large plastic scintillator has been described in Chapter 6.3. The phosphor was NE102A of dimensions 140 x 75 x 5 cm^3 viewed by six 2" photomultipliers positioned with three on each of the 75 cm sides.   The small plastic scintillator has been described in Appendix B.   The phosphor was again NE102A but of dimensions 15 x 10 x 2.5 cm^3 viewed by one 1" photomultiplier.
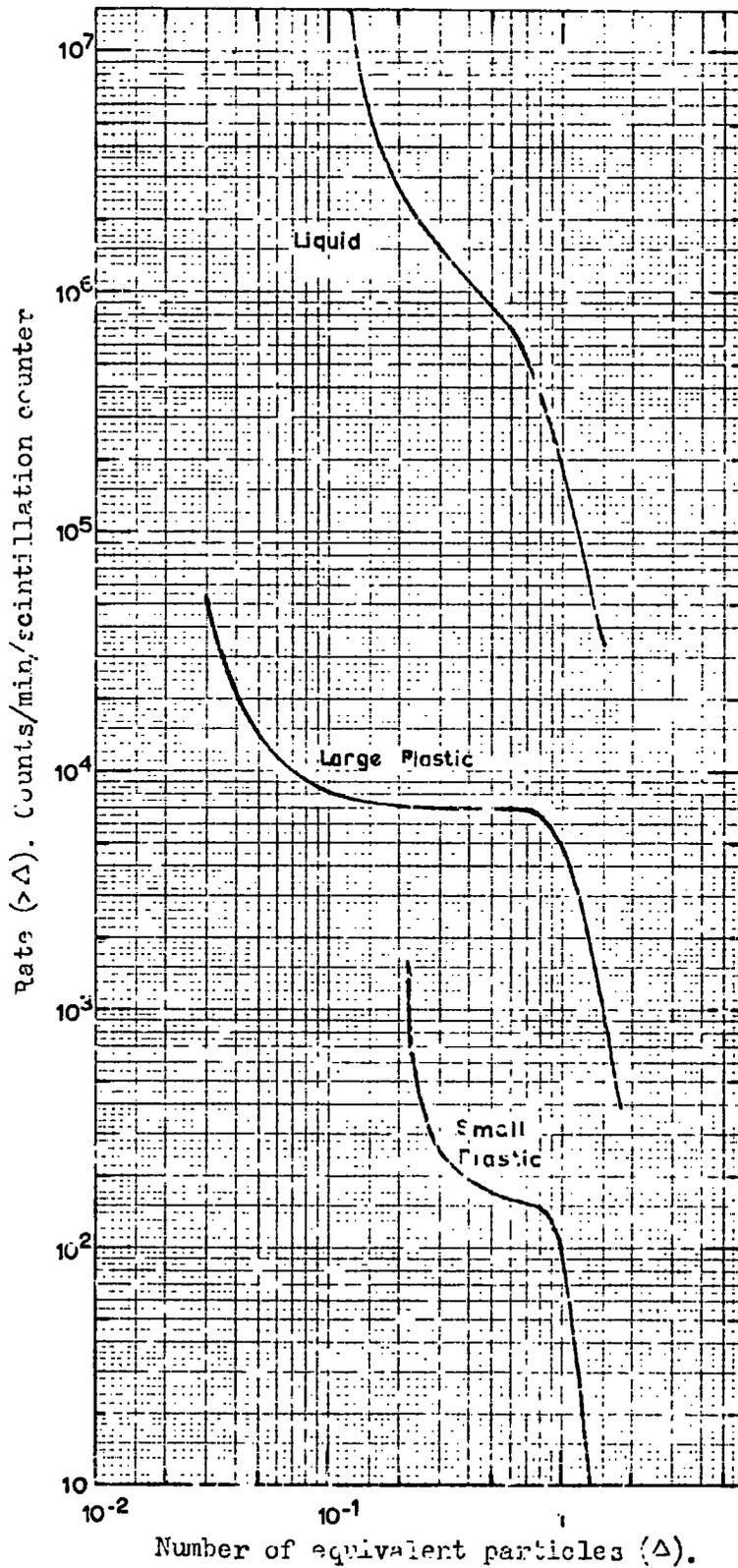
Figure C1
The integral rate-pulse height curves obtained from the three types of scintillators used. The pulse heights have been normalised so that the median pulse height produced by single muons traversing each counter is defined as one equivalent particle.